1.0

4.5
5.0

2.8

2.5

3.2

2.2

3.6

1.1

4.0

2.0

1.8

1.25

1.4

1.6

MICROCOPY RESOLUTION TEST CHART

NATIONAL BUREAU OF STANDARDS 1963 A

Special Report 80-26
June 1980

LEVEL II

12

WORKING GROUP ON
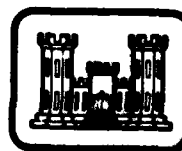# ICE FORCES ON STRUCTURES

A State-of-the-Art Report

T. Carstens, Editor

AD A089674

IAHR

AIRH

DTIC
SELECTED

SEP 2 6 1980

E

80 9 29 106

REPORT DOCUMENTATION PAGE	READ INSTRUCTIONS BEFORE COMPLETING FORM

1. REPORT NUMBER	2. GOVT ACCESSION NO.	3. RECIPIENT'S CATALOG NUMBER
Special Report 80-26	AD-A089 674	

4. TITLE (and Subtitle)	5. TYPE OF REPORT & PERIOD COVERED
WORKING GROUP ON ICE FORCES ON STRUCTURES. A State-of-the-Art Report.	
	6. PERFORMING ORG. REPORT NUMBER

7. AUTHOR(s)	8. CONTRACT OR GRANT NUMBER(s)
Torkild Carstens (Editor)	

9. PERFORMING ORGANIZATION NAME AND ADDRESS	10. PROGRAM ELEMENT, PROJECT, TASK AREA & WORK UNIT NUMBERS
International Association for Hydraulic Research Section on Ice Problems Working Group on Ice Forces on Structures	

11. CONTROLLING OFFICE NAME AND ADDRESS	12. REPORT DATE
U.S. Army Cold Regions Research and Engineering Laboratory Hanover, New Hampshire 03755	June 1980
	13. NUMBER OF PAGES
	153

14. MONITORING AGENCY NAME & ADDRESS(if different from Controlling Office)	15. SECURITY CLASS. (of this report)
	Unclassified
	15a. DECLASSIFICATION/DOWNGRADING SCHEDULE

16. DISTRIBUTION STATEMENT (of this Report)

Approved for public release; distribution unlimited.

17. DISTRIBUTION STATEMENT (of the abstract entered in Block 20, if different from Report)

18. SUPPLEMENTARY NOTES

19. KEY WORDS (Continue on reverse side if necessary and identify by block number)

Force (mechanics)	Underwater structures
Ice	Waterfront structures
Sea ice	
Structures	

20. ABSTRACT (Continue on reverse side if necessary and identify by block number)

Part I. A short review is presented of the literature on thermal ice pressure against extended hydraulic structures such as dams. Some of the methods suggested for the computation of ice loads caused by temperature changes are reviewed. As a means of comparison measurements of thermal ice pressure and empirical values used at present for estimating these loads are referred to.

Part II. Ice forces on structures are determined either by the environmental driving force or by the force to fail the ice sheet and move the ice

DD FORM 1473 EDITION OF 1 NOV 65 IS OBSOLETE
1 JAN 73

20.   (cont'd).

around the structure; which ever is the least.   State-of-the-art techniques for predicting these forces on fixed, rigid structures are presented.   A rigid structure is defined as one where the ice interaction process is not influenced by the deformation of the structure itself.   Structures are considered in three broad categories; structures with sloping sides, structures with vertical sides, and wide structures such as artificial islands.   Both uniform and ridged ice is considered.   The problem of ice ride-up on sloping beaches is also discussed.

Part III.   The modes of interaction between ice and structure are discussed, and the properties of both ice and structure are seen in the context of interaction.   The key parameter of the ice is the dependence of crushing strength on loading rate, in particular the inverse relationship that exists for a certain range and gives rise to negative damping.   Self-excited vibrations leading to limit cycles are explained and some design problems are discussed.

Part IV.   A review of the buckling analyses of floating ice sheets is presented.   The theory used is that of a beam or plate on an elastic foundation.   For beams, the results for all possible boundary conditions are presented and discussed.   For plates, results of numerical solutions for a semi-infinite plate loaded over a part of its boundary are presented and discussed. One solution is presented for an infinite plate loaded radially at a hole in the plate.   In addition, results for wedge-shaped beams and plates are presented and discussed.   Wedge-shaped ice sheets frequently occur due to previous cracking in the ice.

Accession For		
NTIS GRA&I	☒	
DDC TAB	☐	
Unannounced	☐	
Justification_____		
By_____		
Distribution/		
Availability Codes		
Dist.	Avail and/or special	
A		

PREFACE

At its Third Ice Symposium in 1975 in Hanover, New Hampshire, USA, the IAHR
Section on Ice Problems formed the following working groups, proposed by its
chairman, Dr. O. Starosolszky:

    Working Group on Standardizing Testing Methods
    Working Group on Ice Jamming
    Working Group on Ice Forces on Structures

The Section gave the Working Groups the task of presenting state-of-the-art
reports to the Fourth Ice Symposium in Lulea, Sweden, in 1978.

The Working Group on Ice Forces has the following members:

    T. Carstens, Norway (Chairman)
    K.R. Croasdale, Canada
    R.Y. Edwards, Canada
    V.A. Korenkov, USSR
    M. Määttänen, Finland
    D.E. Nevel, USA

It has not been found practical or even desirable to mould the working group
reports in the same form. The present report consists of four parts written
by named individuals. The function of the working group has essentially been
to provide general guidelines at the start and to review the manuscripts at
the end. The report is thus more a result of individual efforts than of teamwork.

The main advantage of this mode of operating is that it produces results faster
than the other mode, in which the collective efforts predominate. To gather
an international group for intensive discussions and unifying modifications of
the submitted drafts is a practical problem of considerable magnitude, and it
is very time consuming.

In this first report we have sacrificed, to some degree, coherence and uniformity,
in order to avoid the worst fate of any report: obsolescence.

The printing and distribution of this and forthcoming reports present another
set of problems. Working group reports cannot be expected to sell and carry
their printing costs. IAHR does not have budgets for such publishing, so out-
side sponsors are necessary. The predicament was overcome by a generous offer
from the U.S. Army Cold Regions Research and Engineering Laboratory, Hanover,
New Hampshire (CRREL). This renowned institution has members in all the working
groups and is very active in international ice research.

The present report is an attempt to distribute information in a useful format to
the international community of ice engineers. Your response will indicate whether
the effort was worthwhile.

Trondheim, August 1979

Torkild Carstens

CONTENTS

PART I

THERMAL ICE FORCES

By J.H. Kjeldgaard and T. Carstens
The River and Harbour Laboratory,
The Norwegian Institute of Technology,
Trondheim, Norway

Abstract

A short review is presented of the literature on thermal
ice pressure against extended hydraulic structures such
as dams.

Some of the methods suggested for the computation of ice
loads caused by temperature changes are reviewed. As a
means of comparison measurements of thermal ice pressure
and empirical values used at present for estimating these
loads are referred to.

As will appear there still exists some divergencies in the
results of the methods suggested and there seems to be a
need for further field measurements to clarify some of the
problems.

INTRODUCTION

When an ice cover is subjected to a temperature increase the
ice will attempt to expand. The forces exerted on the sur-
roundings e.g. on hydraulic structures such as dams will depend
on a number of parameters describing:

- the temperature variation as a function of time and
  depth in the ice cover

- the material properties of the ice

- the geometrical form of the ice cover including cracks
  and other irregularities

- restrictions to expansion along the boundaries of the
  ice cover

The theories suggested for the computation of such ice forces
and the experimental verification of the theories are compli-
cated by the complex mechanical behaviour of ice under load
of long duration and by the variety of forms in wich ice may
occur.
Some of the methods and theories that have been proposed for the
calculation of thermal ice forces are reviewed below.
As will be seen there still exists some uncertainties and
divergencies in this field.

Units used in the reviewed literature:

$1 \text{ kp/cm}^2 = 98066.5 \text{ N/m}^2$
$1 \text{ t/m}^2 = 9806.65 \text{ N/m}^2$
$1 \text{ t/m} = 9806.65 \text{ N/m}$

1.1. THEORIES OF THERMAL ICE PRESSURE

In this section is given a short survey of the theories suggested for calculation of thermal ice pressure. It has been the intention to outline some of the ideas used in the theories and to give some of the fundamental drawbacks that may reduce their utility.

Many of the points mentioned can be found in the works of Korzhavin [1] and Drouin and Michel [2, 3, 4, 18]. In these works also a more quantitative description of the theories can be found.

1.11 Royen (1922)

In 1922 the Swede N. Royen published a method for determining thermal ice pressure [5].

His formula was the basis for the Russian norm SN 76-59 used until 1967. The fundamental law used by Royen was

$$\varepsilon = \frac{c\sigma t^{1/3}}{1+\theta} \tag{1}$$

where

ε : strain in compression (uniaxial)

σ : stress [kp/cm^2]

t : duration of load [hours]

θ : the ice temperature [^{o}C numerical value]

c : an experimental constant $60 \times 10^{-5} - 90 \times 10^{-5}$

The relation $\varepsilon \propto \sigma$ had been found by tests with paraffin wax while $\varepsilon \propto t^{1/3}$ was based mainly on tests with lake ice. Both relations have later been shown to give an inadequate description of the behaviour of fresh water ice.

The uniaxial strain rate from a nonrestricted thermal expansion of ice can be written

$$\frac{d\varepsilon}{dt} = \alpha \frac{d\theta}{dt} \tag{2}$$

where α is the linear thermal expansion coefficient of ice
[/$^{\circ}$C].

Royen equates (1) and (2) keeping σ and θ in (1) constant
during differentiation. It is further assumed that the tempera-
ture increase is linear with time:

$$\theta(t) = \theta_i - \dot{\theta} \cdot t \qquad (3)$$

$\theta(t)$: mean temperature of ice [$^{\circ}$C absolute value]

θ_i : initial mean temperature of ice [$^{\circ}$C absolute value]

$\dot{\theta}$: the mean temperature increase [$^{\circ}$C/h]

By means of equations (1), (2) and (3) Royen finds the maximum
stress developed during a temperature increase

$$\sigma_{max} = 1640\alpha(\theta_i+1) \sqrt[3]{\dot{\theta}(\theta_i+1)^2} \quad [\text{kp/cm}^2] \quad (4)$$

or with $\alpha = 5.5 \cdot 10^{-5}/^{\circ}$C the usual form of Royens equation
becomes

$$P_{max} = 0.9d \ (\theta_i+1) \sqrt[3]{\dot{\theta}(\theta_i+1)^2} \qquad (5)$$

P_{max} : force [t/m]

d : ice cover thickness [m]

To find the value of P_{max} relevant to Sweden, Royen assumes
a minimum air temperature of -40°C, a maximum ice thickness
of 0.75-1.0 m and an initial temperature for the ice of -12°C.
If then the ice temperature is increased to 0°C during 100, 170
or 360 hours as suggested by Royen the corresponding values of
P_{max} will be 34.5, 28.7 and 22.5 t/m for an ice thickness of 1 m.
In admitting a certain elastic deformation Royen assumes a
maximum value of 30 t/m for an ice cover biaxially restrained
in areas where the minimum air temperature is -40°C.

In the light of later research on thermal ice pressure a number of drawbacks are found in Royen's theory, for instance:

1) Paraffin wax does not simulate the properties of fresh water ice.

2) Elastic deformation is ignored.

3) No distinctions are made between different creep states of the ice.

4) Uniaxial theory is used for biaxial restraint.

5) Because the temperature is assumed uniform over the ice thickness, P_{max} will be proportional to the thickness.

1.12 USSR norm SN 76-59. (1959)

The formula in this norm, operative until 1967, was based on the Royen theory with minor modification. See for instance Korzhavin [1].

From observations in Siberia it was found that the initial mean ice temperature θ_i should be expressed as

$$\theta_i = 0.35 \cdot \theta_a \tag{6}$$

where θ_a is the mean air temperature during the preceding 24 hours [$^\circ$C absolute value]

The increase of the ice mean temperature should be

$$\dot{\theta} = 0.35 \frac{\Delta\theta_a}{\Delta t} \tag{7}$$

where $\Delta\theta_a$ is the maximum increase of the air temperature [$^\circ$C] during a given period of time Δt [hours] within the preceding 24 hours.

Finally replacing the constant 1640α by the empirical form
$0.78 \cdot \theta_a^{-0.88}$ the Royen formula becomes

$$P_{max} = 5.52d \; \frac{(0.35 \; \theta_a + 1)^{5/3}}{\theta_a^{0.88}} \cdot (\frac{\Delta \theta_a}{\Delta t})^{1/3} \qquad (8)$$

where   d   :   ice thickness [m]

P_{max} :   maximum force [t/m]

When there is a snow cover (thickness d_s [m]) on the ice the
values of P_{max} should be multiplied by the factor

$$r = \frac{d}{d+9.1d_s} \qquad (9)$$

following the SN 76-59. If the extent L of the ice is more
than 50 m P_{max} should be multiplied by the factor ψ = 0.9-0.6
for L = 50 m - 150 m or more.
According to Korzhavin [1] the pressure values for 10 points
in the USSR will fluctuate from 15 to 30 t/m^2 when based on the
recommendations of SN 76-59.

It is noticed that in spite of the Russian refinements of the
Royen formula the value of P_{max} is still proportional to the
ice thickness.

1.13 Brown & Clarke (1932)

In connection with a hydraulic project in Canada Brown & Clarke
1932 [6] made some laboratory investigations to obtain at least
the order of magnitude of the expected thermal ice pressure.

In the two experiments that were reported, ice cubes were
subjected to a temperature rise that was intended to be linear
with time while two opposite cube faces were loaded exactly as much

as needed to avoid any expansion in that direction. The results
of the experiments were a few (primarily three) points on a graph
showing temperature increase rate versus load increase rate.
As is seen the results are few and furthermore the experimental
equipment was not able to realize the intended test conditions
with any high degree of accuracy.

1.14 Rose (1947)

In spite of the drawbacks Brown & Clarke's experimental results
were used by Rose [7] to make some general computations of ice
pressure. Rose's main contribution to the ice pressure problem
was that he showed how the temperature distribution will develop
in an ice cover that is subjected to a linear temperature rise
at the top.

The computations of ice forces were carried out by first using
finite difference integration of the heat conduction equation
to give the rate of change of temperature at a certain level
in the ice cover. Using this and a curve based mainly on Brown
& Clarke's results, the ice pressure at that level in the ice
was found by summing up the pressure increases. Rose made cal-
culations with or without lateral restraint and also with or
without accounting for absorption of solar energy. According
to Drouin [2] the results found by Rose have been widely known
and used by engineers.

Among the objections made against Rose's results some of the
most important ones might be:

1) The experimental basis is weak.

2) No account is taken of the initial ice temperature,
   only changes are considered.

3) According to Löfquist [8] the summation process used is
   not legal: "An integration of component forces will be
   mathematically permissible only if a linear relation
   exists between the stress and the strain. In the present

case this is true only with a linear temperature rise
according to the experiments. From the physical point
of view, it is not permissible as a rule, to add to a
component of force set up in the ice at a given point
of time, in consequence of restrained temperature expan-
sion, another component of force set up at a later point
of time ......"...... because of stress relaxation.

1.15 Monfore (1947-1953)

A major research project was begun in 1947 by the U.S. Bureau of
Reclamation.   The intention of the project was to determine
the thermal ice pressure on some dams in Colorado. Both in
situ measurements of ice pressure and laboratory investiga-
tions of the creep properties of natural ice were conducted
Monfore [9, 10, 11, 12].

The laboratory investigations were made in much the same way as
the ones by Brown and Clarke, but the equipment was better.
Small cylindrical ice samples could be loaded axially. A meter
in direct contact with the sample measured the axial strain.
The temperature of the ice sample could be controlled by means
of cold air-circulation and the ice temperatures were measured
both at the periphery of the ice sample and at the axis.

Before a test was made the sample was kept at one of the follwing
initial temperatures -30, -20, -10, 0, 10, 20°F for some time.

Then the circulation of air was changed in such a way that the
temperature of the ice was made to increase with one of the
following rates 2, 5, 10, 15 °F/h. During the first 30 minutes
the load was adjusted to give zero total strain every 5 minutes.
Thereafter adjustment of load was done every 15 minutes.

The samples had been taken from two reservoirs where the ice
cover thickness was approximately 45 cm. The samples were

taken from different levels in these covers. They were made in
such a way that the axis of the cylinders were parallel to the
ice cover surface.

Monfore made several tests with the above mentioned temperature
conditions. When the stress necessary to maintain zero strain is
drawn as a function of time (or temperature), the curves look
qualitatively the same. First the stress increases nearly
linearly with time, the curve having a weak tendency of decreasing
slope. The slope decreases more and more and at a certain time
the stress attains a maximum after which it decreases markedly.

The curves look qualitatively the same but by testing different
samples at the same initial temperature and the same rate of
temperature increase, Monfore found a large scatter in the two
characteristic parameters of the load curve: the maximum stress
and the time used to attain this stress. Variation in the order
of 25% was recorded.

To find the reproducibility of the tests a number of samples
were loaded twice under identical temperature conditions. This
showed that the mean value of the difference between 1st and
2nd loading was less than 6%.

This difference in scatter could be attributed to variations in
the crystal structure of the ice. Monfore studied the crystal
orientations in a few samples and did find some marked diffe-
rences but the crystal structure was not used as an independent
parameter in the tests.

The fact that he neglected the crystal structure may be the most
important reason for objections from later investigators.

It is also claimed that when the load is not adjusted more
often than every 5th or 15 th minute the measured stress will
be too high.

A final objection is of course that the tests are uniaxial while
nature is often biaxial.

In spite of the drawbacks Monfore's investigation was a great
step forward in the understanding of thermal ice pressure.

1.16 Löfquist (1952)

In 1952 the Swede Löfquist published the results of a single
experiment with thermal ice pressure [8].
He made use of a cylindrical container with a diameter of 50 cm
appropriately insulated. In this container he let the ice
develop in the same way as it happens in nature by cooling the
water/ice at the top surface.
When the ice had reached a thickness at about 60 cm the ice sur-
face was exposed to an approximately exponential temperature in-
crease from $-30^{\circ}C$ to $0^{\circ}C$ during 25 hours.

During the temperature increase both temperature and the corre-
sponding biaxial stress were measured at several levels in the
ice. It was seen how the temperature profile,
first approximately linear through the ice thickness,
develops into the shape of a semi-pear with a minimum moving
down through the ice. The form of the stress profile also
develops into the shape of a semi-pear with a maximum moving
down through the ice. The stress maximum however is lagging the
temperature minimum by some hours. A maximum total load corre-
sponding to 20 ton/meter was recorded about 14 hours after the
start of the temperature increase. At that time the maximum of
the stress distribution had moved about 1/5 of the way down
through the ice cover.

The cylindrical container used by Löfquist was made of concrete.
He assumes that the thermal and elastic expansion of the concrete
and some cracks in the ice cover during heating have caused the
measured stress to be less than it ought to be.

1.17 USSR norm SN 76-66 (1966)

In 1967 the USSR norm SN 76-59 was succeeded by the one mentioned
above. The norm was translated into English by the National
Research Council of Canada in 1973 [14].

This norm obviously contains a set of formulas quite different
from the ones that were used in the SN 76-59. But in fact we
have found no publication (in non-Russian language) explaining
the sources and the development of the formulas and graphs given
in SN 76-66 for determining thermal ice pressure.
Apparently the theory is the one referred to by Korzhavin 1972
[15]. According to him it is based on the work of B.V. Pros-
kuryakov: "Proceeding from the basic assumption that pressure
developed due to the thermal expansion of ice exceed its yield
point, he regards ice within the range of plastic deformations
as a viscous fluid".
In 1967 Proskuryakov submitted a paper to the 12th IAHR confe-
rence [16]. In this paper he gives a short survey of the pro-
blems of thermal ice pressure and reviews the USSR norms for
determining this pressure, but no details of the SN 76-66 are
given. So for the present it appears to us that only the com-
putational results of the SN 76-66 can be studied.

However one point may be mentioned: The temperatures to be
used as input to the formulas of SN 76-66 are air temperatures
and account is taken of the thermal boundary layer between ice/
snow and air. The formulas used for these two values of the
coefficient of heat transfer are those suggested by O. Devik
[17]. From these formulas it is seen that the thermal boundary
layer will play a significant role in the temperature distri-
bution. This is contradictory to what is said by Michel [3].

1.18 Lindgren (1968)

In 1968 S. Lindgren published the results of an investigation
on thermal ice pressure [13].
The work contained laboratory tests with both uniaxial and
biaxial load. Only little information is given about the struc-
ture of the ice used for the experiments.

The samples that were used by Lindgren for <u>uniaxial tests</u> were of the size $7 \times 7 \times 20$ cm^3. They were made in such a way that a load along the longer axis would simulate an ice cover loaded horizontally.

The samples were subjected to a constant stress at a constant temperature. The results of the tests are thus strain as a function of time. At the temperature -10°C Lindgren used the loads 2, 6, 8, 10 and 14 kp/cm^2 and at the load 6 kp/cm^2 the temperatures -0.5, -5, -10 and -20°C were used.

To reduce the results of the deformation tests to a common form, Lindgren tried to fit the parameters in a linear visco-elastic model composed of a Maxwell and a Voigt element coupled in series. The rheological equation for such a model is

$$\varepsilon = \frac{\sigma}{E_1} + \frac{\sigma}{E_2} (1-\exp(\frac{-E_2 t}{\eta_2})) + \frac{\sigma t}{\eta_3} \qquad (10)$$

where $\quad E_1 \; E_2$: elastic moduli

$\qquad \eta_2 \; \eta_3$: viscosity moduli

$\qquad \quad \varepsilon$: strain

$\qquad \quad \sigma$: stress

Concerning the suitability of such a model Lindgren says: "Several studies have shown that this equation does not give a complete picture of the deformation characteristics of ice. -- However a simple form in accordance with the equation is used in the following. As ice is not linearly visco-elastic the moduli of deformation are therefore governed by stress." After mentioning that: "Only a few tests were carried out and it is therefore only possible to show the general effect of different factors", Lindgren gives the following values:

$$E_1 = (66000 - 800 \cdot \theta) \text{ kp/cm}^2$$

$$E_2 \sim 70000 \text{ kp/cm}^2$$

$$\eta_2 \sim 1.1 \cdot 10^8 \text{ kp sec/cm}^2$$

$$\eta_3 = 18.5 \cdot \sigma^{-1}(0.20-0.08\theta)(\frac{t}{3600})^{0.5} \cdot 10^8 \text{ kp sec/cm}^2$$

where t is time [sec] and θ is temperature [$^\circ$C].

According to Lindgren E_1 seems to be independent of stress
and previous load. It was not possible to show the effect of the
size of crystals. E_1 was determined on the basis of the de-
formation occurring 30 sec after the load was applied. (This
time period may be too long according to [4] because of the
viscous deformation.)
E_2 and η_2 are difficult to determine and only approximate
values are given.
The value given for η_3 is applicable only to "normal crystals"
such as those used for the experiment.
"The value of η_3 is considerably lower when the crystals are
small and shows tendencies to decrease with the period of load".

Lindgren also made experiments with <u>biaxial stress.</u>
In these tests a steel ring with an inner diameter of 80 cm was
placed around a circular ice plate with a diameter of about 80
cm and a thickness of about 7 cm. Then the space in between
was filled with water. The tests were started at a low tempera-
ture after which the temperature was raised. The temperature,
the strain and the stress were recorded as a function of time.

The values for E_1 and E_2 used in the rheological model are esti-
mated to be the same as for the case of uniaxial tests, on condi-
tion that the coefficient for contraction during elastic defor-
mation is ⁎ 0.36. (According to Drouin and Michel [4] this is
a necessary assumption because of difficulties in determining
those parameters.) The value of η_2 is assumed the same as
before. η_3 on the other hand has been assigned a new value,

$$\eta_3 = 31 \cdot \sigma^{-1} (0.30-0.07\theta) \cdot (\frac{t}{3600})^{0.25} \cdot 10^8 \ kp \ sec/cm^2$$

on condition that the contraction coefficient is 0.5 when the
deformation is viscous.

According to Drouin and Michel [4] a fundamental objection to
this work is that the rheological model used by Lindgren cannot
represent the properties of the ice. Further the experimental
results are very scattered. So the final results can only be
an approximation.
One of Lindgrens concluding remarks is: "---- calculations of
the values of maximum ice pressure are somewhat unreliable.
With this in mind, rough estimates can be used to assess maxi-
mum ice pressure."

1.19 Drouin and Michel (1971)

A couple of years after Lindgren's publication Drouin and
Michel (in the following abbreviated D & M) made their con-
tribution to the research of thermal ice pressure [4].
D & M have made a critical survey of former thermal ice pres-
sure research relevant to their work. Furthermore they have
given a thorough treatment of the question of temperature
distribution in an ice cover by conduction considering both
stationary and transient conditions. But the question of
thermal boundary layers has been totally neglected except for
some qualitative considerations in the concluding part of
their work.

As a natural basis for the treatment of the ice pressure pro-
blems they have included information on the temperature varia-
tions in the Quebec area.
By computing the temperature distribution in an ice cover sub-
jected to a cyclic temperature variation at the surface D & M
find that because of attenuation an ice cover thicker than 40
cm can be looked upon as a semi infinite body when ice pres-
sure caused by usual temperature variations are considered.
This fact leads to a great simplification in temperature com-
putation.

D & M have made several laboratory tests with uniaxial as well as biaxial stress to find the connection between time, temperature, stress and the structure of ice.

In <u>uniaxial tests</u> cylindrical samples (length 7.62 cm and diameter 2.54 cm) were deformed along the axis at a constant strain rate and a constant temperature. The results of such a test is a graph showing the applied load versus time.

A number of such tests were made with artificial <u>snow ice</u>. The density of this ice was about 0.89 g/cm^3, the diameter of the grains was about 1 mm and the direction of the crystallographic orientations was random.

Apparently tests were run with a range of strain rates

$$\dot{\varepsilon} = 1.8 \cdot 10^{-8} \text{ sec}^{-1} \text{ to } 1.8 \cdot 10^{-7} \text{ sec}^{-1}$$

and a temperature range of

$$T = -3.2^{\circ}C \text{ to } -28.3^{\circ}C$$

(Some of the tests are not shown on certain graphs and tables.)

The second sort of ice examined was <u>columnar ice of the type S1</u> i.e. where the c-axes of the crystals are vertical or nearly vertical. The stress was perpendicular to the c-axes. Test conditions were

$$\dot{\varepsilon} = 3.7 \cdot 10^{-8} \text{ sec}^{-1} \text{ to } 1.8 \cdot 10^{-7} \text{ sec}^{-1}$$

$$T = -4.1^{\circ}C \text{ to } -26.8^{\circ}C$$

(The number of test results shown vary somewhat from table to table.)

The third type of ice tested was <u>columnar ice with horizontal c-axis (S2)</u>. The direction of stress was in the plane of the optical axes.

After some tests had been made D & M concluded that the samples
of the S2 ice were too small compared to the grain size. Only
two tests with bigger samples are reported (dimensions: height
10.16 cm, diameter 5.08 cm).

The general form of the resulting stress versus time curves
shows a nearly constant increase of stress during the first
period of time. Then the increase becomes less and a maximum
is reached.
In the case of snow ice the stress decreases only little after
the maximum has been reached.
For the S1 ice a marked decrease of stress is found after the
maximum is reached. (The very sudden decrease in the load recor-
ded in some of the tests just after the maximum is attributed to
some sudden lateral deformation of these ice samples.)
The deformation curves for the S2 ice resemble the curves for
snow ice.

D & M use the following formula to give their experimental results
a general form:

$$\frac{d\sigma}{dt} = \dot{\varepsilon}E_a - 2b\beta E_a ((\frac{n_o}{\beta} + \dot{\varepsilon}t) - \frac{\sigma(t)}{E_a})(\frac{\sigma(t)}{2p})^m \qquad (11)$$

where

σ : stress

$\dot{\varepsilon}$: strain rate

t : time

E_a: apparent elastic modulus

n_o: initial number of dislocations

β : rate of multiplication of dislocations

b : the Burger vector

p : a constant

m : a constant

As said by D & M this rheological model is somewhere in between
the conventional models consisting of Maxwell and Voigt elements
on one hand and models making use entirely of theories of mole-
cular mechanisms on the other.

When the constants E_a, n_o, β, p, b, and m have been found for a
certain type of ice the uniaxial pressure from an ice cover made
of this type of ice can be computed if the temperature variations
in the ice are known.

Biaxial stress was also investigated. The ice samples used were
formed as cylinders (height~ 5 cm, diameter ~ 15 or 30 cm). The
cylinders were placed in an invar ring with the same height as
the cylinders and a diameter a couple of millimeters larger than
the diameters of the samples. The space between ring and sample
was filled with water.

During the tests the temperature of the ice was raised from a cer-
tain initial value to $0^{\circ}C$. The thermal pressure was measured by
strain gauges attached to the ring.

Using such a procedure five tests were made with snow ice For
each of the tests the formula (11) was used to find the stresses
that would develop in the uniaxial case under the same tempera-
ture conditions. In this way the maximum measured stress in the
biaxial case could be compared to the maximum computed stress in
the uniaxial case.

The value of the ratio:

$$\sigma(max,biax,snow\ ice) \ / \ \sigma(max,uniax,snow\ ice)$$

were 1.81, 1.51, 1.83, 1.72, 1.56 leading to the following
values of the apparent Poisson modulus: 0.45, 0.34, 0.45, 0.42
0.36.

Some considerations on the validity of the different tests make
D & M exclude the two smallest values from the series of five.
After that they conclude that the snow ice will deform in the
same way as a nearly perfectly plastic material when the state

of maximum stress has been reached.

The arguments made for the exclusion of the two small Poisson
values seem difficult to follow. If all five values are re-
tained the mean value is ~ 0.40. The same value for perfectly
plastic material is 0.50 whereas for isotropic elastic materials
it is in the order of 0.3.

With the <u>ice of the type S1</u> eight biaxial tests were made.
The values for the ratio

$$\sigma(max,biax, S1) / \sigma(max,uniax, S1)$$

were found in the range 1.97 to 1.0. The variation in this
value is attributed by D & M to a variation in the direction of
the optical axis in the biaxial case. For the tests with a high
value of the ratio the directions of the c-axis were found to be
scattered very little about the vertical, whereas a much larger
scatter was found for the samples giving low values of the ratio.
It is confirmed by Lindgren [13] that

$$\sigma(max,biax,S1,c\text{-axis scattered})/\sigma(max,uniax,S1,c\text{-axis vertical}) \approx 1$$

This leads D & M to a convenient conclusion (translated freely
from French): In nature it is impossible that all of the optical
axes of an ice cover consisting of columnar ice are directed
vertically. For this reason the determination of the thermal ice
pressure of columnar ice (not nucleated) that is restricted
biaxially can be based upon the results of maximum stress ob-
tained from samples uniaxially restricted and deformed perpendi-
cular to the optical axis.

With <u>ice of type S2</u> eight biaxial tests are reported. In the
same way as before a comparison of maximum stresses is given.
Due to lack of results for uniaxial tests of S2 ice the
following ratio has been used

$$\sigma(max, biax, S2) / \sigma(max, uniax, S1)$$

The values of this ratio vary between 0.83 and 1.16 with a mean
value of 1.02.

D & M conclude: On the basis of this mean value the magnitude of the thermal ice pressure exerted by an ice cover consisting of nucleated columnar ice is considered, in the scope of this work, as not being able to attain a higher value than the thermal stresses exerted by columnar ice with the optical axes preferentially in the vertical direction.

From the conclusions by D & M cited in the preceding sections it is seen that the results of the uniaxial tests with ice of the type S1 attains a very central and important position in their work. On the basis of these tests they have computed graphs showing the maximum total thermal ice pressure (t/m) that is exerted by an ice cover (composed of S1 ice and uniaxially restrained) as a function of cover thickness and with the initial surface temperature of the ice and the time for increasing this temperature to $0^{\circ}C$ as parameters. Similar curves are shown for a uniaxially restrained cover of snow ice.

1.110 Metge (1976)

Based on observations of cracks in the ice on Lake Ontario near
Kingston, Canada, Metge [22] in an unpublished Ph D thesis to
Queen's University presented some new thoughts on pressure due
to temperature variations. Metge focused not on the continuous
ice sheet, but on the cracks which have so far been almost to-
tally neglected, although they occur in every ice cover. He
suggests two crack mechanisms influencing ice pressure in oppo-
site ways:

Wet cracks, when refreezing, develop thin ice bridges that are
subjected to crushing forces when the ice moves due to thermal
expansion or otherwise. Their sudden failure releases elastic
energy stored in the ice sheet and may cause high impact forces
when the edges of the two ice sheets meet.

Dry cracks, developed during cooling, act as bellows during
warming of the ice, delaying the build-up of thermal pressures.
Formation of dry cracks is often associated with compression in
the lower part of the ice cover as evidenced by flaking.

1.111 Bergdahl (1978)

In 1978 yet another Swedish contribution to the literature on
thermal ice pressure appeared. Bergdahl [23,24] submitted a
doctoral dissertation to Chalmers Institute of Technology and
later summarized his work at the Luleå Ice Symposium.

Bergdahl suggested a rheological equation

$$\dot{\varepsilon} = \frac{\dot{\sigma}}{E} + K D \sigma^n \qquad\qquad (12)$$

where K and n are functions of strain rate and temperature, while
E and D are functions of temperature only. Physically D is the

coefficient of self-diffusion for the ice molecules, and K and n are parameters discribing the viscous deformation (dashpot characteristics in the Maxwell unit).

The model (12) is nonlinear, but lends itself fairly well to numerical computations. If one describes the time history of deformation due to loading and unloading by three terms as in Fig. 1, equation (12) accounts for elastic and viscous deformation, but neglects elastic lag. When considering rare events such as extreme rates of change of temperature, this does not seem a serious deficiency.
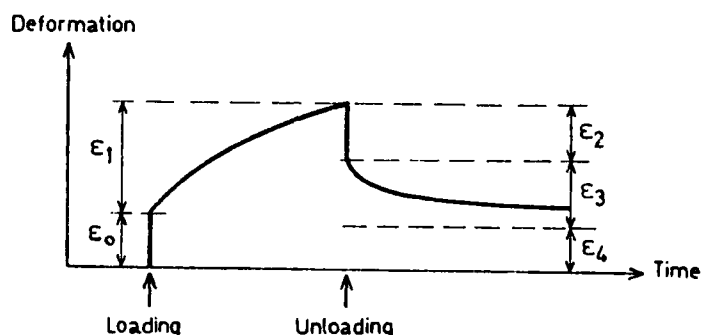
Fig. 1. Time history of ice deformation.

The calculation of ice temperature is thorougly discussed. The resulting ice temperatures for a clear night and an overcast night, assuming constant heat and flux v, are given in Fig. 2 for three ice thicknesses.
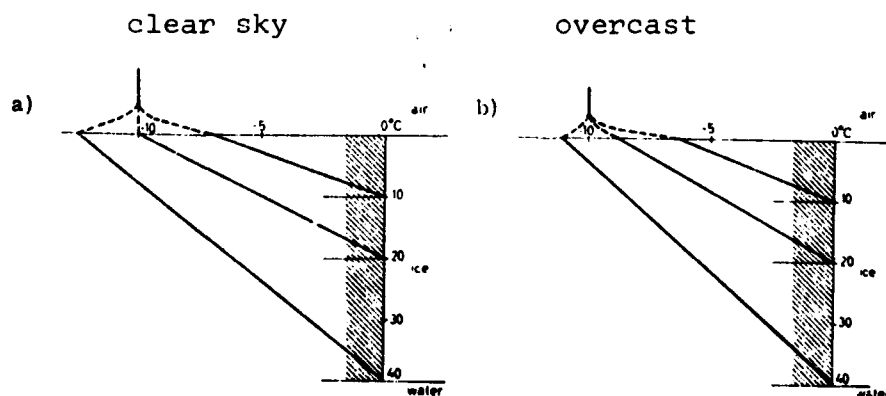
Fig. 2. Temperatures in snow-free ice covers.

The weather conditions for Fig. 2 were: air temperature -10°C, wind speed 2 m/s, and vapour pressure 300 Pa.

It is clear that noen of the simpler assumptions, such as T_{o} = T_{air} (Drouin & Michel) or T_{o} =0,35 T_{air} (USSR, Sn 76-66), can account for more than a few of the examples shown in Fig. 2.

The cases of interest have rising ice temperature, however, and Bergdahl made parametric studies with various numerical schemes. He claims that the method used by Drouin & Michel gives incorrect results, and warns that the choice of boundary conditions is more important than the choice of ice parameters.

1.2. MEASUREMENTS OF THERMAL ICE PRESSURE

Many of the authors mentioned above conclude the description
of their theories by the remark that the theoretical formulas
should be tested against appropriate field measurements.

We have found only a few descriptions of in situ measurements
of thermal ice pressure made recently and in fact none of these
measurements considered the case of thermal ice pressure against
a nearly vertical, flat wall and at the same time reported suf-
ficient data to make possible a comparison between theory and
nature.

The measurements often referred to by investigators are the ones
reported by Monfore about 1950 [11]. Measurements were made at
several reservoirs in the mountains of Colorado. Indenter and
strain gauges were set in thin mortar panels that could be in-
stalled on the face of the walls. Unfortunately these measure-
ments can not be analysed as a function of the temperature condi-
tions because the method used only records the maximum stress
developed during a winter at different levels in the ice. A
mean value of the stresses measured at different levels in the
ice cover is interpreted as the maximum load.
In this way it was found that the maximum load varied between
22.4 and 35.8 t/m in reservoirs with steep and rocky shores
(Eleven Mile Canyon). A maximum load of 14 t/m was found in
the Evergreen reservoir where the shores are moderately steep.
In reservoirs with flat and sandy shores (Antero and Shadow
Mountain) values of 5.4 and 8.6 t/m were measured.

In connection with an application of the linear viscoelastic
theory in a simplified form to the problem of thermal ice pres-
sure on the Saima Channel, Jumppanen [21] reports the result of
a single measurement of ice pressure (1972-73).
Only the pressure measured at a single level in the ice cover
(8 cm below the surface) during 28 hours is reported. It shows
a rather good agreement with the pressure calculated by means
of the theory on the basis of the measured temperature varia-
tions at the same level on the ice cover.

It seems hard to believe that no one has tried to make more extensive measurements of thermal ice pressure recently. According to Drouin & Michel [4] such a measurement should contain the following parameters:

a)   measurement of the stress as a function of time at
      several levels in the ice cover,
b)   measurement of the ice thickness,
c)   measurement of the air temperature,
d)   measurement of temperatures in the ice,
e)   measurement of thickness of snow cover,
f)   measurement of solar radiation,
g)   measurement of direction and speed of wind,
h)   analyses of the structure and the texture of the ice,
i)   measurement of the water level,
j)   a complete and global description of cracks in the ice cover,
k)   measurements of displacements of the ice cover.

1.3. EMPIRICAL VALUES

For different locations and climates one finds empirical
values for the maximum thermal ice pressure used by designing
engineers.

According to Michel [3] empirical values used in Canada at pre-
sent vary form 15 t/m to 22 t/m for rigid structures. For more
flexible structures such as sluice gates values in the vicinity
of 7 t/m are more commonly used.

Drouin [18] gives a somewhat higher value of 15 - 30 t/m for
Canada and suggests himself that when account is taken of cracks
and snow an appropriate value for a thick ice cover moderately
restrained would be 22 t/m.

In [19] the usual practice in North America used to estimate the
total pressure is given as a thrust varying linearly with the
ice thickness. For zero thickness the ice thrust is zero and
for a thickness of 4 feet the thrust is 20 kips per linear foot.
This corresponds to the commonly used design loads of 15 t/m
and 22 t/m when the ice thickness is 2 and 3 feet.

According to Starosolszky [20] in the Soviet Union for the
regions Siberia, Leningrad and Caucasus 30, 20 and 15 tons
per sq. m are recommended as a first approximation for design
purpose.

For the somewhat less severe conditions in Norway 10 t/m is
estimated under usual conditions. Under especially unfavour-
able conditions the value will be as high as 15 - 20 t/m.

1.4. A COMPARISON OF ICE PRESSURE VALUES

In his paper "State of research on ice thermal thrust" [18]
Drouin makes a comparison between the result of some of the
thermal ice pressure theories using a specific example:
- The temperature of the ice surface initially at -40°C
is made to rise at a rate of 2.8°C/h. The ice cover
is uniaxially restricted and without a snow cover.
No solar energy is absorbed. Pressure values are
computed for two thicknesses of the ice cover 0.45 m
and 0.90 m. -

Under these conditions Drouin computes the pressure values by
means of Rose's theory, by means of Monfore's experimental
results combined with an appropriate theory of the temperature
destribution and finally by means of the USSR norm SN 76-59.
(As far as the norm SN 76-59 is concerned it is assumed that
the initial air temperature is -40°C and the rate of change
in air temperature is 2.8°C/h). The results are shown in the
table below.

The table has been extended, first by Kjeldgaard [24]
and later by Bergdahl [23]. Kjeldgaard found the
pressure values based on Drouin and Michel's work [4] for ice
of the type S1 and for snow ice. (It should be noticed that
the pressures given on the graph of [4] for a certain tempera-
ture increase are computed for a sinusoidal variation of the
temperature with time. The values given below have been cal-
culated for a linear temperature increase taking into account
the correction factors given in [4]. For a sinusoidal varia-
tion within the same temperature limits the values would be
approximately 40% larger.)

Also results obtained from the USSR norm SN 76-66 are shown.
In this norm no distinction is made between different types
of ice but the pressure values are very dependent on the velo-
city of wind i.e. the thermal boundary layer. The temperature
data that is to be used in SN 76-66 is air temperature data.
So it is assumed that the initial air temperature is -40°C and
that the increase rate of the air temperature is 2.8°C/h.

Values of the thermal ice pressure have been computed for a
wind velocity of 0, 5 and 20 m/sec.

(It is assumed that the extent of the ice cover is less than
50 m, otherwise the values should be multiplied by a reduction
factor according to SN 76-66.)

TABLE 1.

$T_o = -40^{\circ}C$, $T_1 = 0^{\circ}C$	KN/m^2	
	Ice thickness	
$\frac{\Delta T}{\Delta t} = 2,8^{\circ}C/h$	0.45 m	0,90 m
Rose 1947 (Drouin 70)	47	86
Monfore 54 "	222	232
SN 76-59 59 "	128	255
Drouin & Michel (Kjeldgaard)		
S1 ice "	330	390
Snow ice "	220	270
SN 76-66 0 m/s "	30	60
" 5 " "	310	440
" 20 " "	410	580
Bergdahl 78		
" 0 m/s	459	752
" 5 "	502	830
" 20 "	531	829

The question of the type of restraints relevant to the examples
given in the table will be considered in more detail:

- Drouin has computed the forces exerted by Monfore ice in the
  uniaxial case. In connection with a similar calculation
  Michel [3] mentions that for the biaxial case the results
  for Monfore ice would be about 60% larger using elastic
  theory as the first approximation in extending the results
  from the uniaxial to the biaxial case.
- As far as we know [1] the SN 76-59 does not distinguish be-
  tween the uniaxial and the biaxial case of restriction.

- Referring to the conclusions made by Drouin & Michel in [4] and cited in section 1.9 above, it seems to be in agreement with their train of thoughts to look upon the results of the uniaxial tests with S1 ice as a reasonable estimate of the pressure exerted by biaxially restricted S1 ice as it occurs in nature with some scatter in the directions of the c-axes. Further these results can be taken as a reasonable upper limit of the forces exerted by biaxially restrained S2 ice according to [4].

- In the Russian norm SN 76-66 no distinction is made between uniaxial and biaxial restraints, i.e. the users of the norm do not have to decide which sort of restraints exist in the actual case.

It is seen from the table that the values computed by means of the SN 76-66 are very dependent on the speed of wind w i.e. on the thermal boundary layer in air above the ice/snow surface. The later Canadian investigators Drouin and Michel do not attach the same importance to the boundary layer. In fact Michel in [3] says that the difference between the temperature of the ice surface and the temperature of the air "is small and measurements made for a whole winter on clear ice have shown that it rarely exeeds 3°F (1.7°C). It is thus safe and acceptable to neglect this effect".

Further in [4] Drouin & Michel gives an example of application of their test results for S1 ice. The example is for an air temperature originally at -36°C. To take account of both the effect of the boundary layer and the weak possibility of the initial temperature gradient in the ice being a straight line they assume an initial ice surface temperature of -30°C. No further account is taken of the boundary layer in their example. Thus it seems that the question of temperature distribution above the ice/snow surface is one of the main divergencies between the later methods for computing the ice pressure.

When comparing the theories and methods of computation with each other it should be remembered that they may have developed along

different lines.

For instance Monfore's, Lindgren's and Drouin & Michel's con-
tributions are almost entirely based upon laboratory tests and
theoretical considerations. In this way it has been possible
to study in detail different effects taking part in the problem
and to establish a reliable basis for further research. However,
the next step, to translate these observations into a usable and
safe set of rules for the designing engineer, has not yet been
taken.

The Russian norm SN 76-66 may have gone much further in this
direction. Possibly the Russian theories, whatever their
origin, have been tested against field measurements and adjusted
to the conditions occurring in nature.

1.5. CONCLUDING REMARKS

From the short review of the methods suggested for the computation of thermal ice pressure it appears that the knowledge of the phenomenon has become more detailed during the previous decades.

However, in spite of a considerable amount of experimental work conducted in laboratories, there still exists some divergencies concerning the difficult question of which stress-strain relationships or constitutive laws should be considered appropriate as the basis for the methods of computation.

The somewhat simpler problem of calculating the temperature variation in an ice cover seems to be solved, except for some divergencies concerning the importance of the thermal boundary layer in the air above the ice/snow surface.

In laboratory tests and by theoretical considerations single physical effects have been studied with great care without disturbance from variations in non-relevant associated parameters and a detailed knowledge of effects important to the ice pressure problem has been reached in that way. However, there seems to be a lack of accessible field experiments that show to what extent the theories and methods can give the magnitude of ice pressure occurring in nature where conditions are more mixed.

Such field measurements should take into account all the parameters that at present are thought to play a role in the entire problem of thermal ice pressure or at least a set of parameters that constitutes an independent part of the problem e.g. the temperature distribution including the thermal boundary layer in the air.

Table 1   illustrates a rather striking development which has led to an order of magnitude higher estimates in 1978 than in 1947. It is interesting to note that our increased understanding

and perception has uniformly gone in the direction of increasing
thermal pressures. Perhaps this reflects the prudence of a worst
case design philosophy more than the actual but largely unknown
reality. We are now in the most active period ever of ice re-
search. There will be new information available, and one may
wonder where the upper bond lies. Physically still higher press-
ures than those of Table 1 are conceivable. Bergdahl has pointed
out that an untested combination of simultaneously increasing
air temperature, wind speed and cloud cover will boost thermal
ice pressure beyond the present estimates.

On the other hand the response to this kind of extreme atmos-
pheric forcing depends on the previous history of the ice. If
the ice is too thin, or too thick, or too warm, or has a snow
cover, or is cracked up, the resulting pressures will not be
extreme.

In view of all the parameters influencing the phenomenon, a sta-
tistical approach seems to make sense. One could then either ob-
serve ice pressure directly, or observe inputs in a model and
compute the ice pressure.

The former approach has been advocated by all researchers, but
it is only recently that the necessary instrumentation has been
developed in connection with offshore structures.

The latter approach has been followed by Bergdahl [23]. Based on
12-16 years records of weather and ice conditions he estimated
ice pressures and extrapolated the observed series of annual
maxima to recurrence periods of 100, 500 and 1000 years.

The advantage of using a model is primarily that one can then
generate time series of ice pressures by hindcasting where the
input variables are available. However, even for this case it
is imperative with direct measurements of thermal ice pressure
to verify the proposed model.

REFERENCES

[1]   Korzhavin, K.N. : " Action of ice on engineering structures"
        Novosibirsk, Akad. Nauk. USSR 1962. Also as translation
        TL 260 from CRREL Hanover, New Hampshire, 1971.

[2]   Drouin, M. : "Static ice forces on extended structures"
        (published in proceedings of a conference on "Ice pressure
        against structures" held at Laval University, Quebec, 1966).
        Technical Memorandum No 92.
        National Research Council, Ottawa 1968.

[3]   Michel, B. : "Ice pressure on engineering structures."
        Monograph III-B1b, CRREL, Hanover, New Hampshire 1970.

[4]   Drouin, M. and Michel, B.: "Les poussées d'origine thermique
        exercées par les couverts de glace sur les structures
        hydrauliques". Rapport S-23, Laval University 1971.

[5]   Royen, N. : "Istryck vid temperaturhöjning", Hansenboken,
        Stockholm 1922. Translated as "Ice pressure with increasing
        temperatures." SIPRE bibliography project, Translation 45,
        1955.

[6]   Brown, E. and Clarke, G.: "Ice thrust in connection with
        hydro-electric plant design." Engineering Journal p.19
        1932.

[7]   Rose, E.: "Thrust exerted by expanding ice sheet." A.S.C.E.
        Vol. 112, p 871, 1947.

[8]   Löfquist, B.: "Studies of the effects of temperature varia-
        tions". A.S.C.E. Paper No 2656. Ice pressure against dams
        a symposium, 1954.

[9]   Monfore, G.E. and Taylor, F.W.: "The problem of an expanding
        ice sheet." Proc. Western Snow Long., 16th meeting, 1948.

[10]   Monfore, G.E.: "Laboratory investigation of ice pressure."
       U.S.B.R. Structural Research Laboratory, Report SP-31, 1951.

[11]   Monfore, G.E.: "Ice pressure against dams. Experimental
       Investigation by the Bureau of Reclamation." Proc., A.S.C.E.
       Vol. 78, Technical separate No. 162, 1952.

[12]   Monfore, G.E.: "Ice pressure measurements." U.S.B.R.,
       Structural Research Laboratory, Report C-662. 117, 1953.

[13]   Lindgren, S.: "Effect of temperature increase on ice
       pressure." The Institute for Hydraulic Engineering,
       Royal Inst. of Technology, Stockholm, 1968. "Thermal ice
       pressure" IAHR, Symposium, Ice and its action on hydraulic
       structures, 1970.

[14]   Instructions for determining ice loads on river structures,
       (SN 76-66) Moscow 1967. Translated by N.R.C. as TT-1663
       Ottawa 1973.

[15]   Korzhavin, K.N.: "General research results obtained in the
       USSR on ice-thermal conditions in the vicinity of hydraulic
       structures." I.A.H.R.-symposium, Leningrad 1972.

[16]   Proskouriakov, B.V. and Petrounitchev, N.N.: "Pression
       statique de la glace sur les ouvrages hydrauliques lors de
       sa dilatation thermique." I.A.H.R.-conference, Colorado,
       USA, 1967.

[17]   Devik, O.: "Termische und dynamische Bedingungen der Eis-
       bildung in Wasserläufen, auf norwegische Verh-aåtnisse
       angewandt." Geofysiske Publikasjoner, vol IX, Oslo, 1932.

[18]   Drouin, M.: "State of research on ice thermal thrust."
       I.A.H.R.-symposium, Reykjavik, 1970.

[19]   "Review of Current Ice Technology and Evaluation of
       Research Priorities." Report series No 17, Inland Waters
       Branch, Department of the Environment, Ottawa, Canada 1971.

[20]   Starosolszky, Ö.: "Ice in hydraulic engineering." Division
       of Hydraulic Engineering. Norwegian Institute of Technology.
       Report No 70-1, Trondheim, 1970.

[21]   Jumppanen, P.: "Ice thermal loads against walls of water
       reservoirs." Second conference on "Port and ocean engi-
       neering under arctic conditions." University of Iceland
       1973.

[22]   Metge, M.: "Thermal cracks in lake ice ." Ph.D. thesis,
       Queen's University Kingston, Ontario, Canada, Dec 1976.

[23]   Bergdahl, L.:"Thermal Ice Pressure in Lake Ice Covers".
       Department of Hydraulics, Chalmers University of Techno-
       logy, Report Series A:2.

[24]   Bergdahl, L.:"Inysics of Ice and snow as Affects Thermal
       Pressure", Department of Hydraulics, Chalmers University
       of Technology, 1977 Report Series A:1.

[24]   Kjeldgaard, J.H.:"Thermal Ice Forces on Hydraulic Struc-
       tures. A short literature review." SINTEF-report No.
       STF60 A77043, 1977.

PART II

ICE FORCES ON FIXED, RIGID STRUCTURES

By K.R. Croasdale

Imperial Oil Ltd., Calgary, Alberta, Canada

ABSTRACT

Ice forces on structures are determined either by the environmental driving force or by the force to fail the ice sheet and move the ice around the structure; which ever is the least. State-of-the-art techniques for predicting these forces on fixed, rigid structures are presented. A rigid structure is defined as one where the ice interaction process is not influenced by the deformation of the structure itself. Structures are considered in three broad categories; structures with sloping sides, structures with vertical sides, and wide structures such as artificial islands. Both uniform and ridged ice is considered. The problem of ice ride-up on sloping beaches is also discussed.

2.1 DEFINITION OF FIXED, RIGID STRUCTURES

Fixed rigid structures can be defined as having negligible deformations under the action of ice forces. Any deformations that do occur are heavily damped so that the dynamic response of the structure is not siginficant. In this category, interaction between the ice failure process and the response of the structure does not have to be considered in design.

Examples of fixed rigid structures would be artificial islands (with frozen surfaces), massive concrete or steel docks and break-waters. Conical shaped piers and platforms will generally be rigid enough for their dynamic response to be ignored, and will also be considered in this category of structure. Docks, piers and platforms with cylindrical members might also fall into this category if the length of the cylindrical members is short and the structure is very stiff.

2.2 EXAMPLES OF FIXED, RIGID STRUCTURES

Examples of fixed, rigid structures are shown in the first series of Figures.

An artificial dredged island for petroleum exploration in the Beaufort Sea is shown in Figure 1. Such islands have been built out to 13 m of water and are subject to the forces generated by moving ice up to 2 m thick. They are typically about 120 m in diameter at the water line.

In deeper water an island might be retained by concrete caissons with sloping sides and ice deflectors as shown in Figure 2. This arrangement is being considered for water depths out to 20 m in the Beaufort Sea. At this depth ice features such as multi-year ridges have to be considered in design.

Another possible concept for deeper Arctic waters is the concrete or steel conical platform which might be held on location by friction between the large base and the sea floor (Figure 3). Designs for these structures exist but none have yet been built. One could envisage them being installed out to the 100 m water depth where they would be subject to ice forces generated by the movement of thick polar ice containing ridges up to 30 m thick.

In less severe climates, conical-shaped light piers have been installed in the St. Lawrence Seaway, Canada, Figure 4. These structures are subject to action by sheet ice up to about one metre thick.

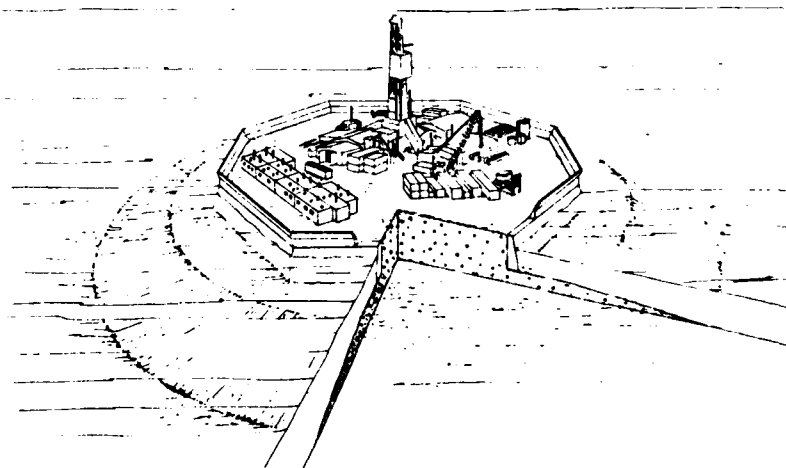Figure 1. Artificial drilling island.

Figure 2. Caisson Retained Island. Schematic showing cutaway through island.
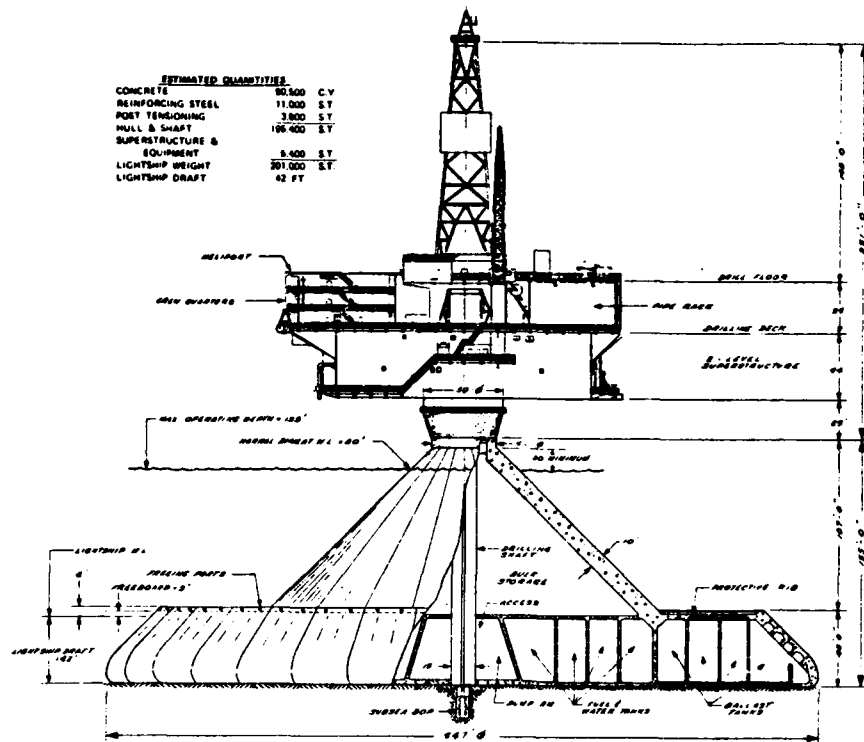
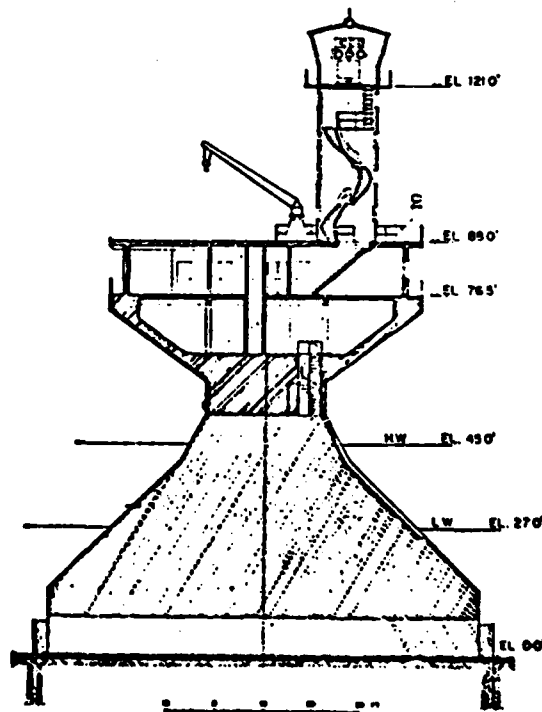Figure 3.   Cone 135, maximum design water depth
= 135'.

Figure 4.   Cross-section of Prince
Shoal Lighthouse.

2.3 LOGIC FOR CONSIDERING ICE FORCES

Before one can accurately predict ice forces on a structure (or even consider the right problem to solve) some preliminary considerations have to be made.

One should be aware for instance that the forces transmitted to a structure by the ice are generated by natural forces such as winds, currents or thermal strains. These natural forces can be concentrated on the structure by large ice sheets and represent an upper limit for the ice forces. The more usually addressed upper limit for the ice forces, is the force to fail the ice against the structure in the easiest mode of ice failure. Sometimes one can select the mode of failure which gives the lowest force but often one has to check several modes.

Another consideration relates to the clearance of ice around the structure; if ice rubble builds-up on the structure the mode of ice failure (and hence the force) can change.

A suggested logic for considering some of the above mentioned points is presented in Figure 5.

Environmental driving forces can be calculated separately and compared with ice interaction forces to indicate the design force. Environmental forces, as will be discussed later in this report are not easily estimated to any degree of accuracy. But usually they are much greater than the ice interaction force so that accuracy is not that important. Sometimes a short ⁺ to the environmental force can be made by using observed ice velociti and floe sizes to estimate kinetic energy prior to impact. If this energy is much greater than the work done in deforming the ice to reach the maximum interaction force then the latter force governs the design force.

Environmental factors such as rate and magnitude of ice movement also input to other parts of the logic diagram as shown.

For the ice interaction force, the mode of ice failure is the most important factor to consider. Intuitively one can expect ice crushing against vertical structures. However it is well known that thin ice can buckle at lower forces than crushing. Furthermore ice rubble in front of a vertical structure can lead to bending failure in a similar way to the formation of first-year ridges. Bending failure will occur against a sloping structure, but the presence of re-frozen rubble or high friction due to ice freezing to the structure can lead to ice crushing at higher loads. All these possibilities may have to be considered.

44

The ice-type governs both the failure mode and the actual interaction force. Such factors as thickness, ridge shapes and sizes, crystal structure, salinity, and temperature are known to be important and will need to be specified.

Structure shape has already been discussed in terms of side angle. For sloping structures, the friction between the ice and the sides is also important in determining the horizontal force. In addition, the width of the structure will influence two things; first the way ice rubble clears around the structure; and second whether ice failure is simultaneous across the full width of the structure.

For certain low-freeboard structures the problem of ice en-croaching onto the structure may have to be seriously considered. As shown in the logic diagram such factors as structure shape, extent of ice movement and characteristics such as strength or thickness will all have to be considered in determining the extent of ice ride-up or pile-up on the structure.

2.4 ICE TYPES

Under the topic of ice type we have to specify ice strength and geometry (e.g. thickness) in order that modes of ice failure and ice forces against any particular structure can be calculated.

In order to calculate interaction forces it is usually necessary to know the following strengths:

- compressive (uniaxial)
- shear
- bending or flexural

It is well known that the above strengths are functions of ice temperature, crystal structure, direction of loading, rate of loading or strain, confining force, sample size, presence of impurities such as salts and air.

It is beyond the scope of this report to discuss the above effects on ice strength but this topic has been addressed extensively in the literature.

Another aspect of ice strength which is important is the integrity of ice rubble piles and first-year pressure ridges. Can they be treated as a pile of granular material or do they also have cohesion due to refreezing of the water between the ice blocks. This problem has not yet been properly addressed.

For uniform sheets, ice thickness in any geographic area is generally known well enough. However, the thickness of ridges is often not known, and assumptions will have to be made.

2.5 ENVIRONMENTAL DRIVING FORCES

Ice motion in large bodies of water is caused mainly by wind stress.

A typical wind force on an ice surface can be calculated using the classical expression for drag (K).

$$K = C_{10} \, \rho_a \, V^2 A \tag{1}$$

where:

C_{10} is the drag coefficient at the 10-metre level

ρ_a is the air density

V is the air velocity at the 10-metre level

A is the "fetch area"

Danys (1977) has recently reviewed the topic of wind induced ice forces. In his paper he lists drag coefficients measured or calculated for a variety of ice surfaces. An average value for a rough ice cover is given as 0.0022.

Other investigators have suggested values for the drag coefficient of arctic sea ice. Karelin and Timoichov (1972) obtained values in the range $0.00335 < C_{10} < 0.0049$ by direct measurements on unridged ice. Banke and Smith (1973) recommend doubling the drag coefficient to allow for the form drag on ridges, whereas Arya (1973) suggests an increase by about 40%. For ridged arctic sea ice a value of $C_{10} = 0.005$ has been recommended (Metge, 1976).

Some typical sheet sizes needed to impose critical ice forces on various structures are given in Table 1. For ice sheet sizes greater than those shown the ice forces will be governed by the ice failure mechanism and not by wind stress. It can be seen that only on relatively small bodies of water will the wind induced ice force control the design load for the structure.

For floes of limited extent moving at a velocity determined by the current or wind, ice forces can be calculated using energy considerations. The initial kinetic energy of the floe is equated to the work done in failing the ice as the edge of the ice floe is penetrated by the structure. Floes below a certain size will be brought to rest before full penetration at lower-than-maximum ice force. However this condition is unlikely to govern ice design criteria.

TABLE 1   ICE SHEET SIZES TO GENERATE TYPICAL ICE FORCES

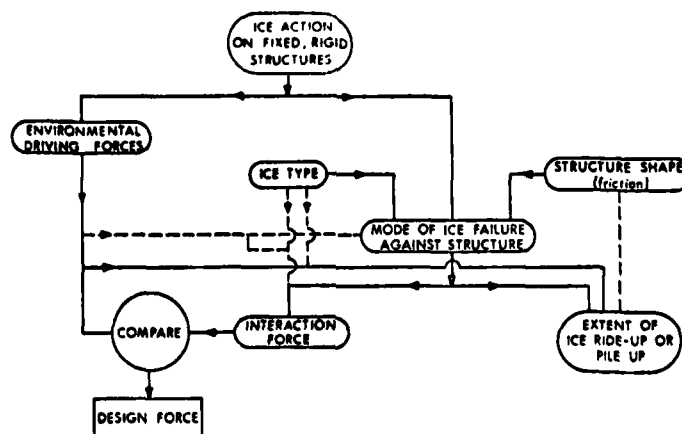| Structure	Typical Force for Ice Sheet Failure (KN)	Ice Sheet Size to Generate Ice Force (For $V = 15$ ms^{-1}) (m) x (m)
Conical Light Pier (3 m diameter)	1500	1600 x 1600
Conical Drilling Platform (60 m diameter)	30000	2630 x 2630
Cylindrical Pier (4 m diameter)	10000	4150 x 4150
Dredged Island (150 m diameter)	500000	18600 x 18600

Figure 5.   Logic for considering ice action on fixed, rigid structures.

2.6 UNIFORM ICE ACTING ON A SLOPING STRUCTURE

2.61 Interaction Mechanism

Consider the simplified two-dimensional system shown in Figure 6. As the advancing ice sheet first encounters the sloping structure, local crushing occurs on the underside of the ice sheet. The local crushing causes an interaction force normal to the structure surface. In addition, because the ice is moving relative to the surface, a frictional force is also generated.

The normal and tangential forces can be resolved into vertical and horizontal components V and H acting at the centre of the crushed area. In the simple two-dimensional model shown in Figure 6, the forces acting on the ice will be V, H, gravity and buoyancy forces; the latter can be considered as an elastic foundation.

As the ice sheet continues to advance the crushed area will increase causing V and H to increase. Assuming an unlimited driving force, V and H will continue to increase until the ice fails. For a properly designed sloping structure the ice should fail in bending.

Except for very steep structures the effect of H on the bending failure of the ice can be ignored. The ice sheet then behaves like a beam or plate on an elastic foundation. The load V to fail the ice sheet governs the initial lateral load on the structure. Subsequent loads are generally higher because of the additional load required to push the ice pieces up the slope.

2.62 Simple Theory - Two-Dimensions

To gain an appreciation of the influence of various parameters it will be useful to consider a two-dimensional system and derive some simple equations.

Consider the initial interaction between ice and the sloping face. The relationships between V, H, N and μ can be derived by resolving forces, that is;

$$H = N\sin\alpha + \mu N\cos\alpha \tag{2}$$

$$V = N\cos\alpha - \mu N\sin\alpha \tag{3}$$

therefore,
$$H = V\left(\frac{\sin\alpha + \mu\cos\alpha}{\cos\alpha - \mu\sin\alpha}\right) \tag{4}$$

In the limit, the maximum value of V will be limited by the strength of the ice sheet with an edge loading. In this simple analysis, assume the ice sheet can be represented by a beam or an elastic foundation. Assume its strength is limited by its bending moment capacity Mo. Most beam strength tests on ice measure bending moment capacity but with the results converted to a flexural strength$\left(\sigma_f\right)$ using simple bending theory, that is;

$$\sigma_f = \frac{6Mo}{bt^2} \tag{5}$$

Where b is the width of the beam and t is the ice thickness.

For a semi-infinite beam on an elastic foundation it can be shown (Hetenyi, 1946) that the maximum bending moment (Mo) due to an edge load(V)is given by

$$Mo = \frac{V}{\beta \, e^{\pi/4}} \sin(\pi/4) \tag{6}$$

Where $\frac{1}{\beta}$ is a characteristic length, defined by,

$$\beta = \left(\frac{K}{4EI}\right)^{\frac{1}{4}} \tag{7}$$

Where K is the foundation constant equal to ρwgb for a floating beam, ρw is the density of water, g is the gravitational constant, E is the elastic modulus, and I is the second moment of area of the cross section ($bt^3/12$).

Combining equations (5), (6) and (7) we get

$$V = 0.68 \, \sigma_f b \left(\frac{\rho wgt^5}{E}\right)^{\frac{1}{4}} \tag{8}$$

and therefore, the initial horizontal force on the structure per unit width is given by

$$H/b = 0.68 \, \sigma_f\left(\frac{\rho wgt^5}{E}\right)^{\frac{1}{4}} \frac{\sin\alpha + \mu\cos\alpha}{\cos\alpha - \mu\sin\alpha} \tag{9}$$

The above can be thoughtof as the component required to break the advancing ice. For subsequent interactions a component is also required to push the ice up the slope. The force system in this latter case is shown in Figure 7. P is the force required to push the ice up the slope, then

$$P = \frac{z}{\sin\alpha} \, t \, b \, \rho ig \, (\sin\alpha + \mu\cos\alpha) \tag{10}$$

Where Z is the height reached by the ice on the slope, and ρi is the density of the ice, then,

$$H = (V + P\sin\alpha)\left(\frac{\sin\alpha + \mu\cos\alpha}{\cos\alpha - \mu\sin\alpha}\right) + P\cos\alpha \qquad (11)$$

substituting for V and P gives

$$\frac{H}{b} = 0.68 \; \sigma_f \left(\frac{\rho w g t^5}{E}\right)^{\frac{1}{4}}\left(\frac{\sin\alpha + \mu\cos\alpha}{\cos\alpha - \mu\sin\alpha}\right) + Zt\rho ig\left(\left(\frac{\sin\alpha + \mu\cos\alpha}{\cos\alpha - \mu\sin\alpha}\right)^2 + \frac{\sin\alpha + \mu\cos\alpha}{\tan\alpha}\right) \qquad (12)$$

Equation (12) above is similar to equation (9) except for the additional term. The equation can be simplified to

$$\frac{H}{b} = \sigma_f\left(\frac{\rho w g t^5}{E}\right)^{\frac{1}{4}} C_1 + Zt\rho ig \; C_2 \qquad (13)$$

where C_1 and C_2 are functions only of α and μ. Values for the coefficients C_1 and C_2 are plotted in Figures (8) and (9) for typical values of α and μ.

In the simple two-dimensional theory given above, the first term can be considered to be the force necessary to break the ice, and the second term can be considered to be the force necessary to push the ice pieces up the sloping structure. As a 2-D theory it might be considered accurate for a very wide structure, but as will be discussed later it is probably inaccurate for narrow structures. For structures which are narrow relative to the characteristic length the zone of ice failure will be wider than the structure itself, also most of the ice pieces will not necessarily ride-up the structure but more around it. Nevertheless it will be useful to discuss the importance of some of the key parameters in the context of the simple 2-D theory.

2.63 Effect of Friction and Slope Angle

For a typical example of a structure with a freeboard of 5 m subject to forces imposed by ice 1 m thick with a flexural strength of 700 kPa, the effect of friction and slope angle is shown in Figure 10. It can be seen that the effect of friction and slope angle becomes significant above an angle of 45°. For a structure with an angle of 55° the horizontal ice force increases from 125 KNm^{-1} for $\mu = 0.1$, to 450 KNm^{-1} for $\mu = 0.5$. For steep angles and high friction the ice may fail in crushing rather than bending. Figure 10 emphasizes the need to maintain smooth surfaces on sloping structures so that ice forces are minimized. Even for very shallow angled structures high friction can increase loads significantly. Other investigators (Bercha and Danys, 1977 and Ralston, 1977) have also shown the importance of friction.
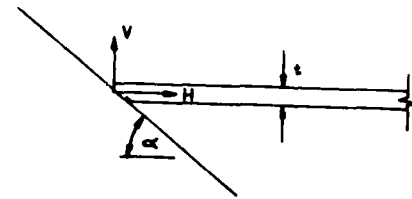
FORCES ACTING ON ICE
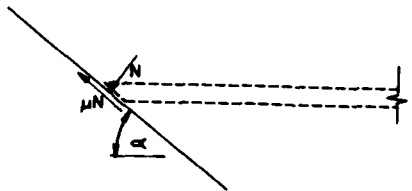
FORCES ON STRUCTURE

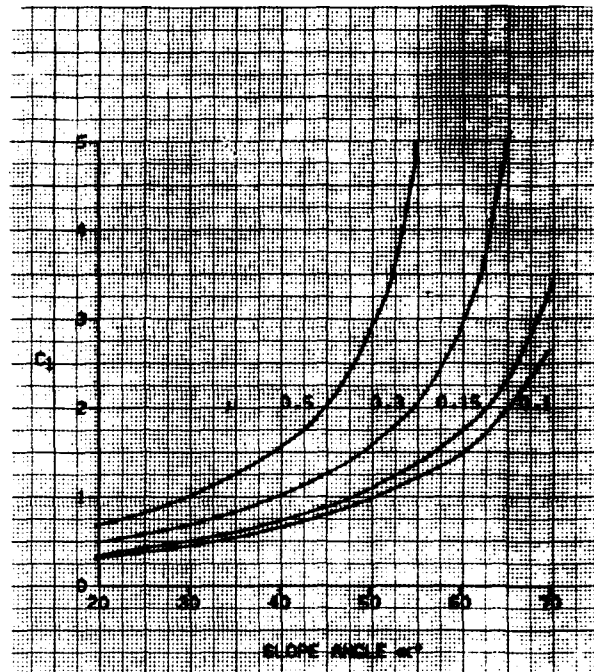Figure 6. Initial inter-
action between ice and
sloping structure.

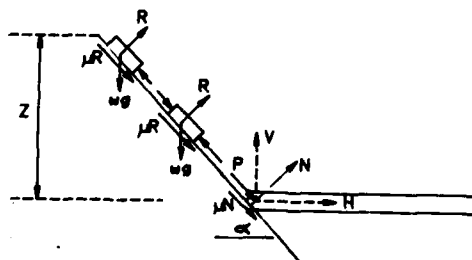

Figure 8. C_1 vs slope angle and friction.

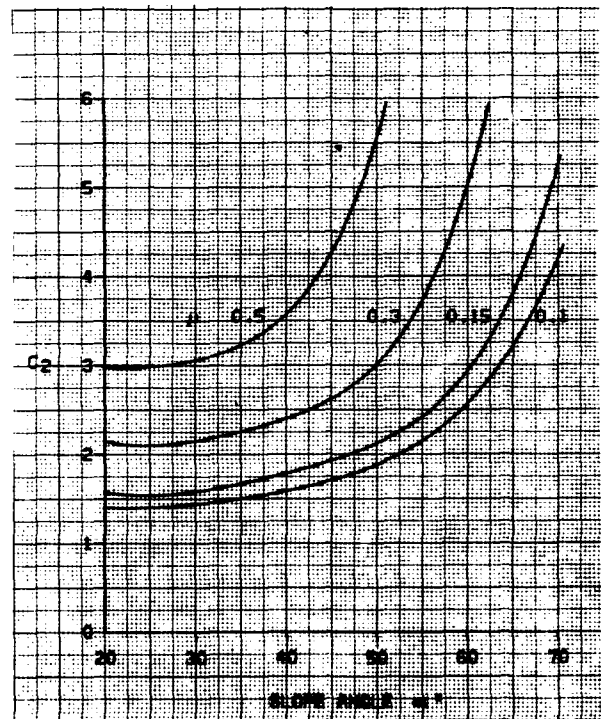Figure 7. General interaction between
ice and sloping structure.

Figure 9. C_2 vs slope angle and friction.

2.64 Effect of Ice Strength

The ice strength affects the ice breaking component but not the ride-up component. As shown in Figure 11, in this simple 2-D elastic analysis, the ride-up force in a typical example is larger than the breaking force, so the effect of ice strength on total force is not as significant as one might suppose. This observation however is not true for narrow structures - as will be discussed later.

2.65 Effect of Ice Thickness

Ice thickness is probably the most significant parameter affecting ice forces on sloping structures. In the simple 2-D analysis, the ice breaking component is proportional to $(t)^{1.25}$ and the ride-up force is directly proportional to t. The effect of thickness for a typical example is shown in Figure 12.

Again, it is interesting to note from Figure 12 that the ice ride-up force is larger than the ice breaking force. However as already discussed, this observation can only be considered relevant to 2-D theory as might be applicable to a very wide structure. For a narrow structure, the ice breaking component will be larger and the ice ride-up component smaller (see the next section).

2.66 Three Dimensional Theory

In the three dimensional case the same mechanisms apply but the zone of ice failure extends wider than the structure. Also for structures of circular section the effective angle for ice ride-up is reduced and ice pieces can slide around the structure without fully riding-up. These effects are illustrated conceptually in Figure 13. Intuitively it will be appreciated that 3-D effects cause divergence from the simple theory more for narrow structures than for wide structures.

For the ice breaking component, the simple beam theory is replaced by a more complex plate theory for which elastic analyses have been made using theories developed for plates on elastic supprts. Nevel (1972) has proposed equations for the ultimate failure of ice plates which can be applied to this problem.

It is generally assumed that the essence of the ice force problem on a conical structure reduces to the predic tion of the forces necessary to fail a series of ice wedges formed by radial cracking of the ice as it advances against the cone, see Figure 13.
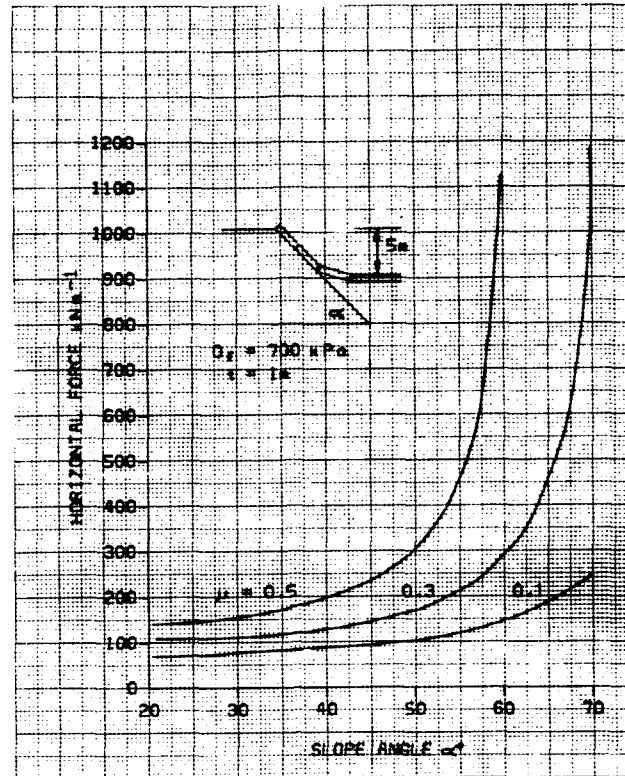
Figure 10. Horizontal force vs slope angle
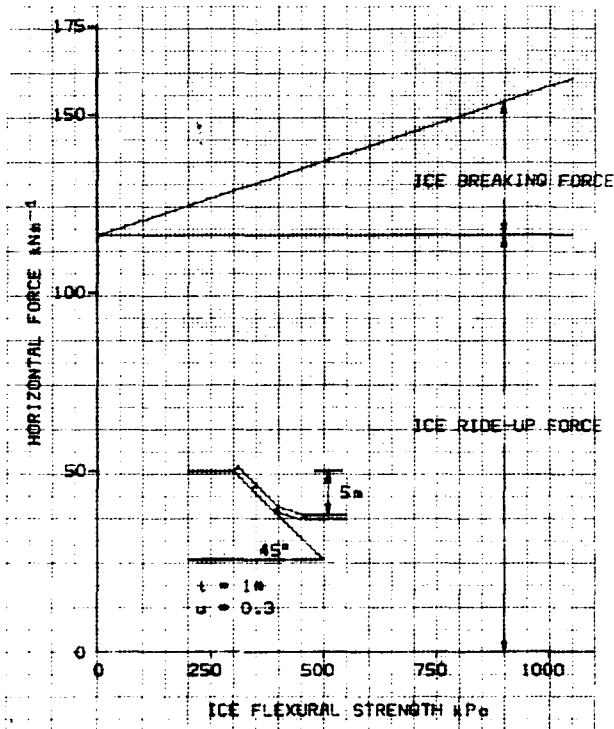and friction (simple 2-D theory).

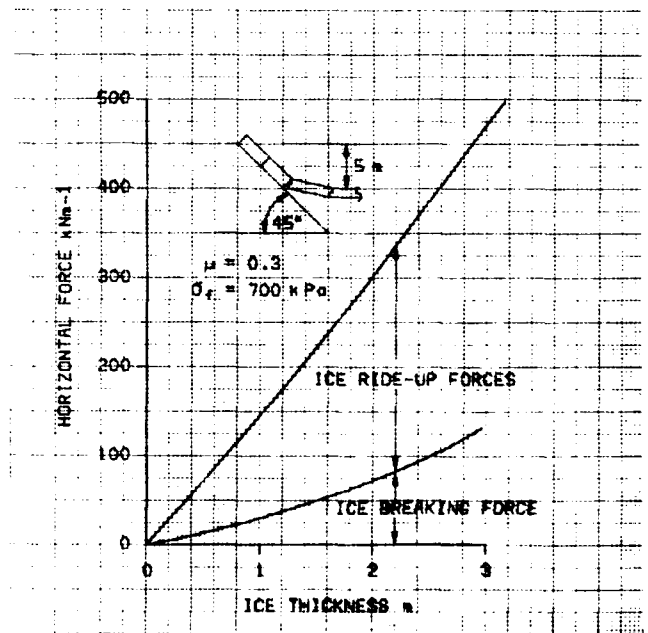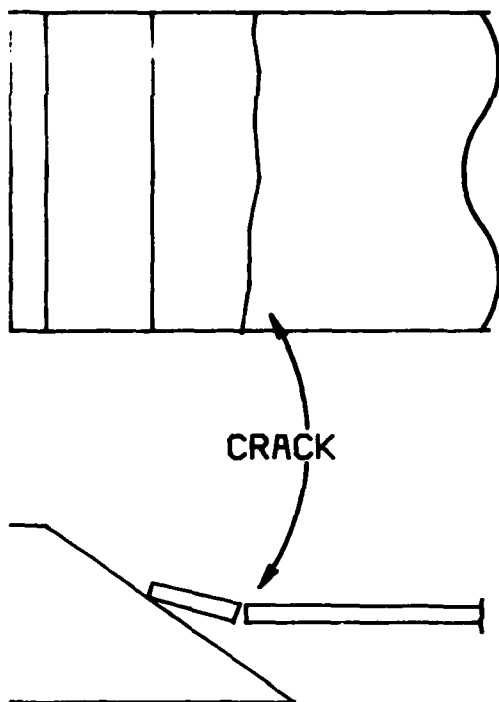Figure 11. Effect of ice strength on
horizontal force (simple 2-D theory).
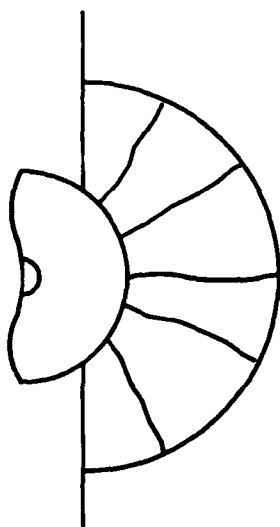

Figure 12. Horizontal force vs ice
thickness (simple 2-D theory).

SIMPLE 2-D THEORY

LENGTH OF TRANSVERSE CRACK
EQUAL TO WIDTH OF STRUCTURE

CRACK

3-D THEORY

LENGTH OF CIRCUMFERENTIAL
CRACK GREATER THAN
WIDTH OF STRUCTURE

Figure 13.   Ice action on sloping structures (3-D effects).

Nevel's (1972) equation for the force to fail these wedges is given as;

$$\frac{6P}{b_0 \sigma t^2} = 1.05 + 2.00(a/\ell) + 0.50(a/\ell)^3 \qquad (14)$$

where P is the failure force on the tip of the wedge, σ is the ice flexural strength, t is the ice thickness, a is the distance from the tip of the wedge over which it is loaded, bo is a constant defining the width of the wedge (b) in the equation

$$b = bo \; \chi \qquad (15)$$

where χ is the distance along the wedge, bo is a constant and ℓ is the characteristic length for the plate given by

$$\ell = \left(\frac{Et^3}{12\rho wg}\right)^{0.25} \qquad (16)$$

Bercha and Danys (1975) have made use of the above theory to present an elastic analysis for the ice breaking component of the ice force on a conical structure. Their results are repeated here in Figures (14) and (15) for structures with water-line diameters up to 18.3 m (60 ft) subject to ice 0.91 m (3 ft) thick.

Bercha and Danys (1975) have also analyzed the effect of in-plane compressive stresses on the flexural failure of the ice sheet. For steep, rough structures the effect can be significant and increases the horizontal force.

An approach for ice forces on a conical structure using plastic limit analysis has been proposed by Ralston (1977). His results can be expressed in the form

$$H = A_4 \left[A_1 \sigma t^2 + A_2 \rho wgtD^2 + A_3 \rho wgt(D^2 - D_T^2) \right] \qquad (17)$$

$$V = B_1 H + B_2 \rho wgt(D^2 - D_T^2) \qquad (18)$$

where D_T is the top diameter and D is the water line diameter. A_1 and A_2 are coefficients dependent on $\rho wgD^2/\sigma t$, and A_3, A_4, B_1 and B_2 are coefficients dependent on the cone angle α and friction μ. Values for these coefficients are reproduced in this report in Figure 16.

It should be noted that Ralston's analysis includes both the forces due to ice ride-up and ice breaking. In equation (17) the first two terms are due to ice breaking and the third term results from the ice pieces sliding over the surface of the cone.

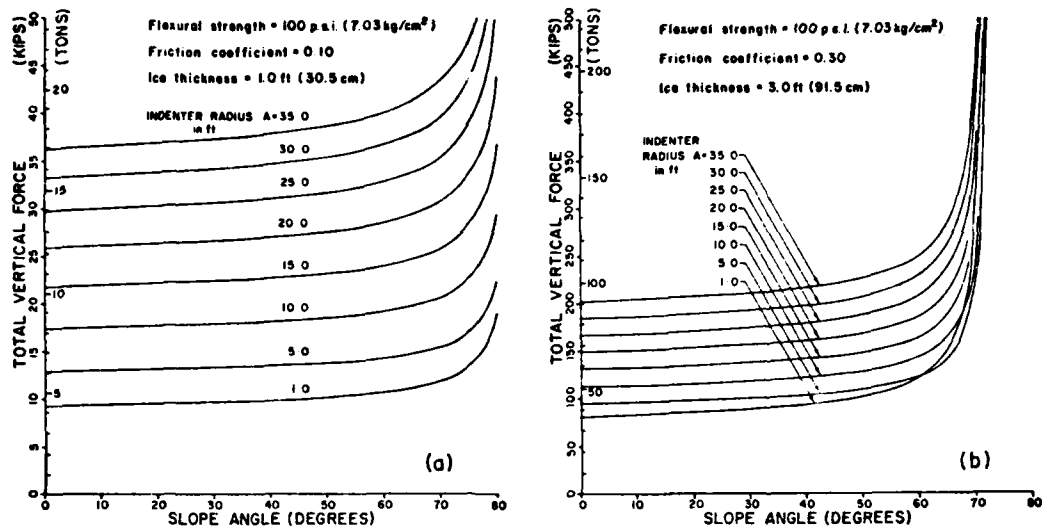Figure 14. Vertical force vs slope angle and indenter radius A for constant flexural strength, friction and ice thickness. (Kip = 1000 lbs.), (Danys and Bercha 1976).
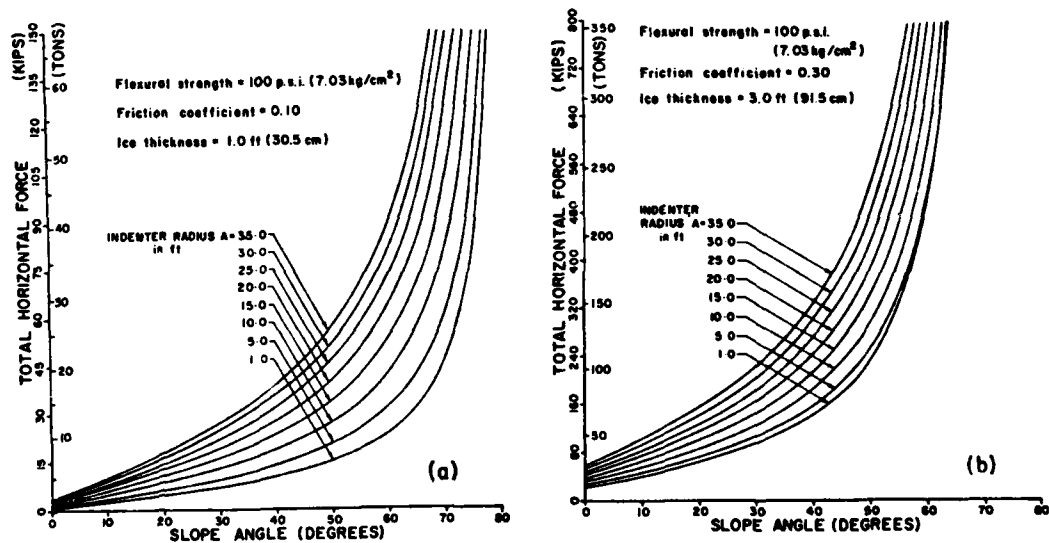

Figure 15. Horizontal force vs slope angle and indenter radius A for constant flexural strength, friction and ice thickness. (Kip = 1000 lbs.), (Danys and Bercha 1976).
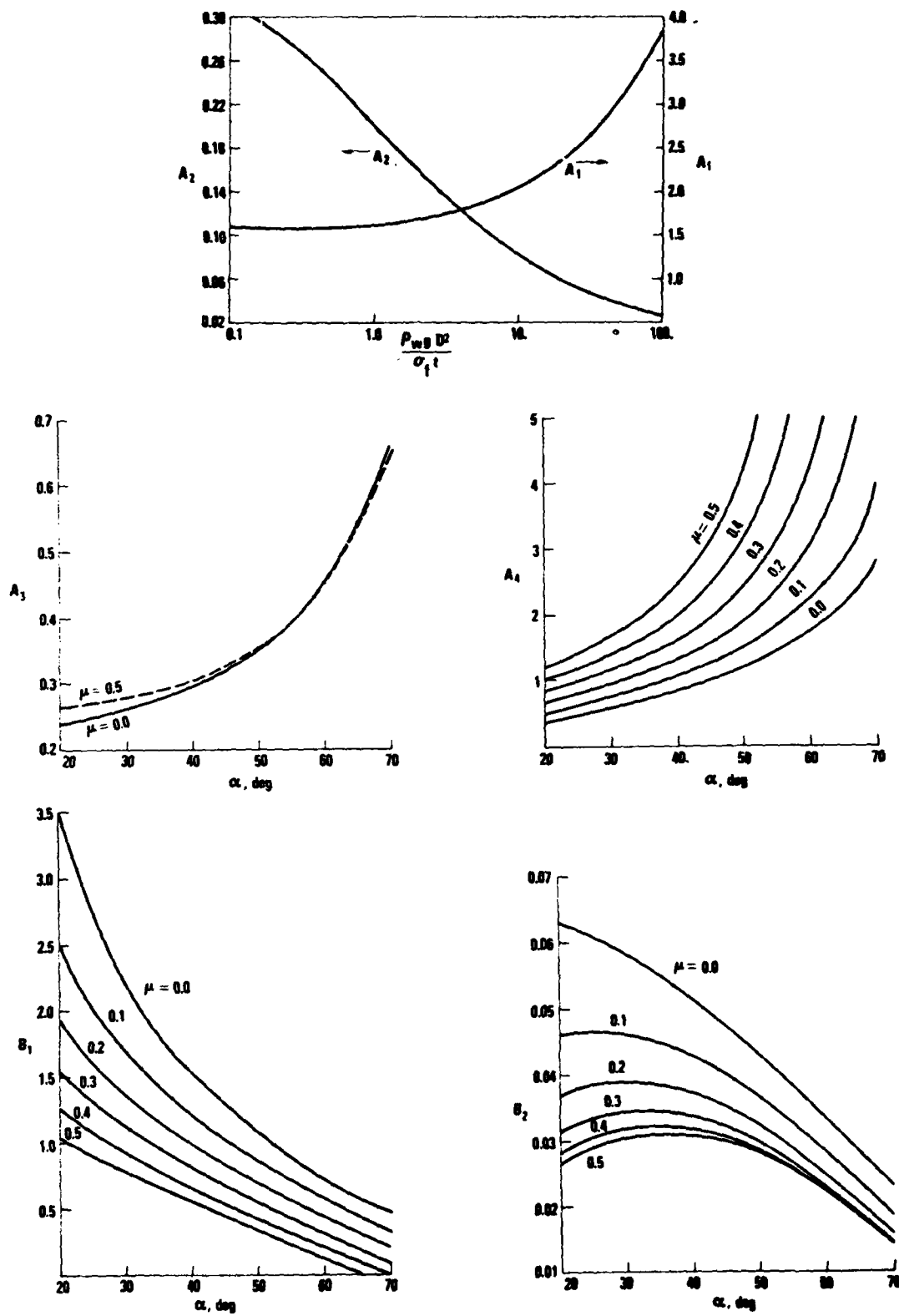
Figure 16. Ice force coefficients for plastic analysis (Ralston 1977).

It's of interest to note that for narrow structures, Ralston's theory predicts the ride-up component to be small compared with ice breaking, see Figure (17). For wide structures the ice ride-up component becomes a larger part of the total force, see Figure (18).

2.67 Experimental Data

At this time there are only two series of laboratory experiments for which data are available. In 1970, tests were conducted in the Arctec model basin on 45° angle cones up to 100 cm in diameter with ice up to 7 cm thick. Results from these tests have been reported by Edwards and Croasdale (1976). In 1971, tests were conducted with cones up to 28 cm in diameter with ice up to 3.5 cm thick by Afanasev, Dolgopolov and Shvaishtein (1971).

An empirical relationship derived by Edwards and Croasdale from their tests is given as;

$$H = 1.6\sigma t^2 + 6.0\rho gDt^2 \tag{19}$$

(for a 45° angle cone with an ice to cone friction coefficient of 0.05).

The investigators proposed that the first term represents the ice breaking portion of the ice force and the second term represents the ice clearing component.

From observations of their tests Afanasev et al (1971) proposed the following formula based on elastic plate theory

$$H = \frac{\sigma t^2 Sx \, \tan x}{1.93\ell} \tag{20}$$

where Sx is the length of the circumferential crack given as

$$Sx = 1.76(\dot{r} + \pi/4\ell) \tag{21}$$

where r is the cone radius at ice level, and ℓ is the characteristic length given by

$$\ell = \left(\frac{Et^3}{12\rho g(1 - \nu^2)}\right)^{0.25} \tag{22}$$

where E is Young's modulus and ν is Poisson's ratio.

Measurements of ice forces on an inclined pier have been published by Neill (1976). The pier was inclined at 23° to the vertical and forces up to 788 KNm^{-1} were measured for ice 0.75 m thick.
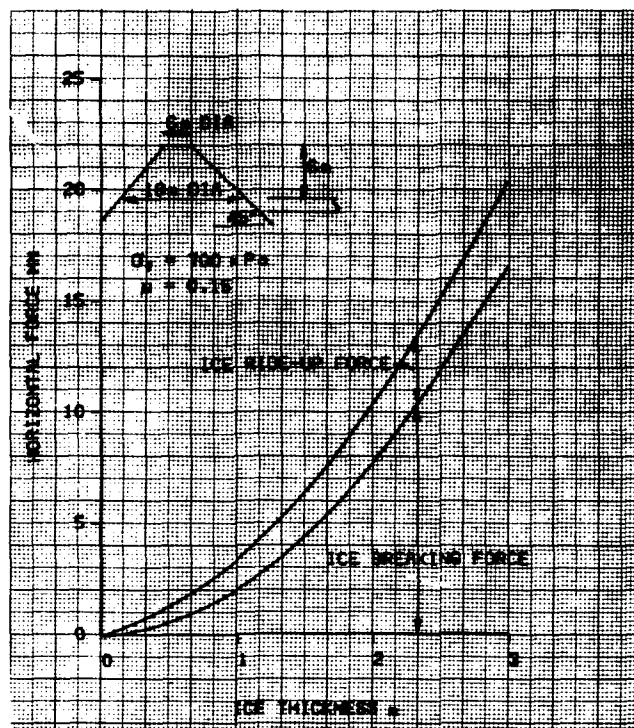
Figure 17. Horizontal force vs ice thickness - narrow structure
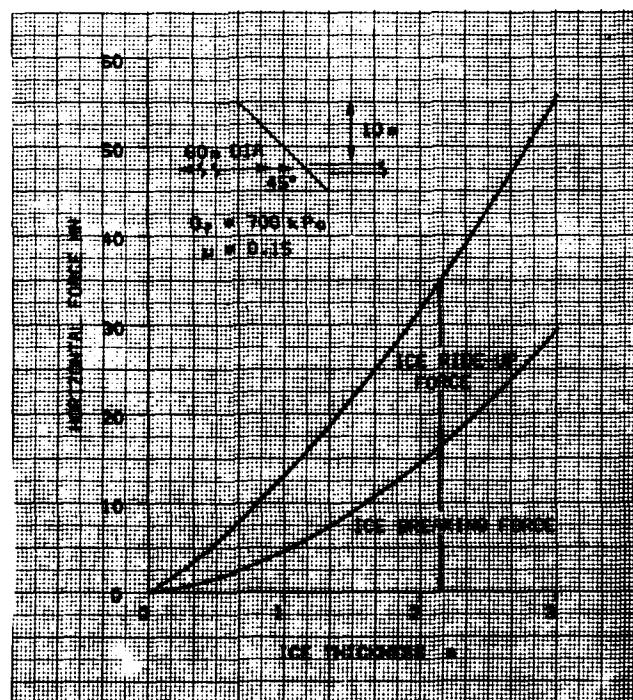(Ralston's theory).

Figure 18. Horizontal force vs ice thickness - wide structure
(Ralston's theory).

Experiments have been conducted in a large outdoor test basin in Calgary on a 45° angle cone with a 3.1 m (10 ft) water line diameter with ice up to 0.6 m (2ft) thick (Robbins et al, 1975, Croasdale, 1977). Results from these experiments have not yet been published.

Tryde (1975 and 1977) has investigated ice acting on a narrow wedge-shaped pier by conducting model tests. He proposed the following empirical method for predicting ice forces on a narrow sloping wedge.

$$H = C_F \sigma_c t D$$

where σ_c is the ice compressive strength and C_F is a 'reduction coefficient' expressed as,

$$CF = \frac{5.2 \; \epsilon^{1/3}}{C^{1/2}}$$

where

$$C = 0.16 \left[\frac{E}{\rho U_c^2 \sin\beta} \right]^{1/2} C_1 / C_2 \; C_3^2$$

where $\epsilon = \sigma/\sigma_c$, where σ is the bending strength and σ_c is the compression strength of the ice, E is the Young's modulus, ρ is the ice density and U_c the velocity of the floe. The coefficients C_1, C_2 and C_3 are given as,

$$C_1 = 1 - \mu \frac{\tan\alpha}{\sin\beta}$$

$$C_2 = \mu + \frac{\tan\alpha}{\sin\beta}$$

$$C_3 = 6(\frac{t}{D}\cos\beta + \frac{C_1}{C_2})$$

where 2β is the included angle at the point of the wedge in the horizontal plane, α is the inclination of the slope of the wedge to the horizontal and μ the coefficient of friction.

Tryde suggests that the value of C_F is most likely to be in the range 0.1 to 0.3, implying that ice failing in bending imposes forces which are 10 to 30% of the ice crushing forces. As far as can be determined Tryde's formula does not account for ice ride-up and is quite sensitive to modulus of elasticity. The formula is not strictly applicable to conical towers.

2.68 Comparison of Formulae

2.68.1 Narrow Structures

In his review of ice forces on piers and piles Neill (1976) used an example of a 10 ft (3.05 m) diameter conical tower to compare various formulae for ice forces on sloping structures. This example is repeated here and extended to include the additional correlations published since Neill's paper. Horizontal forces compared for the four original methods discussed by Neill are presented in Table 2 together with forces calculated using the formulas discussed in this report. Also, typical crushing forces, assuming the structure is vertical sided, are presented.

An immediate observation from the forces shown in Table 2 is that all the more recent formulae and correlations generally give higher forces than the methods originally listed by Neill.

None of the original formulae listed by Neill took account of friction, but even if we set $\mu = 0$ the formulae of Bercha and Ralston still yield higher forces than the first four methods. It should be appreciated that the 3-D math models of Bercha and Ralston presumably assume simultaneous failure of the ice sheet in the affected zone, and this perhaps represents an upper bound. For example in Bercha's model the ice force is derived assuming all the loaded ice wedges fail simultaneously. If in fact they do not, then presumably the peak ice breaking force will be lower.

It is of interest to note that the model data of Edwards and Croasdale if extrapolated to this example gives forces comparable with those predicted by Bercha and Ralston. This fact lends support to the validity of their predictions.

As expected, the simple 2-D theory underpredicts the ice breaking component. This is because the structure width is small compared with the characteristic length of the ice sheet. If we adjust the 2-D force by the ratio of the length of the circumferential crack to the structure width, then the force predicted by the 2-D theory agrees quite well with methods (5) and (7). The length of the circumferential crack $\approx 0.25\pi^2\ell$, where ℓ is the characteristic length defined by equation (22).

TABLE 2 HORIZONTAL FORCE ON CONICAL TOWER
CALCULATED BY TEN METHODS

ASSUMPTIONS: D=10ft. (3.05), t=3ft.(0.91m), σ=150psi (1050kPa)
ν=0.33, E=1x10^{6}psi (7 x10^{6}kPa), α = 45^0
Freeboard= 5ft. (1.53m)

Source of Formula		Breaking Force (kN)	Ride-Up Force (kN)	Total Force (kN)
(1) Afanasev etal (1971)		694	-	694
(2) Dany's Procedure as Reported by Neill (1976)		249	126	375
(3) USSR Code SN 76-66 (Appendix 2)		543	-	543
(4) Korzhavin's Formula		463	-	463
(5) Bercha and Dany's (1975)	μ=0	954	-	954
	μ=0.15	1335	-	1335
(6) Ralston	μ=0	1400	22	1422
	μ=0.15	1964	30	1994
(7) Edward's and Croasdale		1384	150	1534
(8) Simple 2-D Theory (μ=0.15)		84	70	154
(9) Simple 2-D Theory Adjusted (μ=0.15)		1200	70	1270
(10) Tryde (sloping wedge)	E= 7x10^6 kPa	485	-	485
	E= 2x10^5 kPa	1200	-	1200
Crushing Force p = 400 psi (2800kPa) k = 0.5		3886	-	3886
Crushing Force p = 600 psi (4200kPa) k = 0.5		5829	-	5829

Also, we see from Table 2 that even using the most conservative predictions, the forces on the conical tower are significantly less than typical crushing forces on a 10 ft (3.05 m) diameter cylindrical structure.

Finally, we see from the table that for narrow conical structures the ride-up force is small compared to the ice breaking force.

Until better test data is available, designers would be wise to use the most conservative prediction techniques (e.g. Ralston, Bercha and Danys, or adjusted 2-D theory).

2.68.2 Bercha's Example - 18.3 m Diameter Cone

To examine results for a wider structure consider the example of an 18.3 m diameter cone, with the other variables as defined in Table 3. This is the largest diameter structure considered by Bercha and Danys (1975) in their paper.

Again the Ralston formula predicts the highest force, but the ice breaking force is in reasonably close agreement with Bercha and Danys.

The most significant point about the data presented in Table 3 is that the ice ride-up or clearing forces are now quite large. The simple 2-D theory probably over predicts the ride-up forces but both the correlations of Ralston and Edwards and Croasdale suggest ride-up forces of around 1000 KN. Clearly for a structure of this width the ride-up forces cannot be ignored.

2.68.3 A Wide Sloping Structure

The horizontal forces acting on a structure 60 m wide are compared in Table 4. In this case only forces derived using the Ralston formula and simple 2-D theory are compared. The agreement for total force is quite good, but the 2-D theory consistently predicts lower ice breaking forces. This is to be expected for the reasons already discussed.

Again the ice ride-up or clearing forces are very significant and cannot be ignored for such a wide structure. Perhaps more importantly the actual clearing mechanism needs to be further addressed when considering such wide structures.

It should be remembered that the method of calculation of ice
ride-up forces assumes simply that the surface of the structure
is covered by ice pieces; and the force is that necessary to
push the ice pieces up the surface. In reality the ice pieces
may not continue to clear around the structure and a large ice
rubble field may be generated. This ice rubble may then inter-
fere with the ice structure interaction and could lead to even
higher forces. For wide structures, model tests should be
conducted to investigate this phenomenon.

TABLE 3 HORIZONTAL FORCE ON AN 18.3m DIAMETER CONICAL TOWER
(BERCHA'S EXAMPLE)

ASSUMPTIONS: D=60ft. (18.3m), t=3ft. (0.91m), σ=100 psi (700kPa)
ν=0.33, E=1x10^{6}psi (7 x10^{6}kPa), α = 45^0
μ=0.15, freeboard = 20 ft (6.1 m)

	Breaking Force (kN)	Ride-Up Force (kN)	Total Force (kN)
Bercha and Dany's (1975)	1558	-	1558
Ralston (1977)	1964	1196	3160
Simple 2-D Theory	355	1896	2251
Simple 2-D Theory (Adjusted)	845	1896	2741
Afanasev Et Al (1971)	711	-	711
Edwards and Croasdale (1977)	922	900	1822

TABLE 4   HORIZONTAL FORCE ON WIDE CONICAL STRUCTURE

ASSUMPTIONS: D=60m, σ=700kPa, E=7x10^{6}kPa, α = 45°

μ=0.15, freeboard = 10m, t=0.5, 1.0, 2.0m

	t (m)	Breaking Force (kN)	Ride-Up Force (kN)	Total Force (kN)
Ralston (1977)	0.5	1574	4385	5959
Simple 2-D Theory	0.5	559	5625	6184
Ralston (1977)	1.0	4822	8770	13592
Simple 2-D Theory	1.0	1330	11250	12580
Ralston (1977)	2.0	14855	17540	32395
Simple 2-D Theory	2.0	3162	22500	25662

2.7 SOLID ICE RIDGES ACTING ON SLOPING STRUCTURES

Solid multi-year ridges which occur amongst the polar ice represent a severe loading condition for arctic offshore structures. Multi-year ridges up to 15 m thick are not uncommon and are fully consolidated (Kovacs, 1971).

As a first approximation multi-year ridges can be considered as floating beams infinitely long. Failure loads can be calculated using the theory of elastic beams on elastic foundations (Hetenyi, 1946, Croasdale, 1975).

Observations of ridge structure interaction in model tests (Lewis and Croasdale, 1978) indicates that the ridge usually fails first with a centre crack at the point of interaction with the structure (see Figure 19). Using simple beam theory the vertical load necessary to cause this initial crack is given by

$$V_1 = \frac{4\ I\sigma}{y\ell} \tag{23}$$

where I is the second moment of area of the ridge cross section about its neutral axis, σ is the ice flexural strength, y is the distance to the surface in tension (in this case the top surface) and ℓ is the characteristic length given by;

$$\ell = \left(\frac{4EI}{\rho g b}\right)^{0.25} \tag{24}$$

where b is the width of the ridge.

Although when the first centre crack has occurred, the ridge can be considered broken, it cannot pass around the structure without further breaking. Again, observations of tests indicate that the subsequent interaction mechanism is the formation of hinge cracks as shown in Figure 19. The vertical force to cause the hinge cracks is calculated by considering the simultaneous failure of two semi infinite beams on elastic foundations, that is;

$$V_2 = \frac{6.17\ I\sigma}{y\ell} \tag{25}$$

In this case y is the distance from the neutral axis to the bottom of the ridge.

It will be noted from the above equation that the formation of the hinge cracks will generally cause greater loads on a structure than the load due to the initial crack.

For a ridge 15 m deep and 30 m wide with a flexural strength of 700 kPa and elastic modulus of 7×10^6 kPa, the vertical force to create the initial crack is 18,736 KN whereas the force to create the two hinge cracks is 28,900 KN.

The corresponding horizontal forces depend on the cone angle and ice-to-structure friction, that is:

$$H_1 = V_1 \left(\frac{\sin\alpha + \mu\cos\alpha}{\cos\alpha - \mu\sin\alpha} \right) \tag{26}$$

$$H_2 = V_2 \left(\frac{\sin\alpha + \mu\cos\alpha}{\cos\alpha - \mu\sin\alpha} \right) \tag{27}$$

Typical horizontal forces are shown in Figure 19 for the ridge described above acting on a 60^0 cone with $\mu = 0.3$.

More sophisticated analyses of ridge loads can be done using a more realistic ridge cross-section to calculate I and y. Also, the equations given above are for an infinitely long ridge. Ralston (1977) has pointed out that shorter ridges can cause greater loads than infinitely long ridges. The relationship derived by Ralston showing the effect of ridge length is repeated in this report as Figure 20. Obviously as the ridge gets shorter there is more chance of other interactions taking place. The ridge may simply rotate or the ice sheet may fail behind. Therefore Figure 20 should be used with care, and more work is required in this area.

The only published experimental data on ice forces due to ice ridges is that by Lewis and Croasdale (1978). Their work was conducted in 1970 in a saline ice model basin. Model ridges up to 23.5 cm thick and 28.6 cm wide were tested against a 45^0 angle cone.

A summary of their results adjusted to full scale values is given in Table 5. For comparison, theoretical values using equations (25) and (27) are included. The theoretical values are corrected for length using Figure 20.

The comparison between theory and experiment is not good for the small ridge but reasonably good for the deeper ridge. It is possible that the effect of the surrounding sheet ice which was present in the model tests leads to the higher loads observed compared to those predicted.

TABLE 5   RIDGE LOADS: COMPARISON OF EXPERIMENTS AND THEORY
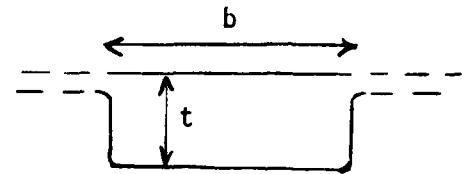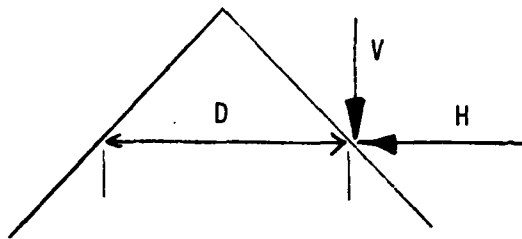
$\sigma = 17 \times 10^5 \text{Nm}^{-2}$ $E = 3 \times 10^9 \text{Nm}^{-2}$

D	b	t	Ridge Length	ℓ	V Exp.	V Theory	H Exp.	H Theory	
								$\mu=0.1$	$\mu=0.3$
(m)	(m)	(m)	(m)	(m)	(MN)	(MN)	(MN)	(MN)	(MN)
12.5	5.9	3.1	120	42	8.46	3.4	14.46	4.2	6.3
12.5	11.3	5.8	120	67	17.29	22.03	27.70	27.21	40.8

2.8 SOLID RIDGES ACTING AGAINST VERTICAL FACED STRUCTURES

Vertical faced structures would not be recommended where multi-year ice ridges are common. Potential ice forces would be very large because the ice ridge would have to fail by crushing, shear or in-plane bending.

2.9 UNCONSOLIDATED ICE RIDGES

First year ridges are largely unconsolidated, that is, they are composed of ice blocks held together by buoyancy, gravity and frictional forces. Ice forces due to first year ridges can be expected to be much lower than due to consolidated ridges. Ice forces can be calculated approximately, the ice is a granular material with an assumed friction angle.

For the arrangement shown in figure 21 (ignoring the ridge sail):

$$\text{Force on structure} = 2F = \frac{2Bt^2}{3}\rho bg\tan\phi \qquad (28)$$

Where B is the ridge width, t is the ridge thickness ρb is the buoyant density of the ice and ϕ is the friction angle of submerged ice blocks.

As an example consider an unconsolidated ice ridge 15 m thick by 30 m wide with $0 = 30^0$, and $\rho bg = 981$ Nm ^{3};

$$2F = 2570 \text{ kN}$$

This is about one tenth the load due to a multi-year ridge of the same dimensions.

2.10 ADFREEZE FORCES

In the nearshore arctic environment the ice surrounding a structure can remain stationary long enough for the ice to freeze to the structure. Also, vertical motions of the ice due to tidal action can be so small that an adfreeze bond can develop between the ice sheet and the structure. Once the ice sheet starts to move again, sliding motion between ice and structure first requires breaking the adfreeze bond. For certain types of sloping structures the force required to fail the adfreeze bond can be significantly greater than the force needed to fail the ice in bending. In these situations the force to fail the adfreeze bond can become the design force for the structure.
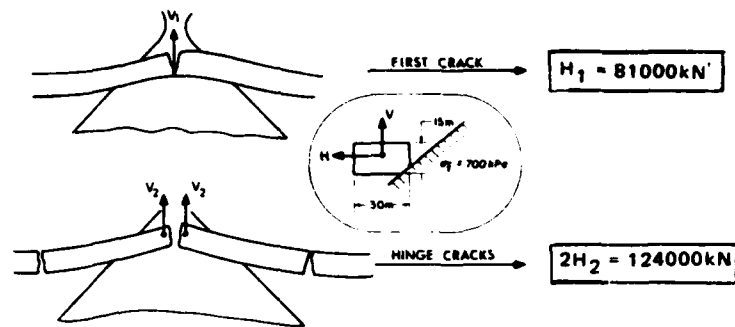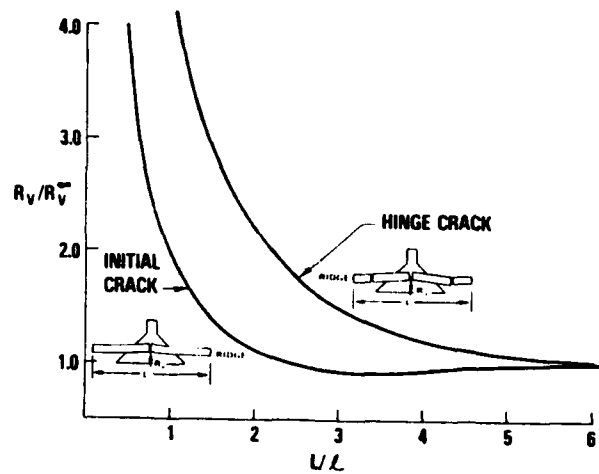
Figure 19.   Ridge failure on cone.

Figure 20.   Elastic interpretation of initial crack and hinge crack forces for multiyear ridges failing against conical structures (Ralston 1977).
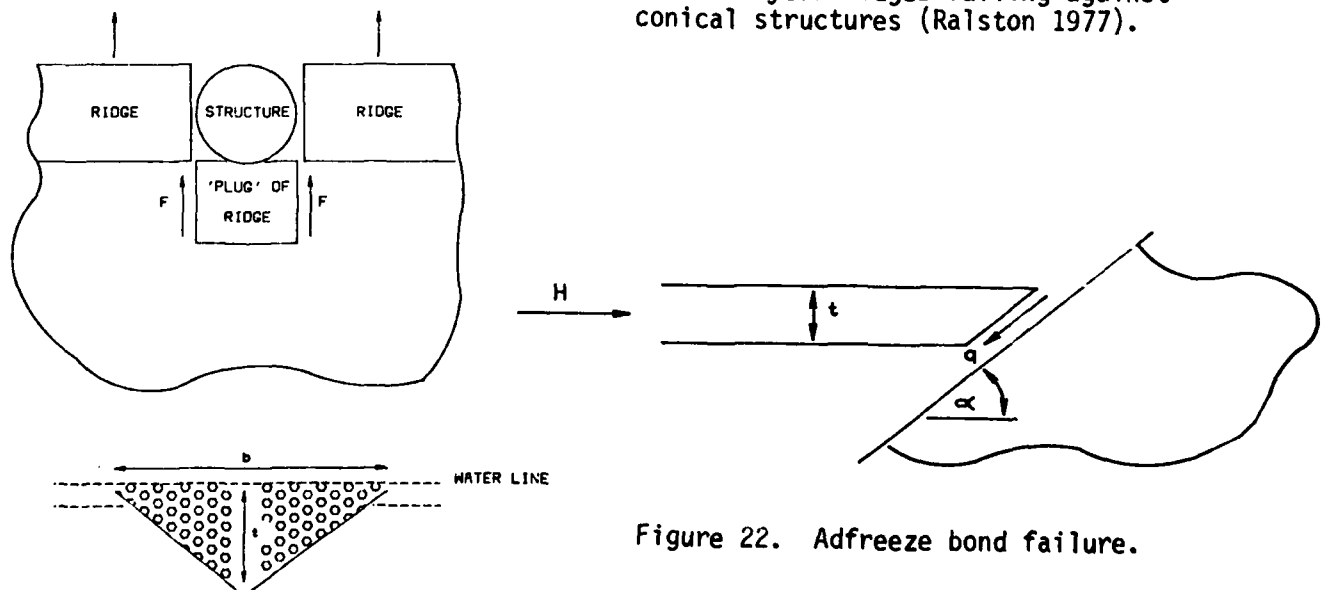

Figure 21.   Simple interaction model for unconsolidated ridge.

Figure 22.   Adfreeze bond failure.

In the arrangement shown in figure 22 the adfreeze force is given by;

$$H = \frac{\pi t q D}{\tan\alpha} \tag{29}$$

where t is the ice thickness, α is the slope angle, D is the structure diameter and q is the adfreeze bond strength.

Little data is available on adfreeze strengths. Adhesion strengths published by Michel (1970) are in the range 140 to 1050 kPa (20 to 150 psi) for fresh ice. More recently Sackinger and Sackinger (1977) have published adfreeze strengths for sea ice on steel. They found that salinity and temperature affected adfreeze strengths. A maximum value of 1590 kPa (227 psi) was measured at a temperature of -23^0 C for ice with a salinity of 0.4 parts per 1000.

2.11   ICE CRUSHING ON A NARROW VERTICAL PIER

2.111 Introduction

The problem of ice crushing against a narrow vertical pier has become a classic problem in the field of ice mechanics. A proper review of this topic would constitute a major thesis and is beyond the scope of this report. For a detailed review of current engineering practice the reader is referred to Neill (1976).

2.112 Empirical Formula

The effective ice pressure or stress acting on a narrow vertical pier can be defined as:

$$p = \frac{F}{tb} \tag{30}$$

where p is the effective ice stress
    F is the ice force
    b is the width of the pier
    t is the ice thickness

The essence of the ice force problem on a narrow vertical pier is to be able to specify the appropriate value of p for the particular ice conditions expected.

Early work (Korzhavin, 1962) to address this problem (primarily for bridge piers) suggested the following empirical relationship for p.

$$p = Imk\sigma \tag{31}$$

where σ is the ice strength in compression
   k is a contact coefficient which equals 1.0 for perfect contact
   m is a shape factor which is close to 1.0 for circular piers
   I is an indentation factor which tends to 1.0 for a wide structure and is equal to 2.5 for narrow structures (d/t=1.0)

In Korzhavin's original equation a velocity term was included, but it is generally accepted that this can be omitted if the ice strength is specified for the appropriate velocity or strain rate.

The usefulness of the above equation to the engineer is limited because of the need to input a value for the ice compressive strength. Compressive strength measured on small ice blocks is notoriously variable, being highly sensitive to crystal orientation, degree of confinement, temperature, strain rate and size of sample.

However, despite this limitation, equation (31) includes some useful concepts for ice pressure on piles. It suggests that for wide structures, with $I = 1$, the maximum pressure approaches the uniaxial ice crushing strength, and for narrow piers, the ice pressure could be 2.5 times greater. The equation also tells us that the ice pressure is a function of the "goodness" of contact between the ice and pier.

2.113 Plasticity Theory

For perfect contact the problem reduces to that of pushing an indentor into the edge of a semi infinite ice sheet. The theory which follows is relevant to the flat indentor configuration shown in Figure 23. (The results for a circular indentor would be similar.) The problem of penetration of an ice sheet by a flat indentor has been addressed by Croasdale, Morgenstern and Nuttall (1977); their solution is repeated here.

We assume ice to be an isotropic, homogeneous ideal elastic-plastic material. Yielding is governed by a relation between the principal stresses known as the yield criterion.

It will be assumed in this analysis that ice behaves like most metals and that yielding is independent of hydrostatic pressure. In this case, the simple Tresca yield condition can be applied, which states:

$$\sigma_1 - \sigma_2 = 2q \qquad (32)$$

where σ_1 denotes the major principal stress, σ_2 denotes the minor principal stress and q denotes the shear strength, and it follows that:

$$\sigma = 2q$$

where σ is the uniaxial compressive strength. Equation (2) states that yield occurs when the greatest shear stress on any plane has reached a limiting value.

The penetration of an ice sheet by a flat indentor can be analysed by the Lower-and-Upper-Bound Theorems of plasticity (Prager and Hodge, 1951, or Calladine, 1969).

The Lower-Bound Theorem states the following: If any stress distribution throughout the loaded body can be found which is everywhere in equilibrium internally and balances the externally applied loads and at the same time does not violate the yield condition, those loads will be carried safely by the body.

The Upper-Bound Theorem is as follows: If an estimate of the plastic collapse load of a body is made by equating internal rate of dissipation of energy to the rate at which external forces do work in any postulated mechanism of deformation of the body, the estimate will be either high or correct.

It should be noted that neither stress distribution in the first case nor the mechanism of deformation in the second need be the correct ones. The true solution is found when both upper and lower bounds converge to the same result. When they do not, the true solution will be between the lowest "upper bound" and the highest "lower bound".

The problem of interpreting the indentation tests is one of computing the resistance offered to incipient indentation of a pier or indentor by the edge of the ice sheet. (In all the indentation tests, a tensile crack first forms at right angles to the direction of loading, so that subsequent crushing failure of the ice sheet is the same as would occur due to edge loading of a thick plate, see Figure 23.)

We can define the solution in the form,

$$p = \sigma I \qquad (33)$$

where σ denotes the compressive strength of the ice, p denotes the average pressure on the indentor at failure and I is the indentation factor which will depend on the geometry of the indentor, the ice thickness and the boundary conditions.

To solve for I is the objective of this analysis, and solutions are derived for two boundary conditions; first with the ice free to slip at the face of the indentor, and second with the ice frozen to the indentor.

The geometry of the arrangement is defined in Figure 23; d is the width of the indentor and t is the ice thickness. When d is much smaller than t, the problem reduces to the classical Prandtl indentor for which there is an exact solution;

$$\frac{p}{\sigma} = 1 + \pi/2 \qquad 2.57$$

Also when d is much larger than t, the lower-bound solution shown in Figure 8 becomes exact, i.e.

$$\frac{p}{\sigma} = 1.0$$

therefore

$$I = 1.0$$

Between these limits, the problem is three-dimensional and I will depend on the ratio of d/t which is sometimes called the aspect ratio. An upper bound solution for this problem will now be derived.

Two kinematically admissible velocity fields are shown in Figure 24. It can be shown that "solution 1" gives a lower upper bound (Morgenstern and Nuttall, unpublished). We will work through one case for d/t = 1.0. The indentor moves with velocity V and external work D_e is;

$$D_e = pd^2V \qquad (34)$$

Internal dissipation due to shearing resistance q occurs along the velocity discontinuity surfaces such as (abde), (bcd), (afe). If the wedges are inclined at θ to the edge of the ice sheet, from symmetry the energy dissipated internally D_i is;

$$D_i = \sigma \left[\frac{d^2 \sec\theta}{2} + \frac{2d^2 \tan\theta}{8} \right] V \operatorname{cosec}\theta \qquad (35)$$

Equating D_e and D_i, we get

$$\frac{p}{\sigma} = \frac{1}{\cos\theta} \left[\tfrac{1}{4} + \frac{1}{2\sin\theta} \right] \qquad (36)$$

To find the critical inclination, we put

$$\frac{\partial(p/\sigma)}{\partial\theta} = 0$$

which gives $0 = 41^0$ and

$$\frac{p}{\sigma} = 1.34$$

i.e. $I = 1.34$.

This calculation can be repeated for several values of d/t to give the curve shown in Figure 25.

If there is adhesion between the interface and the ice sheet, more dissipation of energy takes place internally due to shearing resistance at the interface. Any value of shearing resistance could be assumed at the interface up to the limiting value of q the shear strength of the ice. In this case, accounting for the extra resistance, the solution becomes;

$$\frac{p}{\sigma} = \sec\theta\operatorname{cosec}\theta + \frac{t}{d} \frac{\tan\theta\operatorname{cosec}\theta}{4} + \frac{\cot\theta}{2} \qquad (37)$$

Following minimization with respect to θ, the critical values of p/σ may be found for the range of d/t of interest. Again there is a plane-strain cut-off at d/t = 0. The size-effect curve for the rough indentor is also shown in Figure 25.
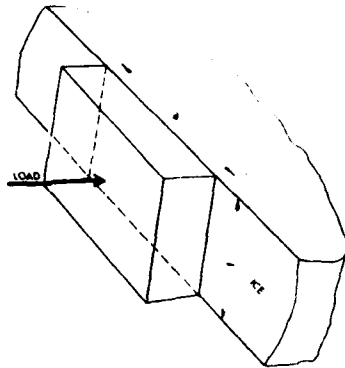
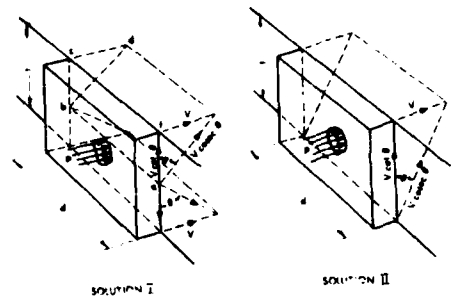Figure 23. Flat indenter.

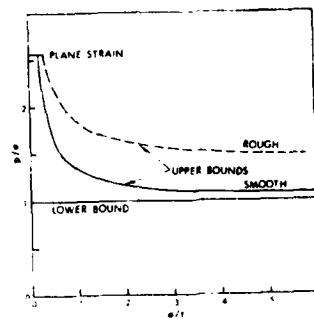Figure 24. Upper bound velocity fields.
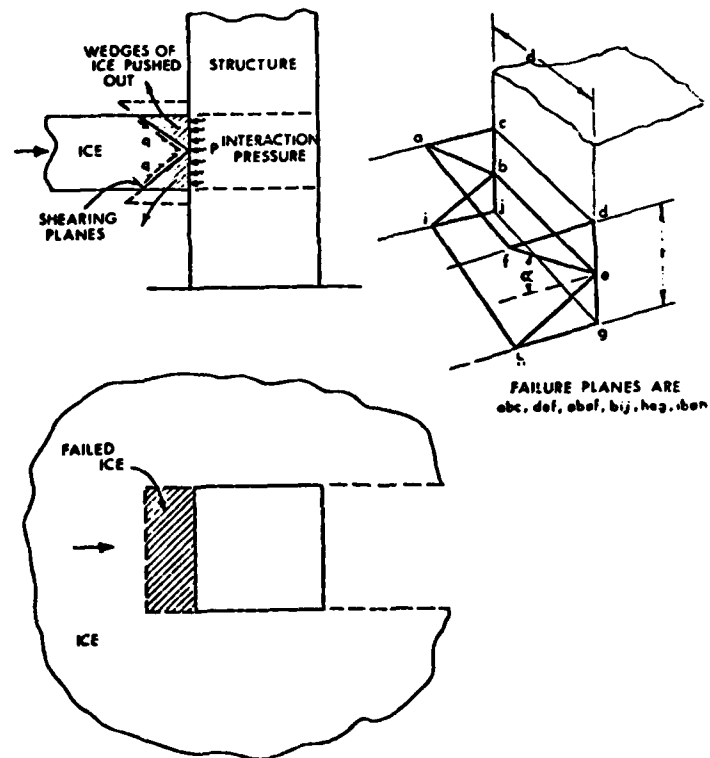

Figure 25. Theoretical solutions.

Figure 26. Wedge-type failure (upper-bound solution).

Solutions can also be found for circular indentors using the same technique (Morgenstern and Nuttall, unpublished) but these will not be discussed here.

The above theory is based on the simple Tresca yield criterion. Other yield criteria have been discussed by Ralston (1977).

2.114 Simplified Theory

The upper bound solution from the previous theory suggest that a flaking type failure occurs for perfect contact between pier and the ice (see figure 26). This failure concept has been observed in the field; although some investigators also report the occurrence of an inplane cleavage crack. (Schwarz etal 1974) However, staying with the wedge type failure and assuming that the failure planes are at 45^0 for all values of b/t then the previous theory can be simplified to;

$$p = \sigma_c (1 + 0.304 \frac{t}{b})$$

(38)

This equation neatly explains the term I in Korzhavin's equation, for as the width of the structure increases the second term becomes negligible and p = σc.

The double wedge failure is obviously only applicable to the initial failure peak for ice in intimate contact with the pier. However, similar reasoning can be used to look at subsequent pressure peaks (figure 27).

Intuitively by considering the area of the failure planes after critical break out it can easily be seen that for subsequent failures (or continuous crushing) the pressure peaks are about half the initial peak. Also the ice pressure for continuous crushing is less sensitive to structure width. The lower pressures for continuous crushing can be considered to be accounted for in Korzhavin's empirical equation by the use of the contact factor, k. Korzhavin recommends values for k in the range 0.4 to 0.7 which are compatible with the 0.5 factor indicated by simple theory.

Tryde (1977) also discussed a wedge-type failure mode for ice crushing, and proposed the empirical formula

$$p = 0.8\sigma_c \left[1 + 2.1(0.4 + \frac{d}{t})^{-1} \right]$$

where σ_c is defined as the uniaxial compressive strength of the ice, and $0.1 \leq D/t \leq \infty$. It is not clear what the basis is for 0.8 factor applied to σ_c.

2.115 Test Data - Indentation

Small scale indentation tests have been conducted by
Michel and Toussaint (1977), Frederking and Gold (1975), Nevel et
al (1972), Zabilansky et al (1975), Hirayama et al (1974) and
others. Field indentation tests have been conducted by Croasdale
(1974, 1977) and by Haynes et al (1975).

A composite plot of some of their results are shown in
figure 28. The results shown indicate a strong dependence on
strain rate and a possible dependence on ice thickness.

The effect of strain rate is discussed at some length
by Michel and Toussaint (1977) they propose that it is the major
parameter in determining ice forces on piles and that strain rate
effects can explain the indentation factor I. Their work also
clearly demonstrated that at high strain rates the ice pressures
during continuous crushing are less than the initial ice pressure
with good contact, see Figure 29.

Frederking and Gold (1975) performed tests at low strain
rates; they suggest that the indentation factor is dependent only
on indentor width, not thickness.

The field indentation tests by Croasdale (1974, 1977)
gave a slight indication of an aspect ratio (b/t) effect (Figure 30).
More important, the ice pressures were generally lower than those
obtained in the laboratory on thinner ice. This could be an
indication of a size effect implying that a larger volume of ice
has a lower average strength. Or the lower field values could be
due to imperfect contact between ice and indenter.

2.116 Theory of Michel and Toussaint

The experimental work of Michel and Toussaint (1977) led
them to develop a theory for indentation assuming a perfectly
plastic material close to the indenter surrounded by a circular
region of ductile deformation. This concept led them to define
strain rate as

$$\dot{\varepsilon} = \frac{V}{4b} \tag{39}$$

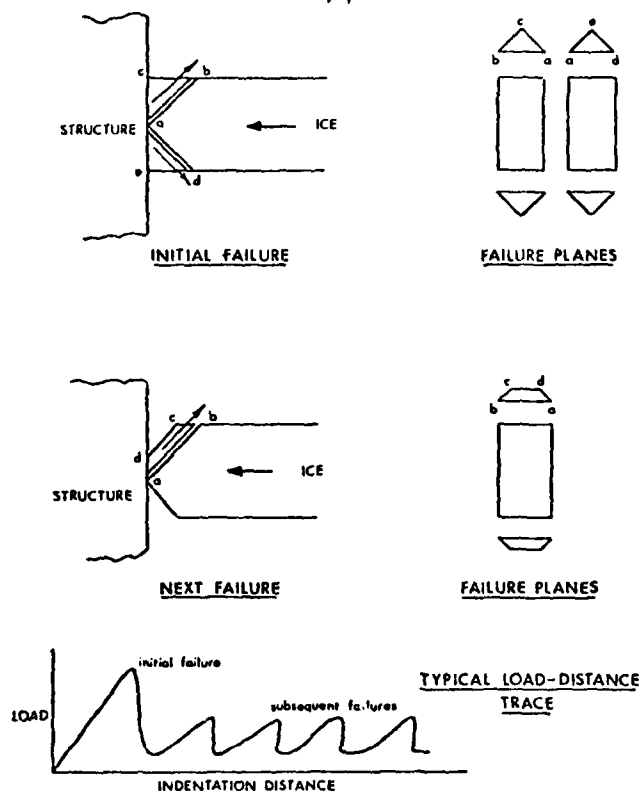where V is the velocity of movement and b the structure width.

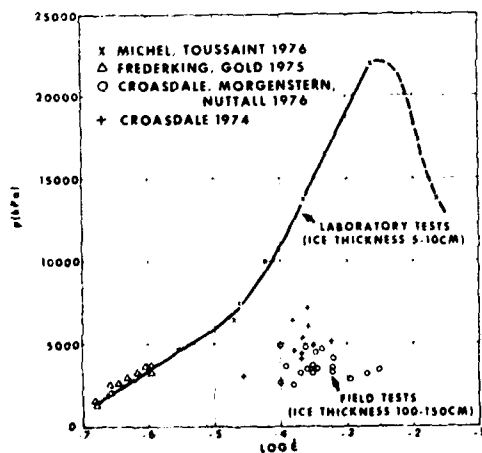Figure 27.   Ice crushing: upper bound solutions.

Figure 28.   Indentation strength
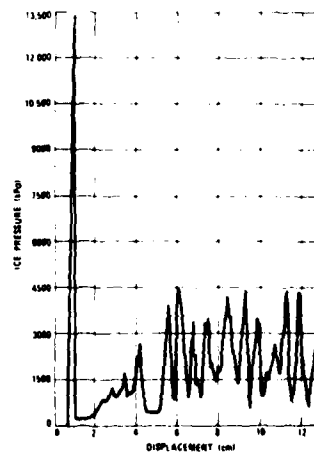(p) vs strain rate ($\dot{\epsilon}$).

Figure 29.   Indentation
pressure vs displacement
(Michel and Toussaint 1976).

Their analysis gave them the expression;

$$p = 2.97\sigma \tag{40}$$

where σ is the uniaxial yield strength in the ductile region (at the appropriate strain rate).

Using equation (40) they reduced a large number of indentation data to uniaxial yield strengths and plotted them with other uniaxial yield strengths to give the composite plot shown in Figure 31. The plot is for S2 ice at -10^0 C. The data agrees reasonably well with that reported by Croasdale et al (1977), showing a maximum strength of about 7600 kPa at a strain rate of around 10^{-4} to $10^{-3} S^{-1}$. As a result of the strong strain rate effect shown in Figure 31, and the proposed dependence of strain rate on structure width, Michel and Toussaint went on to suggest that the variation of effective ice pressure with b/t is because of strain rate dependence.

They proposed the use of three separate equations for ice pressure, each for a specific strain rate range, they are;
(a) For $10^{-8} s^{-1} < \dot{\varepsilon} < 5\times10^{-4} s^{-1}$ (ductile zone)

$$p = 2.97 \, m \, k\sigma_o \left(\frac{\dot{\varepsilon}}{\dot{\varepsilon}_o}\right)^{0.32} \tag{41}$$

where m = 1 for a flat indenter 1.0 for initial good contact, k = 0.6 for continuous crushing, σ_o = 7000kPa for ice at -10^0C, $\dot{\varepsilon}_o = 5\times10^{-4} s^{-1}$.
(b) For $5\times10^{-4} s^{-1} < \dot{\varepsilon} < 10^{-2} s^{-1}$ (transition zone)

$$p = 2.97 \, m \, k\sigma_o \left(\frac{\dot{\varepsilon}}{\dot{\varepsilon}_o}\right)^{-0.126} \tag{42}$$

where k = 0.25 for continuous crushing and the other parameter have values as in (a).

(c) For $\dot{\varepsilon} > 10^{-2} s^{-1}$ (brittle zone)

$$p = 3mk \, \sigma_b \tag{43}$$

where k = 0.3 for continuous crushing and σ_b is the uniaxial crushing strength under brittle conditions

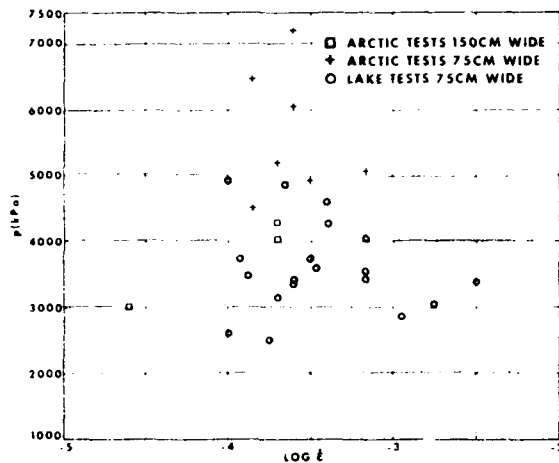Figure 30.   Indentation strength
(p) vs strain rate ($\dot{\varepsilon}$) (field tests)
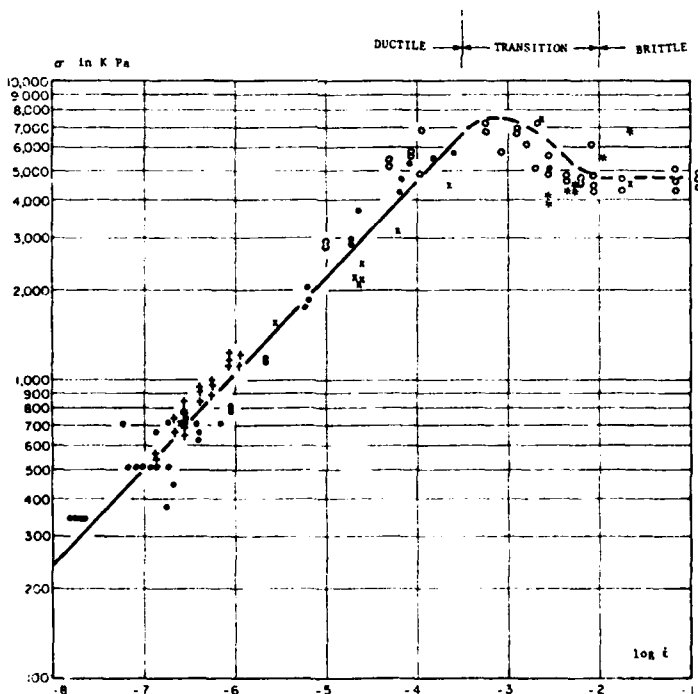(Croasdale 1974, 1977).

Figure 31.   Universal curve for uniaxial crushing
and indentation of S_2 ice at $-10^{\circ}C$: O— Michel and
Paradis (1976), uniaxial; O--- Carter and Michel
(1972), uniaxial; + Frederking and Gold (1975),
indentation; * Hirayama and others (1974), indent-
ation; × present study, indentation.

- The highest values are those derived from Michel and Toussaint for cold ice failing in the ductile condition. Michel and Toussaint themselves do not recommend designing to these values. They note that most ice motions are sufficiently fast to give failures in the brittle condition. It will be noted that their ice pressure for brittle failure of -10^0 C ice agrees reasonably well with that obtained from the wedge theory.

We should also note that even in the arctic the mean ice temperature is unlikely to get much below -10^0 C because of the insulating effect of the snow cover. Furthermore, the values calculated are based on fresh ice; sea ice is weaker and so the ice pressures in crushing would be lower.

It seems as though the wedge formula with k = 0.5 gives reasonable agreement with the guidelines for warm ice. It is recommended that it be used for design where conditions may be different from those of the guidelines e.g. in the arctic. The wedge formula has the advantage of accounting for structure width, thickness, and ice strength. For ice in more or less continuous motion a value of contact factor of 0.5 is suggested. If ice can freeze around a structure, then a value of k = 1.0 or higher may be appropriate. It would seem wise to prevent good contact from occurring by the deployment of waste heat or use of other defence measures.

Further measurements of ice forces on vertical structures, particularly in Arctic regions, is desirable.

For very wide structures a further mitigation of ice forces may occur due to non-similtaneous failure across the width of the structure.

For ice at other temperatures different uniaxial strength values would be used.

2.117 Comparison of Crushing Formulae

Neill (1976) in his review of ice forces compares effective ice pressures used in practice for vertical piles and piers. His comparison is repeated in Table 6. Also, additional ice pressures are included, calculated using the wedge theory, and the equations of Michel and Toussaint (1977).

The ice pressures calculated using the wedge theory (equation 38) are calculated on the basis of a contact factor of 0.5. Also it is assumed that m = 0.9. For the narrow structure, b = 3 m and t = 1m. For the wide structure b = 30 m and t = 1 m. Equation (38) then reduces to;

$$p = 0.59 \, \sigma_c \qquad \text{for the narrow structure}$$

and

$$p = 0.46 \, \sigma_c \qquad \text{for the wider structure}$$

σ_c is taken to be 7000 kPa for ice at -10^0 C and 3000 kPa for ice at -1.5^0 C.

Similar assumptions for ice strength and structure width were made in using the equations of Michel and Toussaint. It was assumed that the ductile ice pressure occurred at the maximum ice strength value. Contact factors were 0.6 for the ductile condition and 0.3 for the brittle condition.

In looking at the values listed in Table 6 several points can be noted.

- The values given by existing guidelines are lower than the highest values given by the formulae.

- The guidelines do not relate specifically to ice temperature or to structure width. It is likely that the design guidelines relate to warm ice as might be experienced at break-up. In which case the agreement with the values given by the formulae for warm ice is quite good.

TABLE 6   COMPARISON OF EFFECTIVE PRESSURES FOR VERTICAL
PILES AND PIERS

Source		Range of Pressures Specified or Implied kPa	
Korzhavin 1962: USSR rivers, spring break-up		490 - 1860	
AASHO and CSA (old), Highway bridge codes		2760	(400 psi)
New CSA Code S-6 (1974), Highway Bridges		690 - 2760	
USSR Code SN 76-66: River Structures		295 - 1320	
Canada Ministry of Transport - Navigation Lightpiers, St. Lawrence		965 - 1210	
Canada Dept. of Public Works - Wharf Piles		1380 - 1720	
Wedge Formula (warm ice -1.5°C)	3 m dia structure	1755	(250 psi)
	30 m dia structure	1390	(200 psi)
Michel and Toussaint (warm ice -1.5°C)	Ductile	4811	(690 psi)
	Brittle	1620	(230 psi)
Tryde (-1.5°C)	3m dia structure	3860	(554psi)
	30m dia structure	2580	(370psi)
Wedge Formula (cold ice -10°C)	3 m dia structure	4095	(585 psi)
	30 m dia structure	3244	(460 psi)
Michel and Toussaint (cold ice -10°C)	Ductile	11226	(1600 psi)
	Brittle	4050	(580 psi)
Tryde (-10°C)	3m dia structure	9070	(1300psi)
	30m dia structure	5990	(859psi)

2.118 Crushing Against Wide Structures

As an ice sheet continuously crushes against a very wide structure, variation in local contact effects enhances the opportunity for non-simultaneous ice failure across the structure width. This suggests that the average ice pressure across a wide structure will be less than for a narrow structure. In non-simultaneous failure, different zones of ice across the width are at different stages of failure at any one time. Local stresses in any one zone could be high, but the average crushing stress across the total width would be low.

An approach using the concept of independent failure zones has been developed by Kry (1978). He uses a statistical approach to estimate the effect of structure width on design ice pressure. It is shown that if movements of the thickest ice are sufficiently limited there is a significant statistical reduction in the expected peak stress for a wide structure compared to a narrow structure.

This is an area where further work and field measurements are required.

2.12 ICE FORCES ON ARTIFICIAL ISLANDS

2.121 Introduction

Artificial islands are being used in the shallow waters of the Arctic Ocean for oil and gas exploration (Croasdale and Marcellus, 1978). These islands are generally quite wide relative to the ice thickness and therefore the mechanics of ice clearing tends to dominate the ice to structure interaction. Islands and wide structures become surrounded by extensive ice rubble fields which can ground. These, rubble fields have to be considered when assessing ice forces (Kry, 1977).

In the cold environment of the Arctic, islands acquire a frozen surface very quickly after construction. If ice forces become large enough there is a danger that the frozen surface of the island can be moved laterally, although no such failures have been observed in the sixteen islands built to date.

Because islands have such large diameters, the ice forces to cause failure are also large. In some situations the environmental driving forces are not large enough to cause island failure, even if the ice were strong enough.

2.122 Typical Island Resistance

Ice movement during different times of the year creates lateral ice forces on dredged islands, which must be resisted by the shearing resistance of the soil along possible failure planes. Three different potential failure planes have been identified for evaluation. These are shown in Figure 32.

Failure plane 1 is considered unlikely because the frozen saturated fill of the island is generally much stronger than the surrounding ice and so the ice will fail first. With failure plane 2, the frozen crust of the island is considered to slide relative to the unfrozen fill below it. In the case of a weak foundation, failure plane 3 through the sea bed might be possible but generally requires a higher lateral force than for failure plane 2.

Approximate calculations of the sliding resistance of an island are quite simple, especially if the material is of good granular quality and its friction angle is known. The other uncertainty is the depth of the frozen layer but this can be predicted from previous measurements or from thermal calculations.

For an island its sliding resistance is given approximately by;

$$R = (\rho_1 V_1 + \rho_2 V_2)\tan\phi \qquad (44)$$

where

V_1 is the fill volume above water level
V_2 is the fill volume between water level and the sliding plane
ρ_1 is the density of the fill
ρ_2 is the buoyant density of the fill
ϕ is the friction angle of the fill

For an island 122 m in diameter at the sliding plane with a freeboard of 4.6 m and 3.1 m between the water level and the sliding plane, and also using ρ_1 = 1925 kgm^{-3} and ρ_2 = 963 kgm^{-3} and $\tan\phi$ = 0.6, then

$$R = 800, 650 \text{ kN}$$

From section 5 a typical environmental driving force might be derived using the expression for wind drag;

$$K = C_{10}\rho_a g V^2 A$$

In this case assume K equals the island sliding resistance and calculate the area of ice required to generate the equivalent environmental force (for a wind speed of 15 m S^{-1}).

$$A = 520 \times 10^6 \ m^3$$

In other words an ice cover 520 square km in extent is needed to generate an ice force with the potential to fail the island. In the landfast ice zone of the Arctic, continuous ice covers of this areal extent are quite common. But in a pack ice situation its unlikely that such a large ice force could be transmitted to the island.

2.123 Ice Action on Islands in Shallow Sheltered Locations - Arctic Ocean

Islands in this category would be in 3 m of water or less and would be in protected areas where ice movement is slow and limited.

2.123.1 *Observations of Ice Action*

A typical scenario for ice action at these sheltered islands would be as follows.

Freeze-up occurs about mid-October and because of the sheltered nature of the locations the ice quickly becomes landfast. From then on, the movement of the ice is similar to that of lake ice with small expansions and contractions occurring under the action of wind stress or thermal expansion.

Observations of the ice around such islands indicate that apart from the occasional tidal crack, the ice is well and truly frozen around the islands and there is little evidence in the form of cracks or ridges, of ice action due to lateral motion. During break-up the ice around these islands usually melts in place.

2.123.2 Ice Forces on Shallow Islands in Landfast Ice

Given that observations of ice around shallow islands indicate a 'frozen-in' condition exists, we can speculate on possible ice failure modes and forces when ice movement occurs.

Figure 33 indicates ice failure mechanisms which could occur.

(a) <u>Buckling</u>

This mode of failure is sometimes observed in the thin ice of refrozen leads. A lower-bound prediction for the ice stress to cause buckling can be derived using simple theory for a slender strip of material on an elastic foundation (Hetenyi, 1946).

$$\text{Critical buckling load, } P = 2\sqrt{KEI} \qquad (45)$$

where K = foundation modulus
       E = elastic modulus
       I = second moment of area

Solving the above for $E = 7 \times 10^6$ kPa and in terms of ice stress (p) and thickness (t) gives:

t	(m)	0.3	1.2	2.15
p	(kPa)	2660	5250	7000

In other words, an ice pressure or stress of at least 7000 kPa would be needed for buckling failure of 2 m of ice. As discussed below, other failure modes probably require less force and, therefore, buckling will not occur (and has not been observed). More accurate predictions of buckling failure are contained in the paper by Sodhi et al (1977).

(b) <u>Failure of Frozen Bond Between Ice and Island</u>

If the adfreeze bond fails then the ice can ride-up the island beach and fail in bending.

Consider the configuration shown in Figure 34 where:

p is the ice stress on the island
t is the ice thickness
q is the adfreeze shear strength of ice to island bond
α is the island beach angle

Then

$$pt = \left(\frac{t}{\sin\alpha}\right)q\cos\alpha$$

i.e. $\qquad p = \frac{q}{\tan\alpha}$

Little data is available on adfreeze strengths of ice to island beaches; for the purpose of this discussion assume q = 1400 kPa and the beach slope is 1 in 3 then;

p = 4200 kPa

Again, this pressure is probably higher than alternates discussed below so adfreeze bond failure is unlikely.

(c) Crushing Failure of Ice or Ductile Flow of Ice

Whether crushing failure or ductile flow occurs will depend on the rate of ice movement or strain rate. At slow strain rates this problem is somewhat similar to that of thermal ice pressures on dams. At high strain rates, ice crushing forces as predicted for a vertical pier can be considered as an upper bound.

As already discussed in Section 11.0 the ice crushing pressure or stress can usefully be discussed using the equation of Korzhavin (1971) namely,

$$p = Imk\sigma \tag{31}$$

where p = ice stress on structure
I = a factor accounting for relative geometry of system. I is nominally equal to 2.5 for narrow structure and equal to 1.0 for wide structure
m = shape factor (equal to 1.0 for flat face and 0.9 for round face)
k = contact factor (1.0 for perfect contact may be higher for frozen in condition)
σ = ice strength in compression

The above equation and its implications have been discussed more fully in Section 11.0.

For a very wide structure, I can be considered as equal to unity. For ice frozen to the island k = 1.0 and whether m = 1.0 or 0.9 is not important. The equation for this application can, therefore, be simplified to p = σ where σ is the compressive strength of the ice.

The problem remains, however, to define the appropriate strength or yield criteria. It is well known that ice strength is a function of temperature, strain rate, crystal orientation, degree of confinement, salinity, and other poorly understood factors such as the size of the piece of ice under stress.

For ice in compression whether it is confined or not, strain rate has a significant effect on the mode of failure and strength. At very low strain rates, ice tends to flow or creep at low stresses with few visible surface failures. At higher strain rates the ice fails in a brittle fashion by flaking or shattering. A typical set of strength versus strain rate data for columnar ice is shown in Figure 31.

The observations of ice action on shallow islands suggest that the ice, as it slowly moves, deforms in a ductile fashion with no obvious failure cracks or flakes. Is this observation compatible with known ice strength data and ice movement rates? Measurements of ice movements in water depths less than about 3 m indicate that a typical maximum movement rate is about 0.3 m per hour. It is not clear what characteristic length should be used to give a strain rate but lets assume it is the island width or diameter.

then $\dot{\epsilon}$ = V/D

where $\dot{\epsilon}$ = strain rate
V = ice movement rate
D = island diameter

than typically
$$\dot{\epsilon} = \frac{0.3}{100.3600} = 10^{-6} \text{ sec}^{-1}$$

This strain rate is compatible with ductile or creep deformation for ice. Furthermore, as indicated in Figure 31, for uniaxial deformation it suggests an ice stress or pressure on the island of about 700 kPa. However, this could rise to 3500 kPa or so, if the plane strain or confined ice strength is more appropriate. On the other hand, small-scale laboratory tests tend to give higher strengths than in the field so the above mentioned ice stresses are likely too high.

In other words, it seems likely that because of the small and slow rates of ice movement at shallow locations, ice forces on shallow islands are governed by the creep or ductile flow characteristics of ice. Therefore, ice pressures on very shallow islands can be expected to be significantly less than on the more exposed islands discussed in the next section.

2.124 Ice Action on Exposed Islands - Artic Ocean

2.124.1 Observations of Ice Action

At deeper locations it takes longer for the ice to become truly landfast, and even then, cyclic ice motion appears sufficient to maintain an active zone of ice failure around the island. Typically, although freeze-up occurs in mid-October the first few weeks are characterized by large movements of ice 0.3 to 0.6 m thick. Under storm conditions, these movements can be several thousand metres causing extensive ice rubble to form around the island.

Once the ice becomes landfast in November or December, ice movements are normally restricted to a few feet per day and are cyclic. Later in the winter, the movement becomes less, but seems sufficient to prevent the active cracks from freezing-up.

2.124.2 Modes of Ice Failure and Ice Forces

A typical sequence of ice action on the beach of an exposed island is shown in Figure 35. Initial movements of thin ice fail at low loads in bending. The ice is too thin to ride-up the island beach so rubble piles are formed.

The mechanics of rubble pile formation are uncertain. In some cases, the rubble forms a ramp up which the oncoming ice sheet advances and fails in bending. At other times the ice penetrates the rubble but again is probably failed in bending by differential buoyancy and weight forces as suggested by Parmenter and Coon (1972) for ice ridge formation. The rubble often grounds, and once a certain height is reached, grows seawards. In the early winter, the rubble height rarely exceeds 6 m. Ice forces at this time might be predicted with the model for pressure ridge formation mentioned above, and will be less than 350 kPa. In any case, the rubble probably protects the island from most of these forces. Because of the rubble resistance to lateral forces the active zone remains on the outside of the rubble which consolidates and freezes into a rigid ice annulus around the island, see Figure 36.

The mechanics of rubble field formation have been discussed by Kry (1977); he also notes that rubble heights can reach 13 m.

Eventually the ice becomes too thick to fail in bending and begins to fail in crushing at much higher ice stresses. However, by now the refrozen rubble is competent enough to maintain the active zone at its outer boundary; but at the same time, transmit the ice forces to the frozen island surface.

For a particular ice crushing stress (p) in the active zone, the ice force (F) generated on the island rubble-pile combination as shown in Figure 36 is given by:

$$F = pWt \qquad (47)$$

where W is the width of the rubble in the direction of ice movement, t is the ice thickness.

If R is the sliding resistance of the rubble then the force on the island is given by:

$$Q = pWt - R \qquad (48)$$

An approximation for R can be made assuming the arrangement shown in Figure 37.

At the sliding plane, the normal reaction per unit area (w) is given approximately by:

$$w = (1 - c)[h_m \rho_i + y (\rho_i - \rho_w)] \qquad (49)$$

where c is the porosity of the rubble
h_m is the mean height of the rubble above sea level
y is the water depth
ρ_1 is the ice density
ρ_w is the water density

Sliding resistance of the rubble is then given by:

$$R = Awtan\phi$$

$$(50)$$

where A is the area of the rubble
ϕ is the friction angle at the base of the rubble (either in the soil or in the rubble, which ever is the least).

For the arrangement shown in Figure 36;

$$R = (WL - \frac{\pi D^2}{4})w\tan\phi \tag{51}$$

For a typical situation assume:

$$D = 97.6 \text{ m}$$
$$W = 137 \text{ m}$$
$$L = 152.5 \text{ m}$$
$$\tan 0 = 0.6$$
$$c = 0.3$$
$$h_m = 3.1 \text{ m}$$
$$y = 7.6 \text{ m}$$
$$\rho_1 = 914 \text{ kgm}^{-3}$$
$$\rho_w = 1000 \text{ kgm}^{-3}$$

Then, sliding resistance of rubble is given by:

$$R = 116 \text{ MN}$$

As discussed in Section 12.2, a typical island might have a sliding resistance of around 800 MN. Thus the effect of the rubble around it would be to increase the total sliding resistance by about 10 - 15%. On the other hand the effective ice loading diameter is also increased; in this case to 140 m or by 40%. In this example then, the effect of refrozen rubble around the island is to decrease the factor of safety against sliding by about 20%.

The preceding analysis is approximate. Kry (1977) has presented a more rigorous analysis, but the general conclusions are the same.

2.124.3 Ice Crushing Stress in the Active Zone

The ice crushing stress in the active zone is not easily determined. The ice crushing pressures given in Section 11.0 can be used as upper bounds, but mitigation of these values can be expected because of the large width of the failure zone (as discussed in Section 11.8), particularly for small movements of the landfast ice.

In-situ ice stress measurements conducted around artifical islands to date indicate ice crushing stresses in the active zone considerable less than the ice compressive strength.
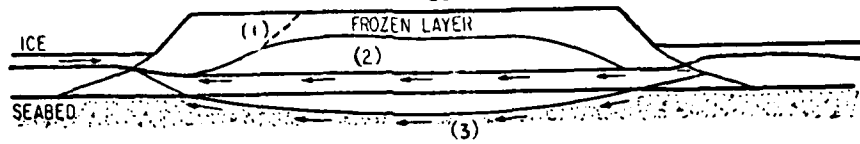
Figure 32. Possible island failure modes: (1) edge failure,
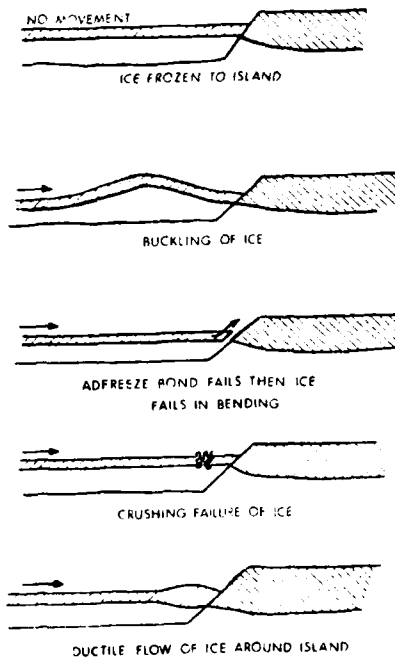(2) failure through island fill, (3) failure through seabed.

Figure 33. Possible ice failure modes; ice frozen to island.

Figure 34. Sequence of ice action on island beach (exposed island): (a) initial movements of thin ice, (b) extensive ice movement causes grounded rubble, (c) active zone remains outside rubble that freezes, (d) thick ice fails in crushing.

Figure 35. Ice action on island and rubble.

Figure 36. Sliding resistance of rubble.

Figure 37. Adfreeze bond failure.

MICROCOPY RESOLUTION TEST CHART
NATIONAL BUREAU OF STANDARDS 1964 A

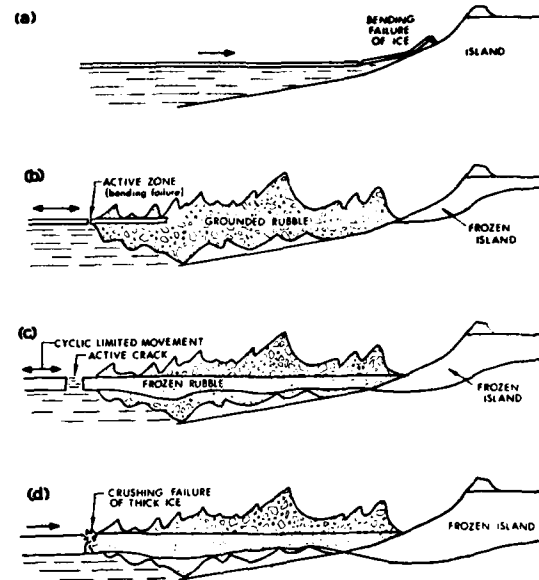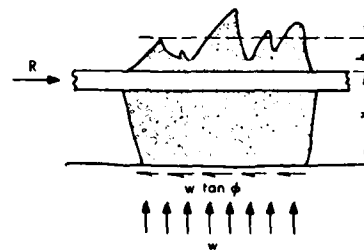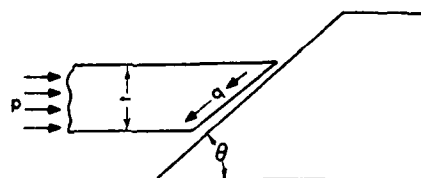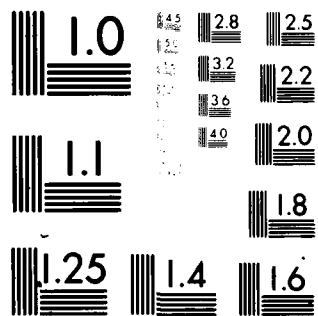## 2.13 ICE RIDE-UP ON ARTIFICIAL ISLANDS

2.131 Introduction

Low freeboard structures with shallow slopes are susceptible to ice encroachment onto their working surfaces. Ice movement against such structures leads either to ice pile-up in front of the structure or to ice ride-up. The nature of simple ice ride-up is illustrated in Figure 38. With ice ride-up, not only can ice encroach onto the working surface, but it advances at the speed of movement of the surrounding ice field. In many cases this would give little time for evasive action.

When designing low freeboard structures with sloping beaches such as artificial islands, it is important to be able to assess the likelihood of ice ride-up. This section examines factors which may limit ice ride-up, and suggests procedures for designing against ice ride-up.

2.132 Reported Ice Ride-Ups

One of the earliest references to ice ride-up was made by the well known arctic explorer Stefansson (1913): "Under such conditions (landward thrust of sea ice under wind pressure) tongues of ice may slip-up on the beach and be shoved inland two or three hundred feet beyond the limit of high tide and thirty or forty feet above sea level".

Until recently, ride-up has been a concern only in the more populated sub-arctic regions such as Scandinavia and the Great Lakes. Several examples of damage to marine structures and shoreline property are given by Bruun and Johanesson (1971), Tryde (1972) and Tsang (1974). These authors have shown that even small ice fields can cause ice pilings of considerable height, up to 10 m for an ice thickness of 0.5 m. Although they refer to "ice pilings", their experience is relevant to ice ride-up because the maximum height of ice pilings is often reached by ice pieces riding up on top of each other (Tsang 1974).

Several analyses of the maximum height of ice pilings have been performed (Allen 1970). They assume that the height is only limited by the horizontal thrust of the ice sheet or its kinetic energy. Other limiting mechanisms (e.g. flexural strength) are explored in the present paper but with specific reference to ice ride-up.

With the recently increased activity in arctic regions, more examples of ice ride-up with thicker ice have been witnessed. Shapiro (1976) described how 1.2 m thick ice was driven ashore near Barrow, Alaska and up the beach as a coherent unit for distances ranging up to 25 m. Irwin (1975) reports a similar occurrence at Lincoln Bay, Ellesmere Island.

More recently, near Barrow, Alaska, ice rode-up a shallow beach up to 105 m from the water line and 3 m above the water level (Hanson, 1978). The ice was from 1 to 1.3 m thick. Elsewhere on the same beach the ice stopped within 25 m from the water line but at a similar elevation of 2.5 m.

Such occurrences emphasize the possibility of ice ride-up on low freeboard structures such as artificial islands.

2.133 Factors Limiting Ice Ride-up

Ride-up can only occur if the capacity of the ice sheet to push is greater than the resistance to movement of ice up the slope. Ice push can be limited either by the environmental driving force or by the strength of the ice sheet immediately in front of the beach. Resistance to ice sliding up the beach can be caused by instability of the broken ice pieces on the beach slope. These limiting factors are discussed.

2.133.1 Simple Slope Resistance

Consider the configuration shown in Figure 39 where P is the force necessary to move the ice pieces up the slope.

Now if, w is the mass of each ice piece
n is the number of ice pieces on the slope
α is the angle of the slope from the horizontal
μ is the coefficient of friction
g is acceleration due to gravity

then,
$$P = \sum_{1}^{n} wg(\sin\alpha + \mu\cos\alpha) \tag{52}$$

In another form, for a simple two-dimensional system,

$$P = Ltb\rho g(\sin\alpha + \mu\cos\alpha) \tag{53}$$

Where, L is the length of slope covered by ice, t is the ice thickness ρ is the density and b is width of the ice on the slope.

If the steady state environmental driving force (F) is greater than the horizontal component of the slope resistance then the potential for ice ride-up exists.

That is, the potential for ice ride-up exists if,

$$\frac{F}{P\cos\alpha} \geq 1 \qquad (54)$$

As an example of slope resistance, consider a beach with a slope angle of 15^0, 30 m long, 100 m wide, ice 1 m thick, and a coefficient of friction of 0.3. Then from equation (53) P = 14.6 MN.

The horizontal component, converted to an ice stress =141 kPa (20 psi). These values will be compared with environmental driving forces in the following section.

2.133.2 Environmental Driving Forces

In the Arctic Ocean, shallow water islands are particularly susceptible to collision with large ice floes during the break-up of the landfast ice. At this time floes several kilometres in extent are not uncommon.

Consider a floe 5 km in diameter with a wind speed of 20 ms $^{-1}$ then the environmental driving force (F) is equal to 21.8 MN (from Section 5). Inserting this value into equation (54) together with the slope resistance for the above example

$$\frac{F}{P\cos\alpha} = \frac{21.8}{(14.6)\cos 15} = 1.54$$

Hence because the environmental driving force is greater than the slope resistance the potential for ice ride-up exists.

For floes of limited extent but which have considerable kinetic energy, an additional check would involve equating the initial kinetic energy of the moving floe to the work done in moving the ice pieces up the beach.

The work done against gravity and friction in moving ice up the slope can be derived using simple calculus and is given by

$$U = 0.5tb\rho g(\sin\alpha + \mu\cos\alpha)L^2 \qquad (55)$$

where t is the ice thickness, b is the ice width, ρ is the ice density, α is the slope angle, μ is the coefficient of friction, L is the length of slope covered by ice, and g is the gravitational constant.

The initial kinetic energy of the moving floe is given by; $\qquad (56)$

$$KE = (1/8)\pi D^2 t\rho v^2$$

where D is the diameter of the floe and v is its initial velocity.

For ice ride-up to the top of the slope, $\dfrac{KE}{U} \geq 1$

that is,

$$\frac{\pi D^2 v^2}{4bL^2 g(\sin\alpha + \mu\cos\alpha)} \geq 1 \qquad (57)$$

Note that the above criterion ignores the work done in bending failure of the ice sheet, but for a long shallow beach this contribution will be small. In any case, ignoring the work done to fail the ice will yield a conservative result.

To view the above criterion in perspective, consider the following example.

A floe 300 m in diameter approaches an island at 1 ms $^{-1}$. The island is 100 m wide, the beach has a 15^0 slope angle and the length of the beach is 25 m. Assume a coefficient of friction between ice and beach of 0.3.

Then,

$$\frac{\pi D^2 v^2}{4bL^2 g(\sin\alpha + \mu\cos\alpha)} = 0.21$$

Hence in this case ride-up by this individual floe is not possible unless other floes impact it from behind and continue to push it against the beach. *The critical diameter of an individual floe for which ride-up in this example is possible is 700 m.*

2.133.3 Ice Sheet Failure

Although the force necessary to push the ice pieces up the beach is caused by the environmental driving force, it is the ice sheet just in front of the beach which transmits the force. If the force due to slope resistance causes edge failure of the ice sheet then pile-up will occur at *the water line and ride-up* will be inhibited.

In general all possible failure modes of the advancing ice sheet should be considered, but in most cases it will be flexural failure which governs.

Consider again the configuration shown in Figure 39. The force P required to push the ice pieces up the slope is generated by vertical and horizontal forces on the edge of the advancing ice sheet.

In the limit, when the ice edge is almost at the slope, then

$$V = P \sin\alpha \tag{58}$$
$$H = P \cos\alpha \tag{59}$$

For a simple two-dimensional system of width b, from (53)

$$V = bt\rho g\bar{Z} \, (\sin\alpha + \mu\cos\alpha)$$

but $L\sin\alpha = \bar{Z}$, the vertical height from water line to the upper point reached by the ice on the slope (in the limit, the freeboard) then,

$$V = bt\rho g\bar{Z}(\sin\alpha + \mu\cos\alpha) \tag{60}$$

and

$$H = bt\rho g\bar{Z}(\sin\alpha + \mu\cos\alpha)\cot\alpha \tag{61}$$

For bending, the in-plane force H can be ignored and the critical condition for flexural failure can be derived by considering a beam or plate on an elastic foundation (Hetenyi, 1946).

For a simple beam of width b, loaded at the end

$$V_c = 0.68\sigma b \left(\frac{\rho g t^5}{E}\right)^{0.25}$$

(62)

where σ is the critical flexural stress V_c is the critical edge load.

Comparing equations (62) and (60), we can see that for ice ride-up to be possible.

$$\frac{V_c}{V} \geq 1$$

that is,

$$0.68\frac{\sigma}{2}\left(\frac{t}{E}\right)^{0.25}\left(\frac{1}{\rho g}\right)^{0.75}\frac{1}{\sin\alpha + \mu\cos\alpha} \geq 1$$

(63)

As an example in the use of equation (63) consider a beach 30 m long with a slope of 15⁰ and freeboard of 3 m, the coefficient of friction is 0.1 and the ice is 1 m thick with a flexural strength of 700 kPa, and modulus of 7 X 10⁶ kPa.

Use equation (13)
$$0.68\left(\frac{\sigma}{2}\right)\left(\frac{t}{E}\right)^{0.25}\left(\frac{1}{\rho g}\right)^{0.75}\frac{1}{\sin\alpha + \mu\cos\alpha} = 1.7$$

which is greater than one therefore ride-up is possible.

It will be noted from equation (63) that the ride-up criterion is directly proportional to ice strength and freeboard, but is influenced less by thickness and elastic modulus. The significance of friction becomes less for steeper slopes.

In the above example, let us consider the effect of increasing the freeboard to 7 m, and the coefficient of friction to 0.3.

Then,
$$0.68\left(\frac{\sigma}{2}\right)\left(\frac{t}{E}\right)^{0.25}\left(\frac{1}{\rho g}\right)^{0.75}\frac{1}{\sin\alpha + \mu\cos\alpha} = 0.48$$

which is less than one therefore ride-up will probably not occur.

The preceding discussion on ice sheet failure is very simplistic and is offered as an example of methodology rather than a precise technique for assessing the limiting condition of ice ride-up. For example, for slopes which continue at a very shallow angle below the water line, there may not be enough clearance for the ice to fail in downward bending as assumed in the equation. In these cases ice would continue to ride-up beyond the limiting condition defined in (63).

To assess the likelihood of other failure modes limiting ice ride-up, consider further the example referred to above. Using equation (60) we can calculate the horizontal stress in the ice sheet close to the beach, it is;

$$\frac{H}{bt} = \rho g \bar{z} \cot\alpha (\sin\alpha + \mu\cos\alpha) = 127 \text{ kPa (18psi)}$$

Such a stress level is too low to cause crushing (by at least a factor of 10) and is also too low to cause buckling except for very thin ice.

2.133.4 Kinematic Instability

For ice to continue to ride-up past a change in slope, certain geometric criteria have to be satisfied, otherwise a kinematic instability can occur. Consider Figure 40 illustrating what might happen at the top of a slope, and also at a point of change in angle of the slope. It will be seen that as the first ice block advances past a change in slope it can tilt clear of the following block thus enhancing the likelihood of a pile-up. However, such an instability can only occur if the ice is thin relative to the change in slope. As shown conceptually in Figure 41 if the ice thickness is great enough, then contact between ice blocks is maintained and the ice can continue to advance.

The limiting relationships between ice thickness, block length and slope angle can be derived as follows.

$$h = \frac{\ell \sin\alpha}{2}$$

If $h < t$ then ride-up can continue.

In reality local edge failure will probably occur if the point of contact is too close to the corner. Thus a more realistic condition might be
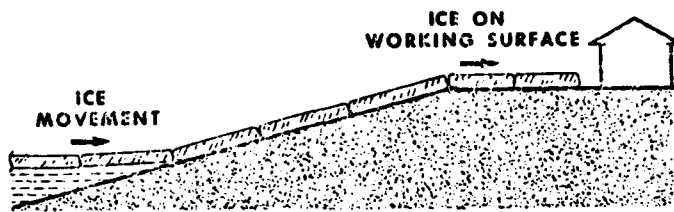
$$h < 0.8 \, t$$

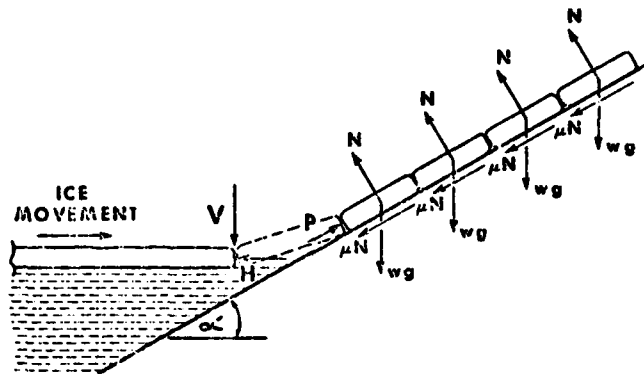Figure 38.. Simple ice ride-up.
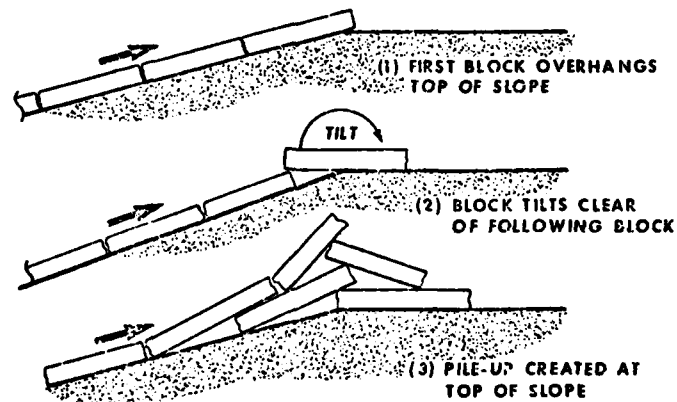

Figure 39. Forces for simple ride-up.

Figure 40. Kinematic instability
(pile-up at top of slope).

Therefore, condition for ride-up to continue is given by

$$t > 0.63 \ell \sin \alpha \tag{64}$$

This limiting condition is plotted in Figure 41. For the curve shown the length of the ice pieces is assumed to be three times the thickness. Other curves could be drawn for different length to thickness ratios.

Figure 41 suggests that for ice one metre thick a change in slope of greater than 30^0 would be needed to cause an instability from this mechanism. For a 1 in 3 (20^0) slope, ice one metre thick would continue past the top of the slope without a pile-up starting. The ice would have to be less than 0.25 m thick for a pile-up to be generated. For longer ice pieces the critical thickness would be greater.

2.133.5 Compression Instability

If the ice pieces are disturbed out of the plane of the slope as they ride-up, a compression instability may develop

Consider the configuration shown in Figure 42 where e is the height of a 'bump' in the slope. Simple equations of equilibrium can be used to relate P to e at the limiting condition of instability.

If for the purpose of this discussion we set α equal to zero and consider a frictionless, two-dimensional system, then

$$P = S = \frac{\ell^2 b t \rho g}{2e} \tag{65}$$

or

$$\sigma_c = \frac{\ell^2 \rho g}{2e} \tag{66}$$

where σ_c is the compressive stress in the ice at the point of instability.

Consider the example of ice pieces 4 m long and 1 m thick riding up a slope 30 m long at a 10^0 angle with a coefficient of friction of 0.3. What would be the height of the eccentricity or 'bump' required to initiate instability and hence a pile-up before the ice pieces reached the top of the slope?

Use equation (53) to calculate simple slope resistance in terms of an ice compressive stress.

$$\sigma_c = (30) \, 900(9.81)(\sin 10 + 0.3\cos 10) \text{ Pa}$$

$$\sigma_c = 125 \text{ kPa}$$

Use equation (16) to calculate value for e

$$e = \frac{(4)^2(900)9.81}{2(125)1000} = 0.57 \text{ m}$$

That is, a 'bump' say 1 m high at the lower end of the slope would lead to a pile-up being generated before the ice pieces could ride-up to the top of the slope.

2.133.6 Jamming

On beaches which have a sudden steepening of slope angle it is possible for the ice to 'jam' at the point of increasing steepness. (See Figure 43). Jamming leads to a sudden increase in slope resistance which can then cause ice pile-up by one of the mechanisms already discussed.

By using simple equations of equilibrium an expression for P can be derived. In this example, for simplicity assume $\alpha = 0$, then by simple mechanics

$$P = \frac{W}{2}(\mu + \frac{\sin\phi + \mu\cos\phi}{\cos\phi - \mu\sin\phi}) \tag{67}$$

The nature of the above equation is that for a particular value of μ a value of ϕ exists for which P becomes infinite and this is the jamming situation.

The 'jamming' situation is governed by the equation,

$$\phi = \tan^{-1}(\frac{1}{\mu}) \tag{68}$$

Variables of ϕ for typical values of μ are given below.

μ	0.1	0.2	0.3	0.4	0.5	0.7
ϕ (^{o})	84	79	73	68	63	55

2.134 Procedures for Designing Against Ride-up

In considering the problem of ice ride-up on a low free-board structure, several distinct steps in the logic can be identified, these are:

(a) Determine Ice Conditions Scenarios

A good knowledge of historical ice conditions is desirable and information on ice movement as a function of ice thickness is needed. Data on ice strength parameters, and coefficients of friction between the ice and beach are also required. In assessing various scenarios in ice conditions it is particularly important to recognize that adverse conditions may only arise infrequently. Statistical techniques may be required to determine design criteria from relatively sparse data. It is also important to recognize mitigating factors. For example, in the Beaufort Sea, dredged islands in shallow water are surrounded by landfast ice during most of the winter. The landfast ice does not move sufficiently to create ride-up problems. Furthermore, when large ice movements do occur in the early winter, the ice is initially very thin and forms rubble piles which protect the island from further ride-up until the ice becomes landfast. It is in fact during break-up, when large sheets of the previously landfast ice are in motion, that ride-up on artificial islands in the Beaufort Sea is most likely. Fortunately at this time the ice is extremely weak and has ablated to about 1.5 m thickness, reducing its ability to ride-up.

(b) Check the Preferred Beach or Island Design

The design of artificial offshore structures is determined by many factors including wave action, ice forces, available construction, equipment and materials, etc. (Croasdale and Marcellus, 1978).

As a first step in assessing the ride-up problems, the design as determined by other criteria (such as wave conditions) should be checked to assess whether ice ride-up is likely to be a problem. In this step, the limiting factors discussed in the previous section should be calculated for the most likely ice condition scenarios. If none of the mechanisms appears to prevent ice ride-up then special design factors may be needed to inhibit ice ride-up.

(c) If Necessary, Incorporate Design Features to Resist Ice Ride-Up

Features can be built into an island to discourage ice ride-up. An obvious solution is to raise the freeboard of the island and steepen the side slopes, but this approach is expensive because of the additional construction material needed.

Obstacles can be placed on the beaches to inhibit ice ride-up. This solution was used on a drilling island in the Beaufort Sea where steel piles were placed in the beach to protect the drilling rig during spring break-up. However, it turned out that the ice was so weak that rubble formed at the water-line and never reached the piles.

Perhaps the best approach is to alter the geometry of the island beach to encourage instability of ice pieces trying to ride-up.

A design using this approach is illustrated in Figure 44. The steep upper slope of the beach causes a jamming action which leads to sufficient force being generated to trigger a compression instability at the point of change in slope of the beach. The resulting pile-up is centered on the point of change in the slope which can be positioned so that the pile-up does not encroach onto the island surface. Equation (67) can be used to specify the angle of the upper slope; and the height of perturbation needed on the slope to initiate a pile-up can be specified using equation (66). For an important structure, model testing to confirm the design is desirable.
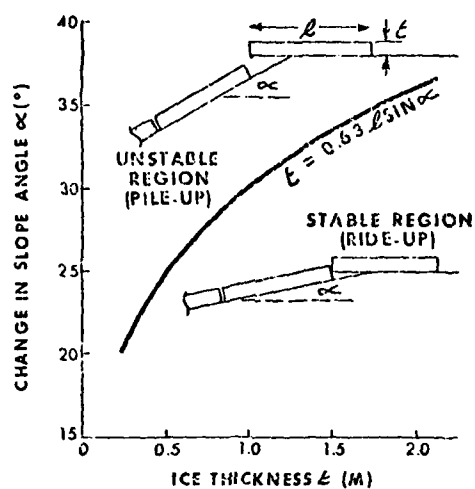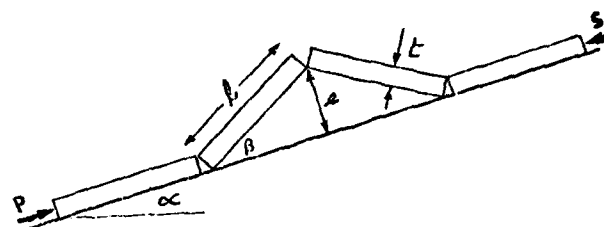
Figure 41. Criterion for ride-up past a change in slope.

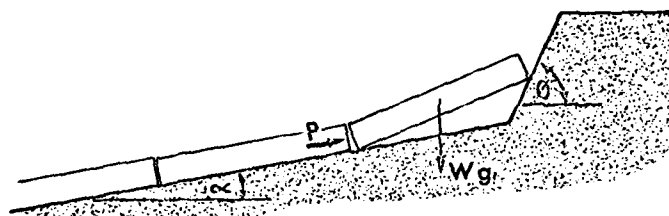
Figure 42. Compression instability.

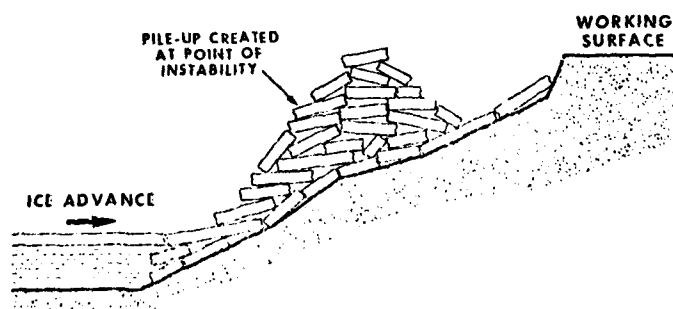Figure 43. Potential jamming of first ice block at change of slope angle.
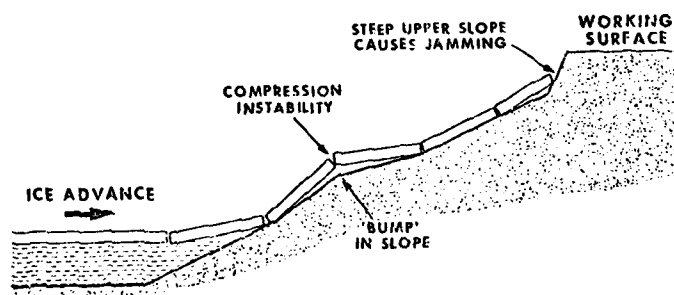

Figure 44. Design to resist ice ride-up.

2.14 REFERENCES

Afanasev, V.P., Dolgopolov, Y.V. and Shraishtein, Z.I., 1971, "Ice Pressure on Individual Marine Structures". In Ice Physics and Ice Engineering, Israel Program for Scientific Translation, 1973, p 50-68.

Allen, J.L., 1970, "Analyses of Forces in a Pile-up of Ice". NRC Technical Memo No. 98, Ottawa, Nov. 1970.

Arya, S.P.S., 1973, "Air Friction and Form Drag on Arctic Sea Ice". Aidjex Bulletin No. 19, pp 43-57, University of Washington, Seattle, W.A.

Banke, E.G. and Smith, S.D., 1973, "Wind Stress on Arctic Sea Ice". Journal of Geophysical Research, 78 (35), pp 7871-7882.

Bercha, F.G. and Danys, J.V., 1976, "Investigation of Ice Forces on a Conical Offshore Structure". Ocean Engineering, Vol 3, No. 5, p 299-310.

Bercha, F.G. and Danys, J.F., 1975, "Prediction of Ice Forces on Conical Offshore Structures". Marine Science Communications, 1975, p 365-380.

Bruun, P.M. and Johannesson, P., 1971, "The Interaction Between Ice and Coastal Structures". First International Conference on Port and Ocean Engineering and Arctic Conditions, University of Trondheim.

Calladine, C.R., 1969, "Engineering Plasticity". Oxford, Pergamon Press.

Croasdale, K.R. and Marcellus, R.W., 1978, "Ice and Wave Action on Artificial Islands in the Beaufort Sea". Canadian Journal of Civil Engineering, Vol 5, No. 1, 1978.

Croasdale, K.R., 1974, "The Crushing Strength of Arctic Ice", "The Coast and Shelf of the Beaufort Sea", Editors - Reed, J.D., and Sater, J.E., Arctic Institute of North America, 1974. pp 377-98.

Croasdale, K.R., 1975, "Ice Forces on Marine Structures". Third International Symposium on Ice Problems, I.A.H.R.

Croasdale, K.R., Morgenstern, N.R., and Nuttal, J.B., 1977, "Indentation Tests to Investigate Ice Pressures on Vertical Piers". Journal of Glaciology, Vol 19, No. 81, p 301-312.

Croasdale, K.R., 1977, "Ice Engineering for Offshore Petroleum Exploration in Canada". Fourth International POAC, Memorial University, St. John's, Newfoundland, 1977. p 1-32.

Danys, J.V. 1977, "On Wind Induced Static Ice Forces on Offshore Structures". Fourth International POAC, Memorial University, St. John's Newfoundland, September 26-30, 1977. p 718-729.

Edwards, R.Y., Croasdale, K.R., 1976, "Model Experiments to Determine Ice Forces on Conical Structures". Symposium on Applied Glaciology, Cambridge, England, 1976.

Frederking, R. and Gold, L.W., 1975, "Experimental Study of Edge Loading of Ice Plates". Canadian Geotechnical Journal, Vol 12, No. 4, November 1975, p 456-457.

Hanson, A., 1978, Private communication. Naval Arctic Research Laboratory, Barrow, Alaska.

Haynes, F.D., Nevel, D.E. and Farrell, D.R., 1975, "Ice Force Measurements on the Pembina River". Second Canadian Hydro-technical Conference, Burlington, Ontario.

Hetenyi, M., 1947. Beams on Elastic Foundations. University of Michigan Press, Ann Arbor, 1946.

Hirayama, K., Schwarz, J. and Wu, H., 1974. "An Investigation of Ice Forces on Vertical Structures". Iowa Institute Hydraulic Research Report, No. 158.

Irwin, G.J., 1975, "Ice Pressures at the Shore of Lincoln Bay". Report No. 729, Defense Research Establishment, Ottawa, October, 1975.

Jazrawi, W. and Davies, J.F., 1975, "A Monopod Drilling System for the Canadian Beaufort Sea". The Society of Naval Architects and Marine Engineers, Sumposium on Ice Breaking and Related Technologies, Montreal, P.W.

Jazrawi, W. and Khana, J., 1977, "Monocone; A Mobile Gravity Platform for the Arctic Offshore". Fourth International Conference on Port and Ocean Engineering under Arctic Conditions, Memorial University, St. John's, Newfoundland.

Karelin, I.D. and Timokhov, L.A., 1971, "Experimental Deter-mination of the Wind Drag on an Ice Sheet". Trudy Arkticheskogo i Antarkticheskogo Nauchno-Isslecovatel' Skogo Instituta, 303, pp 155-165. Also 1972, Aidjex Bulletin, 17, pp 49-52.

Korzhavin, K.N., 1962, "Action of Ice on Engineering Structures" U.S.S.R. Academy of Science, Siberian Branch (1962) Draft Translation by U.S. Army Cold Regions Research and Engineering Laboratory (C.R.R.E.L.), 1971.

Kovacs, A., Weeks, W.R. and Hibler, W.D., 1971, "Pressure Ridge Characteristics in the Arctic Coastal Environment". First International Conference on Port and Ocean Engineering Under Arctic Conditions, University of Trondheim.

Kry, P.R., 1977, "Ice Rubble Fields in the Vicinity of Artificial Islands". Proceedings of the Fourth International Conference on Port and Ocean Engineering under Artic Conditions (POAC), Memorial University, St. John's, Newfoundland, Canada, Sept. 1977.

Kry, P.R., 1978, "A statistical Prediction of Effective Ice Crushing Stresses on Wide Structures". IAHR Ice Symposium, Lulea, Sweden, 1978.

Lewis, J.W. and Croasdale, K.R., 1978, "Modeling the Interaction Between Pressure Ridges and Conical Structures". IAHR Ice Simposium, Lulea, 1978. (preprint).

Lo, K.Y., 1970, "The Operational Strength of Fissured Clays". Geotechnique (London), Vol 20, No. 1, pp 57-74.

Michel, B., 1970, "Ice Pressure on Engineering Structures". CRREL Monograph 111 B1b, Corps of Engineers, U.S. Army, Hanover, New Hampshire, 1970.

Michel, B., and Toussaint, N., 1977, "Mechanisms and Theory of Indention of Ice Plates". Symposium on Applied Glaciology, Cambridge, England, 1976. Published in Journal of Glaciology, Vol 19, No. 81.

Morgenstern, N.R. and Nuttall, J.B. Unpublished. The Interpretation of Ice Strength from In-situ Indentation Tests. (Report to Imperial Oil Limited, APOA Project No. 16, 1971.)

Neill, C.R., "Dynamic Ice Forces on Piers and Piles. An Assessment of Design Guidelines in the Light of Recent Research". Canadian Journal of Civil Engineering, Vol 3, No. 2, 1976, pp 305-41.

Nevel, D.E., "The Ultimate Failure of Floating Ice Sheets". Proc. of IAHR Symposium, Lennigrad, 1972, pp 17-22.

Parmenter, R.R., Coon, M.D., 1972, "Model of Pressure Ridge Formation in Sea Ice". Journal of Geophysical Research, Vol 77, No. 33, pp 6565-6576, 1972.

Prager, W. and Hodge, P.G., 1951, "Theory of Perfectly Plastic Solids". New York, John Wiley and Sons.

Ralston, T.D., 1977, "Ice Force Design Considerations for Conical Offshore Structures". Fourth POAC Conference, St. John's, Newfoundland, 1977.

Robbins, R.J., Metge, M., Taylor, T.P., Verity, P.H., 1975, Test Techniques for Study of Ice Structure Interaction. POAC Third Conference, Fairbanks, Alaska, 1975.

Sackinger, W.M. and Sackinger P.A. (1977), "Shear Strength of the Adfreeze Bond of Sea Ice to Structures". Fourth International POAC, Memorial University, St. John's, Newfoundland, p 607-614.

Schwarz, T., Hirayama, K. and Wu, H.C., 1974, "Effect of Ice Thickness on Ice Forces". Offshore Technology Conference, Houston, 1974.

Shapiro, L.H. and Harrison, W.D., 1976, "Mechanics of Origin of Pressure Ridges, Shear Ridges and Hummock Fields in Landfast Ice". Annual report, Contract No. 03-5-022-55, Geophysical Institute, University of Alaska, Fairbanks, March 1976.

Stefansson, V., 1913, "My Life with the Esquimau". McMillan, New York, 1913.

Tryde, P., 1972, "A Method of Predicting Ice Pilings". Prog. Report 25, Institute of Hydrodynamics and Hydraulic Engineering, Technical University of Denmark, April 1972, p 17-23.

Tryde, P., 1977, "Ice Forces". Journal of Glaciology, Vol 19. No. 81, 1977.

Tsang, G., 1974, "Ice Piling on Lakeshores". Scientific Series Report No. 35, Canada Centre for Inland Waters, Burlington, Ontario, 1974.

Zabilansky, L.J., Nevel, D.E. and Haynes, F.D., 1975, "Ice Forces on Model Structures". Second Canadian Hydrotechnical Conference, Burlington, Ontario.

PART III

ICE FORCES ON FIXED, FLEXIBLE STRUCTURES

By Mauri Määttänen

University of Oulu, Oulu, Finland

Abstract

The modes of interaction between ice and structure are discussed, and the properties of both ice and structure are seen in the context of interaction. The key parameter of the ice is the dependence of crushing strength on loading rate, in particular the inverse relationship that exists for a certain range and gives rise to negative damping.

Self-excited vibrations leading to limit cycles are explained and some design problems are discussed.

3.1 Definitions and structure category

The necessary condition for the ice-structure dynamic interaction is that either the displacement of structure or elastic deformation of ice takes part in the ice crushing phenomenon. Physically this means that one or the other of the components is capable of storing energy and releasing it later in another phase when crushing is easier.

Depending on the relative magnitudes of elastic deformations of ice and displacements of structure at the contact area the interaction problem can be divided into three modes: elastic ice displacements are insignificant, displacements of structure are insignificant, and both are significant. In many cases the difficult problem of the general third mode can be replaced by the simpler first or second modes.

The appearance of the ice-structure dynamic interaction is most profound in slender single-pile bottom-founded cantilever-type structures with small internal damping. Typical examples are piles, light-piers, lighthouses or monopod-type platforms (Fig. 3.1). Piles in groups, such as in bridges or in platforms, may also exhibit dynamic interaction during ice crushing, either in conjunction or separately.

Stiffness, mass and damping distributions in the structure also affect the interaction phenomenon. Ice-induced vibrations in structures ranging from 0.5 to 15 Hz have been reported under field conditions. If natural frequencies of structure lie in this range, dynamic interaction is more likely. The shape of natural modes is essential, since the amplitude of the natural mode at the ice action point strongly affects the excitation capability of ice force on that particular mode.

The source of energy for the ice crushing and the ice-structure interaction has its origin in wind drag or water currents. This topic is treated in Part II. In this section a brief overview is given on how to consider the effects of parameters in dynamic ice-structure inter-action following the scheme in Figure 3.2.

80 m

30 m

(m)
20
15
10
5
0
-5
-10
-15
-20
-25
-30
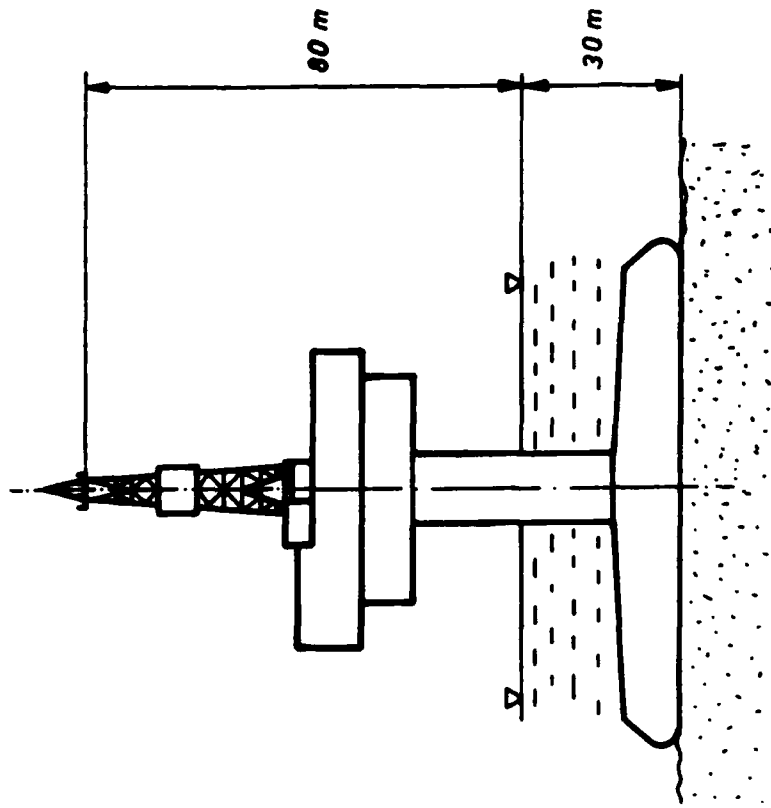
a) Steel lighthouse
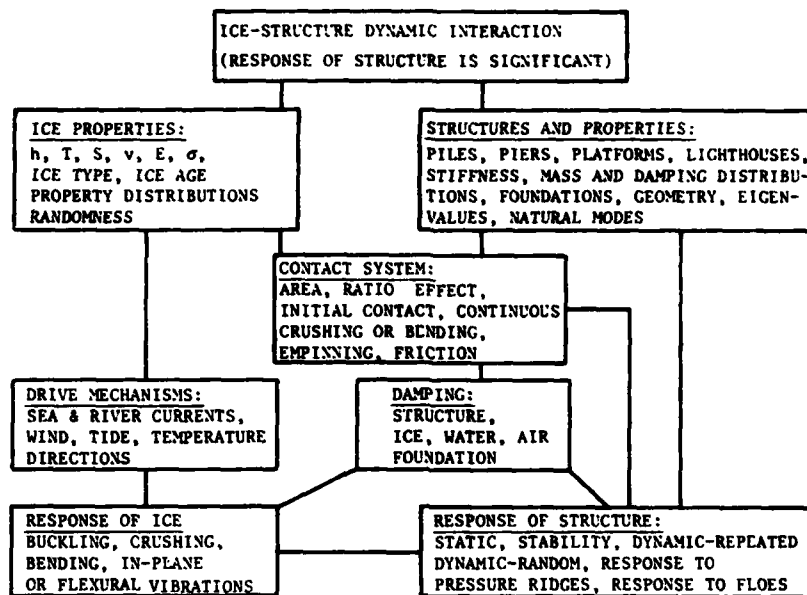
b) Pier

c) Monopod
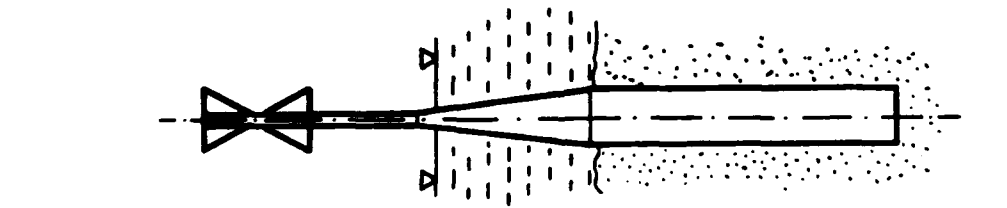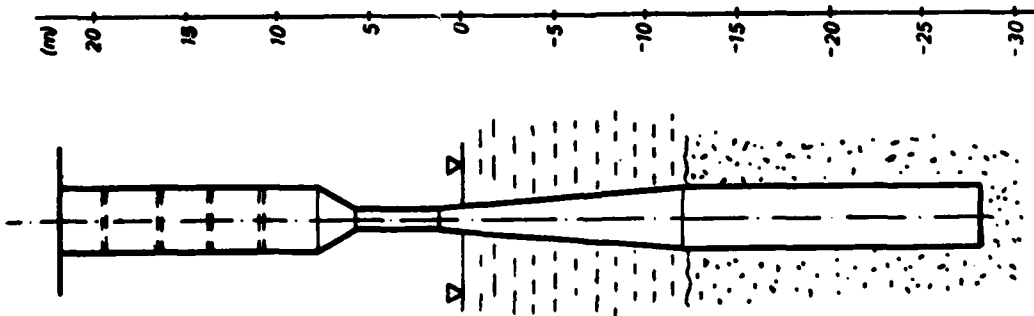
Figure 3.1

Figure 3.2

3.2 Ice properties

The strength properties of ice are dependent on its grain size and type, grain orientation, temperature, salinity and loading history. The most important parameter required is crushing strength, which means the stress value at which ice is failing against the structure. In this meaning both uniaxial compression strength values and the average failing stress value on the whole projectional ice action area are used. During ice crushing a three dimensional state of stress exists. Hence three dimensional yield conditions are required. The research in this area has not yet proceeded so far as to give accurate enough yield conditions for ice crushing purposes.

The size of the projectional area of the structure against which ice is crushing is usually so large when compared to the crystal size of ice that analysis need not be carried out at the crystal size scale but an average crushing strength σ_c for practical calculations can be used. Hirayama et al. (8) have observed that σ_c dependence on grain size appears only with $d/d_{cr}<25$, and Michel et al. (12) with $d/d_{cr}<7$ ($d =$ diameter of pile, $d_{cr} =$ diameter of ice crystals). In practice the grain size of columnar grained ice is from 1 to 20 mm, Gold (4), increasing with ice thickness. Hence, the average crushing strength from the grain size point of view is justified for actual structures.

The properties of ice vary through the thickness of an ice sheet. The main effect is due to temperature and salinity profiles. As the thickness of ice is usually small when compared to the height of a pile, averaging of properties through the thickness does not have any significant effect on structural response or on ice interaction. The effect of grain size and orientation may be handled in a similar way. The properties of a natural ice sheet in macro scale do not change in its plane but are different perpendicular to its plane. The effect of averaged properties can be observed by repeating calculations using a new combination of these parameters for ice crushing strength.

During the ice-structure interaction the viscoelastic behavior of ice must also be considered. During dynamic interaction the frequency of ice-induced vibrations with actual structures is however so high that the effect of viscoelastic behavior of ice can be disregarded. According to Gold (4) the behavior of ice is essentially elastic if it is loaded to failure within two seconds. This requirement is well satisfied with the observed range of frequencies from 0.5 to 15 Hz.

The key parameter in ice and structure interaction is the dependence of crushing strength on loading rate. The first measurements of crushing strength as a function of stress rate are by Peyton (17). His results from uniaxial compression tests of Cook Inlet ice samples (Fig. 3.3), indicate a decreasing strength with increasing stress rate. A similar trend was also measured on total ice force, both with laboratory and field test piles. The reduction in failure stress and ice force was about 50% from the maximum.
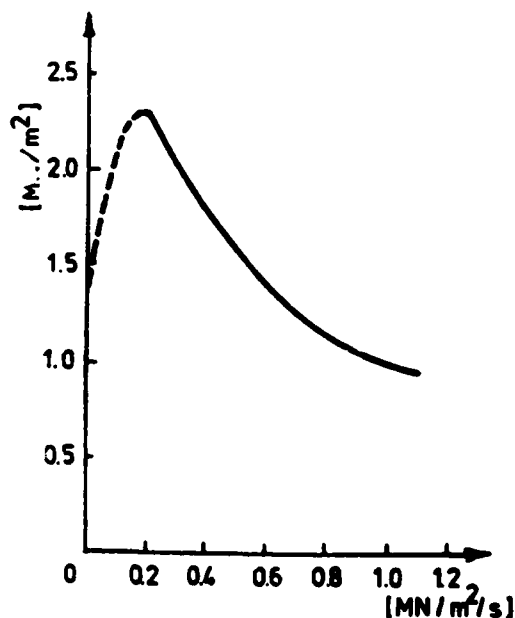

Figure 3.3 Crushing strength vs. strain rate, Peyton (17)

Michel et al. (12) carried out indentation tests with a square
indentor in the laboratory and also collected results from other authors
for crushing strength versus strain rate curve (Fig. 3.4). Ice behavior
is divided into three parts: the ductile region, the transition zone
and the brittle region, with boundaries as shown in Fig. 3.4. In the
brittle region failure occurs more randomly and the above curve repre-
sents an average crushing strength. Michel observed thinning of the ice
sheet by peeling off wedges from the upper and lower surfaces. Thinning,
together with strain rate, causes an average decrease to about 60% of
the maximum strength at the beginning of the transition zone.
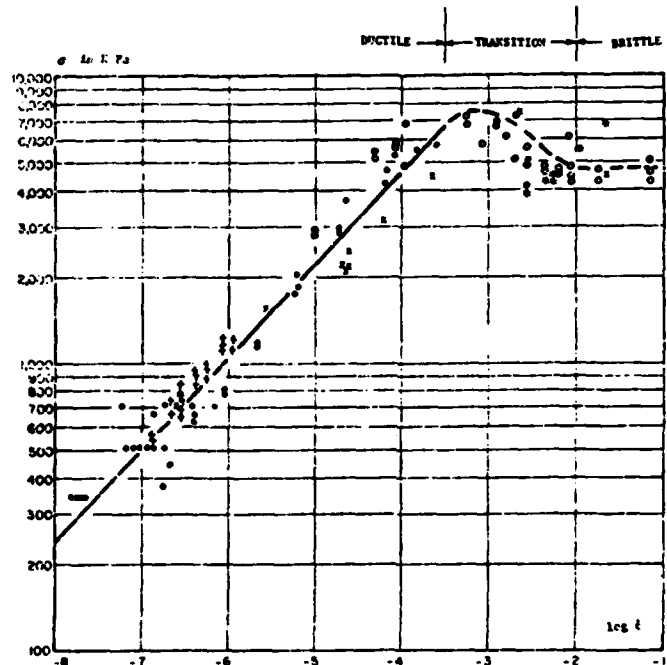
Figure 3.4 Crushing strength vs. strain rate, Michel et al. (12)

Wu et al. (24) achieved in their laboratory tests strength-strain
dependence as shown in Fig. 3.5. They pointed out the effect of temp-
erature: with decreasing temperature the transition from ductile to
brittle occurs more abruptly and with lower strain rates. In uniaxial
tests the reduction in strength is much greater than in the plane state
of stress. The transition to brittle is explained by means of a disloca-
tion theory. With high strain rates dislocation velocity is too low to
allow ductile behavior by plastic yielding and, therefore, cleavage
fracture and linking of grain boundary cracks occur. This also explains
the more random crushing behavior in the brittle region.
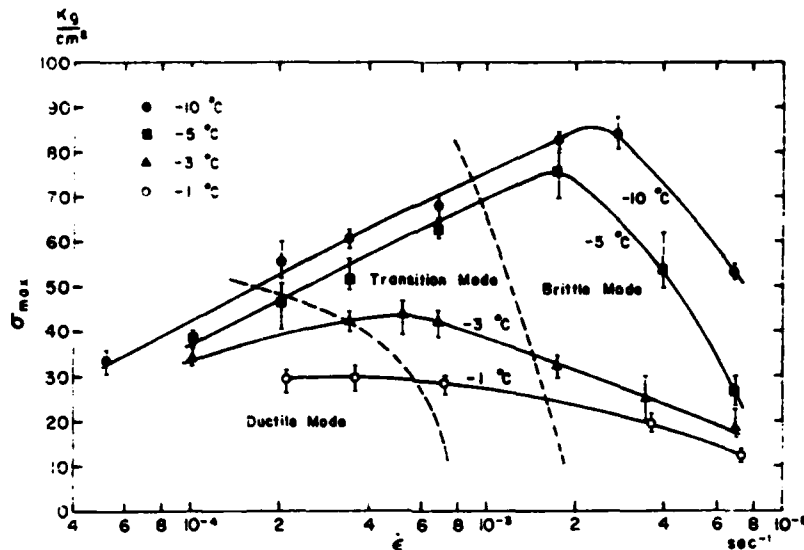
Figure 3.5   Ice crushing strength vs. strain rate and
             temperature, Wu et al. (58).

All researchers are of the same opinion with regard to the in-
creasing of ice strength with increasing loading rate in the ductile
region. Almost all agree that maximum strength occurs in the transition
zone, after which the average strength decreases considerably in the
brittle region. Exceptions are, for instance, Nevel et al. (16) and
Haynes et al. (6), who observed both in laboratory and in-situ field
tests that the speed of an indentor had no effect on crushing strength.
However, if stress rates are calculated it appears that almost all of
their data points fall in the brittle region.

The results of measurements by Hirayama et al. (8) showed the usual
reduction in average strength in the brittle region. However, no reduc-
tion was observed for a maximum value curve, which was defined in such a
way that 90% of all measured values lie under this curve.

Haynes (7) conducted uniaxial compression tests with dumbbell-
shaped snow ice specimens. His preliminary tests, three samples, indi-
cated that ever-increasing strength values can also be achieved beyond
the ductile region. This result is not, however, average, but from
carefully controlled small test samples, in which probability for initial
defects is very low and great strength values can be expected. Comparing
this to Hirayama's 90% curve and Peyton's measurements, it can be con-
cluded that for actual structures an average reduction in ice strength
in the brittle region exists. From the structural response point of

view, then, it makes no great difference if the reduction is due to strain rate, or thinning of the ice sheet, or uneven contact between ice and structure. The peeling off and local brittle failures occur simultaneously along the contact area, thus yielding to reduction in average ice force.

The definition of strain rate in the crushing strength curves is confusing as presented in the published research papers. There exist definitions which have only right dimensions, such as the concept of fracturing frequency (velocity divided by the crushing length per cycle), and velocity divided by the plastic zone width before the indentor, or the width of indentor or ice thickness.

In the elastic region, with uniaxial tests, the strain rate can be easily measured directly or calculated by dividing the velocity of crossheads by the length of test sample. In actual crushing the situation is more complicated: a two- or three-dimensional state of stress exists and difference must be made between the cases of initial stress increasing before yielding and continuous crushing.

The physically correct way to define strain rate is that of Gold (4) according to the dislocation theory. Considering elastic effects only the strain rate will then be directly achieved from the stress rate by dividing by the modulus of elasticity. The stress rate can be calculated by taking the time derivative from the stress history of a point in the ice sheet approaching the indentor. This method has been used by Blenkarn (7) and his formula for the maximum stress rate of ice before a circular indentor is

$$\dot{\sigma} = \frac{4\sigma_c v_o}{\pi a} \tag{3.1}$$

where σ_c is the maximum stress, v_o the velocity of ice sheet and a the radius of indentor. Depending on the shape of indentor, similar equations can be obtained starting from the corresponding stress field.

Frederking et al. (2) calculated the strain rate in the elastic region by integrating displacements, eliminating the shear modulus using strain values and taking the time derivative, which gives the strain rate as a function of displacement rate. At the indentor edge the latter is the same as indentor velocity. This definition is not valid after the yield point has been exceeded. As the stress or strain equals the yield point, the definitions of strain rate according to stress rate and displacement rate should yield equal results. However, depending on the value of modulus of elasticity and yield stress, a difference of two to three decades in the strain rate magnitude exists. It seems that the

strain rate obtained from displacement rate is only valid during the
initial loading and the strain rate obtained from the stress rate is
valid during continuous crushing. The discontinuity between the two
methods needs further research.

Randomness in the ice properties also affects the ice-structure
interaction. The meaning of grain size and orientation, salinity and
temperature variations is not so important from the structural response
point of view as variations in ice thickness, existence of cracks and
leads, piled-up layers of ice or pressure ridges. Although all in-situ
measurements indicate the existence of randomness, no general classifi-
cation has been made. Reddy et al. (19) describe a method to utilize
the observed random response of the structure further. The aerial
strength distributions have been observed in Soviet Design Codes, but
the randomness of ice properties is not directly observed anywhere.

3.3 Contact system

The mode of ice failure against a structure may vary with the
properties and thickness of ice. In this context only vertical or
almost vertical structures are considered. Typical failure mode is then
crushing if the slope from vertical is less than about 20° and the
friction between the ice and structure is not especially low. However,
a bending type of ice failure may occur even with vertical structures
with thin ice, which first buckles and then fails by bending. In this
case no significant ice-structure interaction response has been reported.
Buckling loads with thin ice are usually insignificant when compared to
crushing loads with nominal design ice thickness.

The best contact with the ice and structure is after the ice has
frozen to the structure with extensions downwards due to better heat
conductivity of the structure. The initial ice load peak becomes high
when the ice starts to move, although the strain rates at the beginning
of movement are so low that significant stress relieving due to visco-
elasticity occurs. In the case of slightly conical structures it has
been observed that the contraction of ice during cooling tends to lift
the freezing ice collar upwards and break it into segments, which prevents
the formation of high initial ice loads.

In classical formulas for ice force, e.g. Korzhavin, the effect of
contact phenomena is taken into account by two factors: I for the
shape of the structure and m for the unevenness of contact. These
factors are based on experimental measurements. It should be noted that
the value of the contact unevenness factor depends strongly on ice
properties and loading rate. Cold ice has greater strength but it is
more brittle, especially at high loading rates, which leads to lower

contact factors. In bridge piers in rivers the ice loading usually occurs during spring when the ice is warm and its strength low but contact factors greater. In design, all combinations should be considered. The usual range for the shape factor of the structure is from 1.0 for a flat indentor to 0.9 for a circular one and for the contact unevenness factor from 1.0 to 0.5.

A typical expression for ice force acting against a vertical pile is eq. 3.2 by Korzhavin:

$$F = Imk\sigma_c hd \tag{3.2}$$

which includes, in addition to the earlier mentioned factors I and m, a coefficient k which takes into account the observed dependence of ice force on the diameter of structure to ice thickness ratio, e.g. Fig. 3.6. This so-called "ratio effect" has been studied widely. Frederking (3), Gold (5) and Michel et al. (12) are of the opinion that the increase in effective crushing strength with small d/h ratios results from the strain rate effect. Considering a constant strain rate and using the power law in the ductile region a somewhat similar curve to Fig. 3.6 is achieved. However, then all values of the ratio effect k could be obtained just by changing ice velocity. In nature a wide range of velocities may appear.
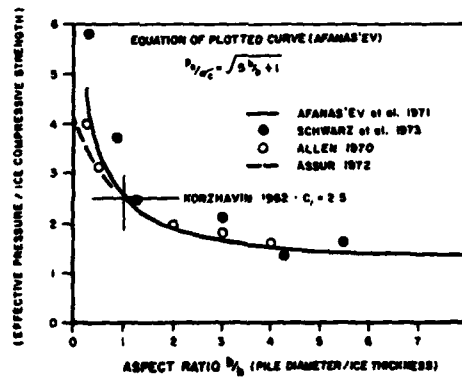
Figure 3.6 The dependence of effective σ_c on d/h, Neill (15).

In addition to, or included in, contact and aspect ratio coefficients other phenomena occur during ice crushing and have an effect on ice force. In the ductile region a small area of ice becomes plastic before the pile, which increases the effective diameter of the structure. The plastic region is not very wide but it extends more in the direction of ice movement, about 1.6d with a flat indentor, Michel et al. (12).

Schematically for a circular pile the situation is according to Fig. 3.7. The increase in effective diameter increases relatively more ice force with low d/h values, since pushing away ice rubble then requires relatively more tolerance between elastic ice and pile. Maybe this is one of the reasons for the diameter to ice thickness effect.
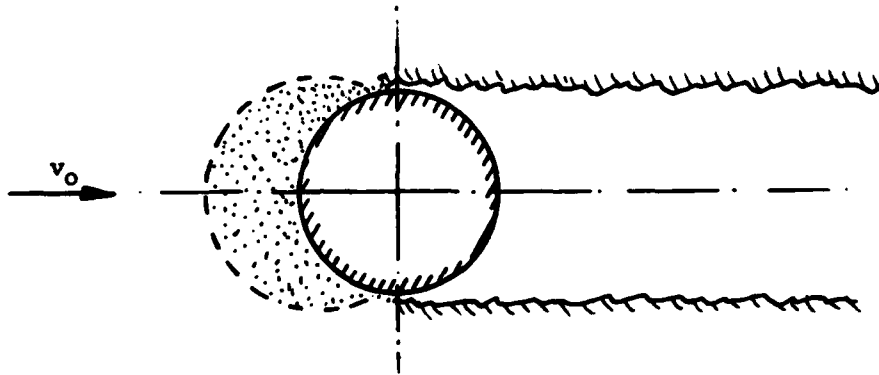
Figure 3.7 Plastic zone in crushing

In the brittle region during crushing the ice sheet is thinning by flaking or peeling off wedges from the upper and lower surfaces. Radial cracks and lateral cracks in the ice middle plane may appear. These yield a decrease in the ice thickness and relief in the state of stress which results in a reduction in the ice force. This gives a physical reasoning for the contact unevenness factor. The factor due to the shape of the structure can also be based on the promotion effect of the formation of radial cracks.

Although the contact between the ice and structure would be complete, the maximum ice pressure would not occur simultaneously. The failure of ice crystals with most unfavorable directions will start first before others have reached the yield level. As the crushing starts it may spread very fast to the whole contact area. Thus the magnitude of ice force will always be somewhat random and smaller than that calculated according to maximum ice strength.

During the dynamic ice-structure interaction the crushing strength, and the contact pressure, depend on the loading rate, which depends on the relative velocity v_r between ice and structure

$$v_r = v_0 + \dot{\Delta}_n - \dot{\delta}_n \qquad (3.3)$$

where $\dot{\Delta}_n$ and $\dot{\delta}_n$ are ice and structure velocities at the contact point n. As the crushing strength σ_c in eq. 3.1 is measured in uniaxial compression and as the pressure against a circular pile obeys approximately the cosine law, eq. 3.4, Frederking et al. (2),

$$\sigma_c (\dot{\sigma},\theta) = \sigma_c (\dot{\sigma}) \cos \theta \tag{3.4}$$

the final stress rate will be

$$\dot{\sigma} = \frac{4\sigma_c (\dot{\sigma}) v_r}{\pi a} \cos^2 \theta \tag{3.5}$$

To solve this equation it is required to iterate using a suitable crushing strength vs. stress rate curve. After the stress rate is solved the total ice load can be integrated along the periphery of the circular pile. The above equations can be similarly obtained for other indentor shapes. Alternatively a strain rate formulation could be used. In this way starting from the ice crushing strength vs. stress rate curve Määttänen (14) solved the interaction problem for circular piles in the case in which ice elastic deformations can be neglected.

In the first year pressure ridge in which the ice floes are not frozen together into one solid ridge, the dynamic interaction is relatively less severe than the maximum ice force. The contact with separate floes takes place only in a few corners or edges, and pushing aside loose floes causes great damping effects, which is observed in laboratory tests, Keinonen et al. (9). However, no measurements in-situ have been reported. In-situ observations, by this author, of a steel lighthouse showed as large vibration amplitudes in a pressure ridge as in the original even ice sheet. On the contrary in a concrete, caisson-type lighthouse considerably smaller vibrations occurred in a pressure ridge than in the even ice sheet.

Friction also plays an important role in the dynamic ice-structure interaction. Its main contribution is to damping and it will be treated separately in the next chapter. To the contact system the effect of friction is otherwise insignificant on the ice force but it may change the intended bending failure of ice against a sloped structure to crushing failure with considerably greater ice forces in the slope angle range between 10 to 30 degrees from the vertical.

3.4 Damping

In the ice-structure dynamic interaction the effect of damping is most significant in the case of self-excited ice-induced vibrations. The amount of damping controls to a great extent the amplitudes of limit cycles and may suppress totally the self-excited vibrations so that a

situation of "static" crushing may develop. In the case of transient ice forces such as the edge of an ice floe hitting against the structure damping has only a minor effect on structural response.

Total damping consists of structural and foundation hysteretic dampings, hydrodynamic damping of water and aerodynamic damping of air and of friction between the ice and structure. Also the energy dissi- pated to crush and grind ice into rubble may be regarded as a damping effect. On the other hand, the decreasing part of the ice crushing strength curve as a function of loading rate can be interpreted as a negative damping effect. All these are interfering during dynamic ice- structure interaction which makes it very difficult to eliminate the real positive damping from the total damping in measurements.

Most structural and hydrodynamic dampings are nonlinear in relation both to deformation and its time derivative. The usual concept is to linearize damping and to use equivalent linear damping coefficients, Lazan (10). As damping forces are usually very small when compared with stiffness or mass forces the vibratory response deteriorates only insignificantly while the nonlinear damping dissipates as much energy per cycle as the linear viscous damping.

Damping in structures is hysteretic and only slightly, or not at all, dependent on the rate of loading, Lazan (10). Aerodynamic damping is usually negligible and hydrodynamic damping is linear in small Reynolds numbers, Skop et al. (21). Foundations exhibit both hysteretic and hydrodynamic damping effects, but usually they are small, Ross (20). Considering a velocity dependent damping force, in which the above effects are combined, the positive damping behaviour can be visualized schematically according to Fig. 3.8. If in the same figure the negative ice-induced damping force near the steepest descent point in the crushing strength curve is plotted, it is observed that the positive damping overcomes the negative and hence no self-excited vibrations should occur. However, the always present random variations cause great enough velocities to move the point of action to the area where the negative damping is determined and self-excited vibrations may develop. If the curve of positive damping is linearized, the greatest error will be just near the point of origin, where a stable origin may be predicted as unstable. In practice the constant part is small at the origin for the positive damping force when compared with possible negative ice damping forces. Hence, linearization means operation on the safe side in design.

The negative damping effect of ice should be observed following the ice crushing strength curve with relative velocity. In addition, ice crushing also includes positive damping. These effects are the energy required to crush and grind ice into rubble, pushing the rubble away,
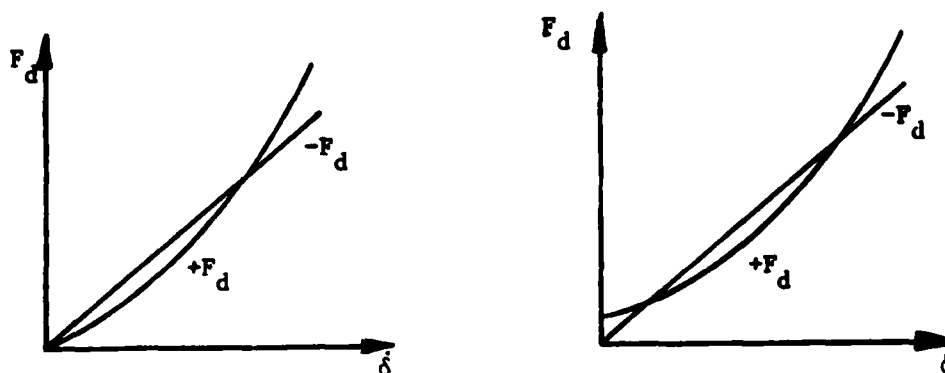
Figure 3.8 Effect of damping curv shape

and friction between ice and structure. Partly these effects can be taken into account already in the ice crushing strength curve, where in the brittle region the average ice force values are used instead of considering them to be zero after bursting like failure of ice. In the ductile region positive damping effects are negligible - practically no crushing - and, therefore, no additional positive ice damping effects are required. Crushing strength curves measured in the laboratory include these effects but no special attention has been paid to damping phenomena. Corresponding curves with actual size in-situ structures are not yet available and one must be careful when the results of laboratory tests are extended to full size structures.

The easiest way to observe structural and hydrodynamic dampings is to use natural mode relative damping coefficients, which can be measured most reliably. Relative damping coefficients have been reported to be from 2% by Blenkarn (1) to 6% by Matlock (11) and 10% by Määttänen (13). In the cases of Blenkarn and Määttänen positive and negative ice-induced dampings were interfering; in some cases energy required for ice crushing dissipated all the elastic energy of the structure, suppressing vibrations in half a cycle. Ross (20) reports a value of 2.5% for a steel tube vibrating freely. As for the structure and water alone, without ice effects, relative linear damping coefficients of from 3 to 6% are reasonable for the lowest modes.

3.5 Response of ice

The available information on dynamic response of ice is rather limited. The travelling and attenuation of stress waves have been

studied in connection with the elastic properties of ice but not in
connection with the dynamic ice-structure interaction. In the latter
case the elastic deformations of ice are usually so small that they are
not considered to be significant.

Depending on the relative magnitudes of elastic deformation of ice
and displacement of structure at the contact area the interaction problem
can be divided into three modes: elastic ice displacements are in-
significant, displacements of structure are insignificant, and both are
significant.

In the first mode ice interaction can be taken into account only
through the stress rate dependent crushing strength curve. In the second
mode the structure is infinitely stiff and its only interaction is
reaction force, which for its part is again stress rate dependent. In
the third mode both the ice and structure experience elastic displace-
ments simultaneously, and the dynamic equations of equilibrium for both
have to be solved simultaneously but separately with the only inter-
connection by the stress rate dependent ice force at contact points.

In the case of slender pile structures the first mode of interaction
is a sufficiently accurate approximation. In-field observations (13)
suggest this and the validity of approximation can be justified also by
calculations. The elastic ice displacement u_r for a circular pile in
the middle of an ice field is, according to Frederking et al. (2),

$$u_r = \varepsilon_r \cdot a \left[0.550 \left(\frac{a}{L} - 1\right) + 0.450 \ln \frac{a}{L} - 0.277\right] \tag{3.6}$$

where ε_r is the maximum radial ice strain at the contact point, a =
radius of pile, and L is the distance to the fixed boundary of the ice
field. Evidently infinite ice fields induce infinite displacements in
static loading. In practice all ice fields are finite and the order of
magnitude of u_r can be determined by taking a typical pile diameter
$d = 2a = 1$ m, $\varepsilon_r = 5 \cdot 10^{-4}$ (maximum elastic strain just before yielding
in a short duration loading) and varying L/a ratio:

Table 3.1 Elastic ice displacement

L/a	u_r (mm)
10^2	0.72
10^3	0.98
10^4	1.24
10^5	1.50

In slender pile structures the deflection due to maximum ice force is typically several centimeters so that the elastic displacement of ice is insignificant also in static loading. In the case of dynamic ice-structure interaction the effects of elastic ice deformations should be calculated using the wave equation. The order of practical L/a ratio can be bounded by considering the time during which an elastic wave starting from the interaction point travels to the edge of an ice field and back. Observing the attenuation and considering the periods of interaction frequencies from 0.5 to 10 Hz as the time limit for elastic waves to proceed with a typical velocity of 2800 m/s, the limit of ice field size L will be only 2800 ... 140 m in the case of a 1-m-diameter pile. Hence, also in infinite ice fields the elastic deformation of ice is limited from the interaction point of view.

Theoretically the in-plane vibrations of an ice sheet could be solved using the wave equation. In practice, however, initial conditions are not adequately known. The existence and effective range of in-plane vibration should be measured in-situ. In connection with in-plane vibrations, flexural vibrations may also occur during dynamic ice-strucure interaction. It is evidently the latter type of vibration which can be felt under an observer's feet on the ice.

The failure mode of a thin ice sheet acting against a vertical pile is buckling instead of crushing if the thickness of the ice is less than a critical value. In this case the maximum ice force will be small and usually insignificant when compared to design ice thickness ice forces. However, the possibility of resonance exists again, since the length of the buckles is constant for constant ice sheets and, hence, the velocity of ice determines the frequency of appearing ice force peaks.

When ice gets thicker, the failure mode changes to that of crushing. In the transition buckles may start to initiate and, depending on ice thickness, either buckling or crushing will be the failure mode. With thicker ice the initialization of buckles may be the origin for flexural vibrations.

Ice failure by bending is dominant with ice acting against inclined sloped structures. Methods for calculating ice forces are given in Chapter 2 by Croasdale. Again the length of subsequent bending failures is constant for a given ice sheet, and the frequency of resulting ice force peaks is determined by the velocity of ice. The possibility of resonance exists, but sloped structures are usually so stiff that no significant energy change between ice and structure occur, making dynamic interaction less pronounced.

3.6 Response of structure

Analytical numerical methods for predicting the dynamic response of structures are currently so effective that any structures can be analyzed

easily if time-dependent loading functions are known. In the case of ice-structure interaction the system is autonomous and, hence, the appearing ice force is the result of dynamic response of both the structure and ice. The problems encountered in numerical analysis are mostly due to inadequate knowledge of ice forces. The damping phenomena are also complicated since the loading-rate dependent part of the ice force is interfering with damping. Hence, great attention should be paid while using measured ice force functions as input for numerical analysis.

One of the most powerful methods for dynamic analysis of structures is to use finite element idealizations (23). This leads to the dynamic equation of motion

$$[k] \{\delta\} + [d] \{\dot{\delta}\} + [m] \{\ddot{\delta}\} = \{f(t)\} \qquad (3.7)$$

where $[k]$, $[d]$ and $[m]$ are the stiffness, damping and mass matrices of the discretized system, $\{\delta\}$ is the displacement vector of discretization nodes, and $\{\dot{\delta}\}$ and $\{\ddot{\delta}\}$ are its time derivatives, the vectors of modal velocities and accelerations. Schematically a similar equation as 3.7 can be written for the discretized ice floe as well:

$$[K] \{\Delta\} + [D] \{\dot{\Delta}\} + [M] \{\ddot{\Delta}\} = \{F(t)\} \qquad (3.8)$$

In the case of large or infinite ice fields, the wave equation must be used instead of eq. 3.8.

The loading vectors $\{f(t)\}$ and $\{F(t)\}$ have nonzero terms only in those modes in which ice is acting against the structure. These terms are identical in both equations and cause the interconnection between ice and structure. The appearing interactive ice force is loading rate dependent (Section 3.2, eq. 3.2, 3.4 and 3.5). Considering the nodal point n, the ice force ϕ_n can be expressed as a function of relative velocity, eq. 3.3 between ice and structure at the point n:

$$\phi_n = \phi_n (\dot{\delta}_n, \dot{\Delta}_n, v_o) = f_n = F_n \qquad (3.9)$$

Substituting this into eq. 3.7 and 3.8 it is observed that the system is autonomous, since time does not appear as an independent variable.

Initial conditions for the group of equations 3.7 and 3.8 are that $\{\dot{\delta}\}$, $\{\delta\}$, $\{\dot{\Delta}\}$ and $\{\Delta\}$ are zero vectors, and $\{f\}$ and $\{F\}$ vectors contain only that constant part of the interaction force that corresponds to constant initial ice velocity v_o. The appearance of vibrations occurs only if either or both of systems 3.7 and 3.8 are dynamically unstable.

The condition of stability can be deduced by solving the roots of the dynamical equations of motion. These are usually complex conjugate pairs, eg. for mode j

$$\lambda_j = \rho_j \overset{-}{+} i\, \omega_j \qquad (3.10)$$

The real part ρ_j, net damping, expresses the rate of decay or increase of possible vibrations in mode j and ω_j expresses its angular velocity. If $\rho_j < 0$, vibrations will die out exponentially and the situation is stable with no vibrations occurring in mode j and with ice crushing exposing constant loading against the structure. If $\rho_j > 0$ vibrations in mode j will grow exponentially with time, the system is dynamically unstable and self-excited vibrations will occur. Although the initial situation is static, only a small disturbance is required to start vibrations with growing amplitudes. Always present random variations in ice properties are enough to initiate self-excited vibrations.

For absolute dynamic stability it is required that all roots have negative real parts. In practice it is enough to check only those modes which can contribute significantly to dynamic response. With pile structures the observed range up to 15 Hz is adequate.

An approximate stability condition for mode j can be calculated from eq. 3.11, (14)

$$\zeta_j > \frac{\overline{X}_{nj}^2 \, \psi_{nn}}{2M_{jj}\, \omega_j} \qquad (3.11)$$

where $\overline{X}_{nj}$ is the amplitude of natural mode j at the ice-action node n, M_{jj} is the mass for the jth principal mode ($M_{jj} = \{x\}_j^{T}[m]\{x\}_j$, where $\{x\}_j$ is the natural mode vector), ω_j is the undamped angular velocity in mode j and ϕ_{nn} is defined as the rate of ice force from eq. 3.9:

$$\phi_n = \psi_{nn} \cdot \dot{\delta}_n \qquad (3.12)$$

Eq. 3.11 states that mode j will be stable in case the relative modal damping ζ_j is greater than the negative ice-induced damping through the term ψ_{nn}. While deriving eq. 3.11 it was supposed that ψ_{nn} is small. Hence, eq. 3.11 is valid only when the right hand side is smaller than about 0.15 and this requirement should be extended to all significant natural modes. Hence, results from eq. 3.11 are in close agreement with those of eq. 3.10.

The stability condition deduced from the roots of dynamical equations of motion gives only answers to the question of stability in the small. This means that amplitudes must be small. The ice-structure interaction is strongly nonlinear and with increasing amplitudes the rate dependence of ice force is changing. After a certain limit for relative velocities the negative damping effect of ice disappears as the point of action in the ice crushing strength curve moves out of the descending part (Fig. 3.4). Hence, ever increasing amplitudes are impossible. After a while the structure reaches a steady level of vibration amplitudes: limit cycles.

Dynamic stability in the large and limit cycles can be solved from eq. 3.7 and 3.8 by integrating them numerically. A small initial disturbance is required after which the nonlinear ice crushing strength curve is followed with changing relative velocities. If the initial disturbance decays, the system is stable; if after the initial disturbance vibrations start to grow, the system is dynamically unstable in the small. Limit cycles are then achieved simply by continuing integration until amplitudes and shape of vibration patterns no longer change.

The possibility of losing contact between ice and structure can also be easily observed in numerical integration. The contact is lost whenever the relative velocity gets negative after which a gap forms. At this stage the interaction force will be zero. A new contact and ice force according to the rate-dependent crushing strength curve is retained after the gap has closed. This kind of behavior during crushing has been observed in the field.

From the energy balance it is easy to deduce that steady limit cycles will exist and the system is dynamically stable in the large. The external energy imparted to the structure by ice will not grow forever with increasing amplitudes and relative velocities but the energy dissipated by damping will increase monotonically. Sooner or later, then, asymptotically a constant situation develops in which the net energy change is zero during each cycle of vibration.

The dynamic response and stability conditions of steel lighthouses and piers were solved analytically with the method described above (14). Only the first mode of interaction, elastic deformations of ice are insignificant, was analyzed. Results showed conformity with the observed and measured vibration patterns and limit cycle frequencies.

Another explanation for the rise of ice induced vibrations is given by Peyton (17) and further refined by Neill (15). Peyton explains that the frequency of ice crushing is a property of ice. Neill explains that ice tends to break into floes of a certain size. Hence, the velocity of ice determines the frequency. In either case no actual ice-structure interaction exists.

The breaking pattern proposed by Neill is dominant with inclined structures and also in the case when initial buckles occur. With brittle ice and vertical indentor radial cracks first appear and proceed before circumferential cracks appear. After this ice floes are pushed aside until new contact is achieved and the process starts again. In this case the resulting frequency of force peaks is mostly determined by the properties and velocity of ice and the shape of indentor, not by the stiffness or mass properties of structure. The response of the structure may then be integrated from eq. 3.7 by using an appropriate known or supposed time-dependent ice force function. With ductile ice, e.g. when ice starts to move in the spring, the crushing can occur without radial cracks and ice is ground into small pieces. In this case dynamic interaction is possible only by considering the loading-rate dependence of ice crushing strength.

The dynamic response of the structure may include transients, vibrations with constant amplitudes and frequencies and vibrations with random amplitudes and frequencies. The latter form is most common but from the structural safety point of view constant frequency vibrations are most dangerous because a resonant condition is always possible. Theoretical calculations seem to support the observed behavior of structures, to vibrate more likely in those natural modes that are unstable.

The frequency of ice-induced vibrations can be solved by integrating limit cycles numerically. An upper bound can be calculated more easily from eq. 3.13 (13)

$$f = \frac{k \, v_o}{\sigma_c \, hd} \qquad\qquad (3.13)$$

where k is the spring stiffness of the structure in the point of action and in direction of the ice force, v_o ice velocity, σ_c effective ice crushing strength, h ice thickness and d the diameter of pile. This equation does not take into account the time of deflection springback during crushing and the elastic deformation of ice. Hence, its accuracy is worse with higher frequencies where springback time becomes more important. Depending on the type of structure the limit cycle frequencies calculated by numerical integration have been about 0.6 to 0.9 of those of eq. 3.13. However, considering the range of possible ice velocities v_o or ice thickness L it can be concluded that eq. 3.13 is practical in predicting the possibility of resonance.

The transient response of structure during the initial hit of an ice edge or ice floe can be integrated also using eq. 3.7 and 3.8. Due to dynamic amplification maximum deflections and stresses in the structure

may rise up to two times that in the case of static crushing. Simplifying
the structural system to a one degree of freedom system and considering
only the maximum ice force without interaction but with rise time dependent
on the ice velocity, the amplification due to initial hit can be found
out directly from the curves of Timoshenko, et al. (22). Another possi-
bility instead of continuing crushing after the initial hit is the case
when the ice floe empinns to the pile and continues to vibrate with the
pile. The increased mass decreases the natural frequency but it causes
no additional loading (compared to initial hit loading) to the structure,
since then ice cannot impart any more energy to the structure.

Basically all ice-induced vibrations during crushing are random
by nature. This is due to random variation of ice thickness, strength,
crystal size and orientation, existence of pre-cracks, leads or layered
ice, etc. Thus, the resulting ice force will vary randomly and as the
time to failure with constant ice velocity will depend on the maximum
ice force, also the frequency of ice force peaks will be random.

Reddy et al. (19) have treated the ice-structure interaction as a
random phenomenon. The presented method is valuable in predicting
the random response of structures under ice loads in case probabilistic
properties of ice loads are known. However, only a limited amount of
data is available to date. The method to broaden the frequency range
of observed peaks in measured power spectras gives additional safety.
The applicability of generalized power spectras for other structures
is rather limited since the ice-structure interaction is autonomous and
a highly-nonlinear phenomenon. Changes of structural or ice parameters
may change, e.g. the condition of stability to opposite. Hence, the
original spectrum is no longer valid.

In the case of first year pressure ridge loading the dynamic re-
sponse of the structure will be equal to or less severe than in the case
of even ice sheet, and not in direct relation to the total ice force
(field observations by this author). The reason is that the essential
energy exchange in the dynamic ice-structure interaction will not work
since separate ice floes cannot deform elastically to a significant
extent but will, instead, dissipate much energy in local crushings.
Therefore, the first-year pressure ridge loading can be treated more
like a static loading condition. In the case of a multi-year ridge
energy exchange is possible and then also dynamic interaction. Measure-
ments, however, are lacking.

3.7 Design considerations

From the dynamic ice-structure interaction point of view the type
of structure chosen is most important. Low aspect ratio structures are
more stiff and their natural frequencies higher than those of high aspect

ratio structures. Low aspect ratio structures are not as sensitive to ice-induced self-excited vibrations, see eq. 3.11, but their total design ice force may be higher. This may happen also for conical structures that break ice by bending in case allowance is required for water level changes, which makes diameters and with it ice forces great.

Moving ice field with bending failure against inclined structures is giving an excitation with constant frequency, which depends on the properties and velocity of ice and the angle of slope. Pulsating ice force will be the result in every case. In the case of crushing failure the arising of a pulsating ice force depends on the properties of both ice and structure. With a successful design it will be possible to achieve a situation where the most significant natural modes will be dynamically stable. This gives possibilities for static crushing with no vibrations at all. However, also in this case, structures must be designed against transients and random ice force fluctuations.

The concept of a structure dynamically stable against ice-induced autonomous vibrations is to date more theoretical than practical, although experiences and a small number of measurements have verified the expected behavior of a dynamically stable lighthouse.

Resonant vibrations are the most dangerous loading condition. The whole range of changing ice velocity, strength and thickness values should be considered, with eq. 3.13 for the case of crushing failure and with a corresponding equation for the case of bending failure of ice.

Factors of safety in design should be reasonably great. Uncertainties in effective crushing strength, amount of decrease of crushing strength during transition from ductile to brittle ice failure and damping phenomena during the crushing process require more additional safety than normally used in dynamic loading conditions.

Both in-field and laboratory measurements are required to achieve a better understanding of all those phenomena that are occurring during dynamic ice-structure interaction. By field measurement the probabilistic properties of interaction force can be logged. While analyzing measurements a mathematical model of the structure is required in order to eliminate mass force and also partially damping effect out of the interaction force. The further utilization of measured known spectra requires the knowledge of dynamic stability characteristics in both test and application structures. By laboratory measurements the effects of basic parameters on interaction phenomena can be tested one after another. Also in this case the mathematical model is an essential part while analyzing and utilizing results.

REFERENCES

1. Blenkarn, K.A.: Measurement and Analysis of Ice Forces on Cook Inlet Structures, Offshore Technology Conference, Dallas Texas, 1970.

2. Frederking, R. and Gold, L: Ice Forces on an Isolated Offshore Pile, POAC-71, Technical University of Norway, Trondheim, 1971.

3. Frederking, R. and Gold, L: Experimental Study of Edge Loading of Ice Plates, Canadian Geotechnical Journal, Vol. 12, No. 4, November 1975.

4. Gold, L.W.: The Failure Process in Columnar-Grained Ice, NRC Technical Paper No. 369, Ottawa, 1972.

5. Gold, L.W.: Engineering Properties of Fresh-Water Ice, Symposium of Applied Glaciology, Cambridge, September 1976.

6. Haynes, F.D., Nevel, D.E. and Farrell, D.R.: Ice Force Measurements on the Pembina River, Alberta, CRREL Technical Report 269, Hanover, 1975.

7. Haynes, F.D.: Effect of Temperature and Strain Rate on the Strength of Polycrystalline Ice, CRREL, Hanover, January 1977.

8. Hirayama, K., Schwartz, J. and Wu, H-C.: Model Technique for the Investigation of Ice Forces on Structures, POAC-73, University of Iceland, Reykjavik, 1973.

9. Keinonen, A.: A paper to be published by IAHR proceedings, Luleå, 1978.

10. Lazan, B.: Damping of Materials and Members in Structural Mechanics, Pergamon Press, Oxford, 1968.

11. Matlock, H., Dawkins, W.P., and Panak, J.J.: A Model for the Prediction of Ice-Structure Interaction, Offshore Technology Conference, Dallas, Texas, 1969.

12. Michel, B. and Toussaint, N.: Mechanisms and Theory of Indentation of Ice Plates, Symposium on Applied Glaciology. Cambridge, September 1976.

13. Määttänen, M.: Experiences of Ice Forces Against a Steel Lighthouse Mounted on the Seabed, and Proposed Constructional Refinements, POAC-75, University of Alaska, Fairbanks, 1975.

14. Määttänen, M.: On Conditions for the Rise of Self-excited Ice-induced Autonomous Oscillations in Slender Marine Pile Structures, Finnish-Swedish Winter Navigation Board, Research Report No. 25, Finnish Board of Navigation, Helsinki, 1978.

15. Neill, C.: Dynamic Ice Forces on Piers and Piles. An Assessment of Design Guidelines in the Light of Recent Research, Canadian Journal of Civil Engineering, Vol. 3, p. 305-341, 1976.

16. Nevel, D.E., Perham, R.E. and Hogue, G.B.: Ice Forces on Vertical Piles, CRREL Report 77-10, Hanover, April 1977.

17. Peyton, H.R.: Sea Ice Forces, Conference on Ice Pressure against Structures, NRC Technical Memorandum No. 92, Laval University, Quebec, 1966.

18. Peyton, H.R.: Ice and Marine Structures, Ocean Industry, Parts 1, 2 and 3, March, September and December 1968.

19. Reddy, D.V., Cheema, P.S. and Swamidas, A.S.J.: Ice Force Response Spectrum Modal Analysis of Offshore Towers, POAC-75, University of Alaska, Fairbanks, 1975.

20. Ross, H.E.: Dynamic Response of Offshore Piling, Offshore Technology Conference, Dallas, Texas, 1971.

21. Skop, R.A., Ramber, S.E. and Ferer, K.M.: Added Mass and Damping Forces on Circular Cylinders, Naval Research Laboratory Report 7970, Washington, 1976.

22. Timoshenko, S., Young, D. and Weaver, W.: Vibration Problems in Engineering, John Wiley & Sons, New York, 1974.

23. Zienciewicz, O.: The Finite Element Method in Engineering Science, McGraw Hill, London, 1977.

24. Wu, H.C., Chang, K.J. and Schwartz, J.: Fracture in the Compression of Columnar Grained Ice, Engineering Fracture Mechanics, 1976, Vol. 8, pp. 365-372.

PART IV

A REVIEW OF BUCKLING ANALYSES OF ICE SHEETS

by D.S. Sodhi and D.E. Nevel

Abstract

A review of the buckling analyses of floating ice sheets is presented. The theory used is that of a beam or plate on an elastic foundation. For beams, the results for all possible boundary conditions are presented and discussed. For plates, results of numerical solutions for a semi-infinite plate loaded over part of its boundary are presented and discussed. One solution is presented for an infinite plate loaded radially at a hole in the plate. In addition, results for wedge-shaped beams and plates are presented and discussed. Wedge-shaped ice sheets frequently occur due to previous cracking in the ice.

INTRODUCTION

When an ice sheet impinges on a vertical structure, the generated force cannot be larger than the force needed to fail the ice sheet in either the crushing mode or the buckling mode, whichever requires less force. Although considerable experimental and analytical research has taken place to determine the horizontal forces ice exerts on structures in the crushing mode, comparatively little effort has been devoted to the study of ice sheet failure in the buckling mode. The concentration on the crushing mode probably has occurred because most structures placed in ice-infested waters have a small aspect ratio (ratio of structure width to ice thickness), and so cause the ice sheet to fail by crushing. However, it has been observed by many investigators during small-scale tests (Hirayama et al. 1973, Nevel et al. 1977, Zabilansky et al. 1975, Afanas'ev et al. 1972) and in the field (Perham 1977) that an ice sheet fails in the buckling mode when the aspect ratio is large (generally greater than 6), as with wide structures encountering thin ice.

Since buckling is a possible mode of failure for an ice sheet as it impinges on a vertical structure, it is necessary to study the buckling of floating ice sheets, which have been analyzed as beams or plates resting on elastic foundations. The force offered by the elastic foundation is assumed to be linearly proportional to the deflection of the ice sheet, an assumption that is valid as long as the ice sheet does not submerge completely under the water surface or emerge completely out of water. This assumption is also adequate for the linear buckling analysis that determines the load for the incipience of instability, but it is not valid for the post-buckling or dynamic behavior of an ice sheet.

This review is presented in two sections: 1) buckling analysis of beams on elastic foundations and 2) buckling analysis of plates on elastic foundations.

BUCKLING ANALYSIS OF BEAMS ON ELASTIC FOUNDATIONS

Beams of rectangular cross section

The deflection and buckling analysis of beams on elastic foundations has been presented by Hetenyi (1946). It is summarized briefly here for the sake of completeness.
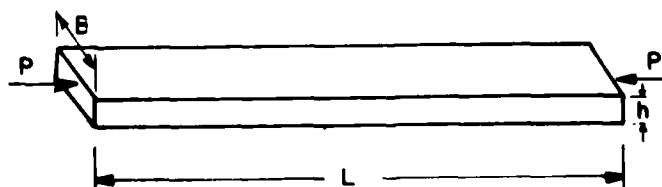

Figure 1.   Geometry of a beam with a rectangular cross section resting on a elastic foundation with compressive axial load P.

The differential equation governing the buckling of a beam with a rectangular cross section (Fig. 1) resting on elastic foundations and subjected to an axial compressive force P can be shown to be:

$$EI \frac{d^4w}{dx^4} + P \frac{d^2w}{dx^2} + KBw = 0 \qquad (1)$$

where   E = modulus of elasticity
              I = area moment of inertia
              w = transverse deflection of the beam
              x = distance along the beam
              B = width of the beam
              K = modulus of foundation (specific weight of water in the
                   case of floating ice sheets)

The characteristic length of a beam, $L_b = (EI/KB)^{1/4} = (Eh^3/12K)^{1/4}$ (h being the thickness of the beam), is an important parameter because it expresses the relative magnitude of beam stiffness to foundation stiffness in terms of an influence length parameter. Equation 1 may be rewritten by introducing a nondimensional length variable $\xi = x/L_b$:

$$\frac{d^4w}{d\xi^4} + 2\lambda \frac{d^2w}{d\xi^2} + w = 0. \qquad (2)$$

where $2\lambda = P/(BKL_b^2)$.

The general solution of eq 2 is a linear combination of four $e^{m\xi}$ terms where m is a complex number, and the solution takes three different forms, depending on whether the value of λ is greater than, equal to, or less than 1. The determination of the buckling load depends on the form of the solution assumed and the boundary conditions prescribed at the ends of the beam. The boundary conditions may be any one of the following: frictionless (shear force and bending moment are zero), hinged (deflection and bending moment are zero), or fixed (deflection and slope are zero).

The procedure for determining the buckling load from the general solution of eq 2 is outlined in the Appendix. The buckling load depends explicitly on the boundary conditions imposed at the ends of the beam and implicitly on the length of the beam. A buckling load exists for each mode of buckling of the beam, but we are only interested in the lowest buckling load of a given beam. The lower envelope plots of the nondimensional buckling pressure $P/(BKL_b^2)$ with respect to the ratio of beam length to characteristic length, L/L_b, are given in Figure 2 for the six different boundary combinations.
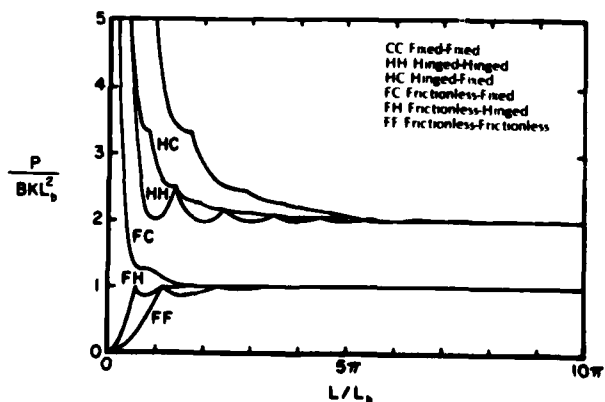

Figure 2.   Lower envelope plots of nondimensional buckling pressure $P/(BKL_b^2)$ with respect to the ratio of length to characteristic length, L/L_b.

Several observations can be made by observing the plots in Figure 2. When the length of a beam is small compared to the characteristic length, the buckling load of a beam on elastic foundations consists mainly of the Euler buckling load. For long beams, the Euler buckling load is low and the elastic foundation influences the buckling mode and thereby the buckling load of the beam. For beams that are long relative to the characteristic length L_b, the nondimensional buckling pressure $P/(BKL_b^2)$ approaches 2, except when one end is frictionless, in which case the nondimensional buckling pressure $P/(BKL_b^2)$ approaches 1. For short beams with frictionless-frictionless or frictionless-hinged boundary conditions, the nondimensional buckling pressure $P/(BKL_b^2)$ increases from 0 to 1 as the ratio L/L_b increases from zero to infinity because the rigid body movements of these beams are present in the solution and the Euler buckling load of such beams without the elastic foundation is zero. Since the buckling load can be small for small values of L/L_b in the frictionless-frictionless and frictionless-hinged cases, instability of this kind may exist when a broken ice sheet is pushed on a beach, causing an ice pile-up or rubble field to form near the shore.

Beams of linearly varying width (tapered beams)

The buckling analysis of tapered beams is of considerable interest because such a situation may occur when an in-plane force acting on an edge of an ice sheet creates vertical cracks originating from the area of loading and radiating outward into the ice sheet.

Referring to the geometry of the tapered beam shown in Figure 3, the differential equation governing the buckling of such a beam may be written as:

$$\frac{Eh^3}{12} \frac{d^2}{dx^2} \left[\frac{Bx}{R} \frac{d^2w}{dx^2} \right] + P \frac{d^2w}{dx^2} + K \frac{Bx}{R} w = 0 \qquad (3)$$

where B is the width of the beam at $x = R$ (see Fig. 3 for the definition of R) and the other parameters have been described previously. The buckling load P is determined by seeking a nontrivial solution which satisfies the imposed boundary condition at the ends of the beam. For a semi-infinite beam, a fixed boundary condition is imposed at infinity, and a prescribed boundary condition (either frictionless, hinged, or fixed) is imposed at x = R.
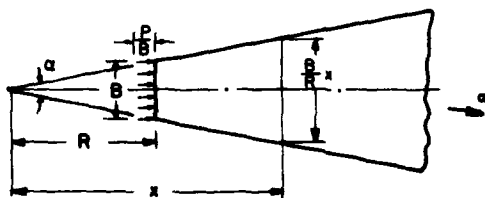

Figure 3.   Plan view of a semi-infinite tapered beam resting on an elastic foundation with total axial force P.

Equation 3 may be written in the following form by introducing a nondimensional variable $\xi = x/L_b$, where $L_b = (Eh^3/12K)^{1/4}$:

$$\frac{d^2}{d\xi^2}\left[\frac{\xi}{R/L_b}\,\frac{d^2w}{d\xi^2}\right] + \frac{P}{BKL_b^2}\,\frac{d^2w}{d\xi^2} + \frac{\xi}{R/L_b}\quad w = 0. \quad (4)$$

It is evident from the above equation that the nondimensional buckling pressure $P/(BKL_b^2)$ of a semi-infinite tapered beam depends on the boundary condition imposed at x = R and on only one geometrical parameter, R/L_b.

Kerr (1978) made an attempt to solve eq 3 by an approximate method using a solution having two degrees of freedom and a buckling load derived for fixed and hinged boundary conditions at x = R. Kerr (1978) postulated from his analysis that the expression for the buckling load should be in the form of the sum of two terms, the first being linearly dependent on B and the second being a function of taper angle α. But this is not the case according to the discussion presented here and the closed form solution presented by Nevel (1979).

Nevel (1979) obtained the exact solution of the differential equation (3) and confirmed that $P/(BKL_b^2)$ does depend only on R/L_b and boundary conditions imposed at x = R. The results obtained by Nevel (1979) have been plotted in Figure 4 along with the results obtained from a finite element analysis (Sodhi 1979).

This buckling analysis of tapered beams is valid only for small values of taper angle α, and the use of plate theory would be more appropriate for the cases when α is large.
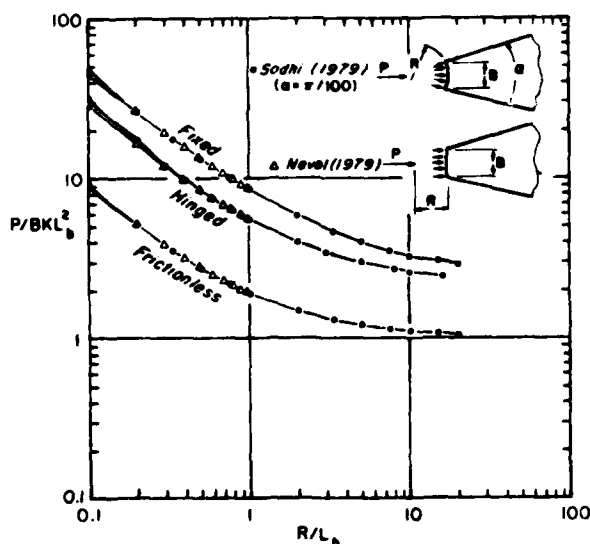

Figure 4.   Plot of nondimensional buckling pressure $P/(BKL_b^2)$ of a tapered beam with respect to R/L_b.

BUCKLING ANALYSIS OF PLATES ON ELASTIC FOUNDATIONS

The buckling behavior of a floating ice sheet is governed by the following differential equation:

$$D\nabla^4 w + Kw = N_{xx}\frac{\partial^2 w}{\partial x^2} + 2N_{xy}\frac{\partial^2 w}{\partial x\partial y} + N_{yy}\frac{\partial^2 w}{\partial y^2} \quad (5)$$

where

D = flexural rigidity of ice sheet

w = transverse deflection of the ice sheet

x,y = Cartesian coordinates on the middle plane of the ice sheet

∇^4 = biharmonic operator

K = modulus of foundation (specific weight of water in the case of floating ice sheets)

N_{xx}, N_{xy}, N_{yy} = in-plane stress resultants (force per unit length) which are linearly dependent on the total in-plane force P

The general procedure for solving eq 5 is to determine the expressions for N_{xx}, N_{xy}, and N_{yy} by solving a plane stress problem and then to solve the eigenvalue problem that determines the buckling load and the mode of buckling are determined. To find the non-dimensional form of the buckling load, we normalize the coordinates (x,y) with respect to the characteristic length of the plate

$$L_p = \left(\frac{Eh^3}{12(1-\nu^2)K}\right)^{1/4}$$

where ν is Poisson's ratio, to get $\xi = x/L_p$ and $\eta = y/L_p$, and we can rewrite eq 5 in the following form:

$$\nabla^4 w + w = \frac{P}{KL_b^3}\left(N_{\xi\xi}\frac{\partial^2 w}{\partial\xi^2} + 2N_{\xi\eta}\frac{\partial^2 w}{\partial\xi\partial\eta} + N_{\eta\eta}\frac{\partial^2 w}{\partial\eta^2}\right) \qquad (6)$$

where $N_{\xi\xi} = \dfrac{N_{xx}L_p}{P}$, etc., are the nondimensional expressions. The non-dimensional buckling load $P/(KL_b^3)$ is determined according to the procedure listed above, and the nondimensional buckling pressure is obtained by dividing $P/(KL_b^3)$ by the aspect ratio B/L_p (width of structure/characteristic characteristic length of ice sheet) to obtain $P/(BKL_b^2)$, which has the same form as that obtained for uniform beams and tapered beams.

A closed form solution of eq 5 or 6 may be obtained for simple plate geometries and for uniform in-plane stresses, but it is very difficult to obtain a solution for complicated plate geometries and boundary conditions, it is advantageous to seek solutions using numerical techniques. The only closed form solution known to the authors is that of Takagi (1978) who presented a solution of the buckling problem of an infinite elastic plate floating on water and stressed uniformly along the periphery of an internal hole. In this case, the two-dimensional problem is reduced to a one-dimensional problem using the condition of symmetry, and the equation governing the linear buckling is

$$D\left(\frac{d^2}{dr^2} + \frac{1}{r}\frac{d}{dr}\right)^2 w + Kw = p\frac{R^2}{r^2}\left(-\frac{d^2w}{dr^2} + \frac{1}{r}\frac{dw}{dr}\right) \qquad (7)$$

where r is the radial coordinate, and p is the pressure applied at $r = R$. By introducing $\zeta = r/L_p$, we may rewrite eq 7 as

$$\left(\frac{d^2}{d\xi^2} + \frac{1}{\xi}\frac{d}{d\xi}\right)^2 w + w = \frac{P}{KL_p^2}\frac{(R/L_p)^2}{\xi^2}\left(-\frac{d^2w}{d\xi^2} + \frac{1}{\xi}\frac{dw}{d\xi}\right). \qquad (8)$$

It is evident from the above equation that the nondimensional buckling load $p/(KL_p^2)$ is dependent on the ratio R/L_p and the boundary condition imposed on the circular edge $r = R$. Plots of the lowest nondimensional pressure $p/(KL_p^2)$ with respect to R/L_p are given in Figure 5 for three boundary conditions imposed at $r = R$ (frictionless, hinged, or clamped). The value of Poisson's ratio ν is taken to be 0.3 in the computation of buckling pressure when a frictionless or hinged boundary condition is specified at $r = R$. The nondimensional buckling load varies in a similar manner with respect to R/L_p as in the case of tapered beams, but the values are much higher for low values of R/L_p, which may be attributed to the development of hoop stresses around the hole. The asymptote of the buckling pressure for high values of R/L_p is 4 for hinged and fixed boundary conditions and 1.07 for the frictionless boundary condition. The corresponding values for a floating ice beam are 2 and 1.
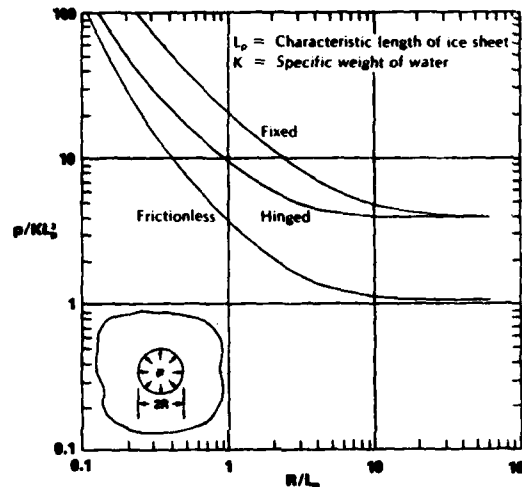

Figure 5.   Plots of the lowest buckling pressure $p/(KL_p^2)$ with respect to R/L_p for an infinite ice sheet stressed uniformly along the periphery of an internal hole (Takagi 1978).

In the following, only those studies that are relevant to the buckling of floating ice sheets in ice-structure interactions are discussed. The solutions in these studies were obtained by employing one of the numerical techniques.

1. Sodhi and Hamza (1977), using a finite element method, presented a buckling analysis of a semi-infinite ice sheet loaded by a uniformly distributed load over a finite length of a straight boundary (see Fig. 6). This study assumed a frictionless boundary condition on the straight edge and fixed boundary conditions on the edges at infinity.

2. Wang (1978a,b), using a combined Fourier decomposition and finite difference method, solved the buckling problem of a semi-infinite ice sheet as it moves against a rigid cylindrical structure (see Fig. 7). In this study, both frictionless and fixed boundary conditions are considered on the circular boundary, frictionless boundary conditions on the straight boundaries, and fixed boundary conditions on the edges at infinity.

3. Sodhi (1979), using a Fourier decomposition and finite element method, solved the buckling problem of a semi-infinite wedge-shaped ice sheet (see Fig. 8) that is loaded by a total load P, distributed on the cylindrical surface to create a radial stress field (i.e.

$N_{rr} = \frac{2P}{(\alpha+\sin\alpha)} \frac{\cos\theta}{r}$, $N_{\theta\theta} = 0$, $N_{r\theta} = 0$) in the ice sheet. The boundary conditions considered in this study are fixed on the edges at infinity, frictionless on straight radial edges, and fixed, hinged, or fixed on the circular edge.
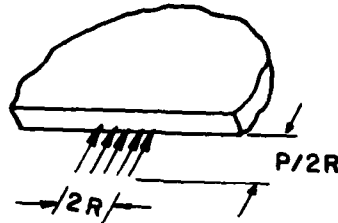

Figure 6.   Geometry of semi-infinite ice sheet acted on by a uniformly distributed load over a finite length.
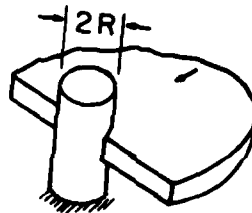

Figure 7.   Geometry of a semi-infinite floating ice sheet moving against a rigid cylindrical structure.
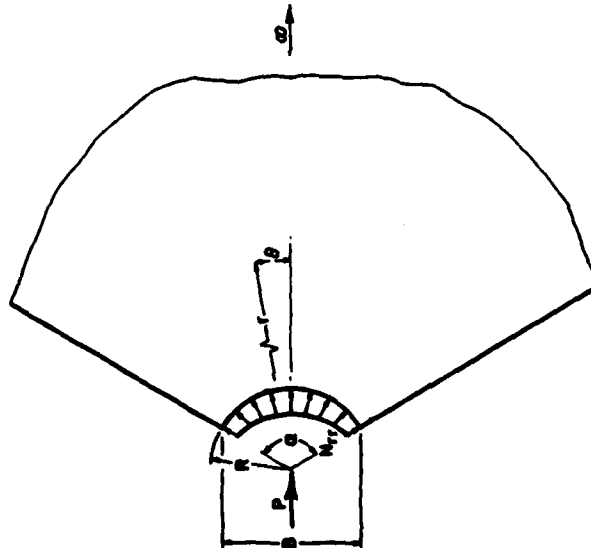

Figure 8.   Geometry of a semi-infinite wedge-shaped floating ice sheet.

The results of the first two studies and a particular case of the third study are presented in Figure 9 in the form of plots of $P/(2RKL_p^2)$ with respect to $2R/L_p$, where $2R$ is the structure width or length over which the load P is distributed. The results of the three studies are close to each other for the frictionless boundary condition, whereas the results of the second study are higher by 40% than those of the third study for the fixed boundary condition. This difference can be explained by noting that the stress field in the ice sheet is not strictly radial when fixed boundary conditions are used to determine the pre-buckling stress field.
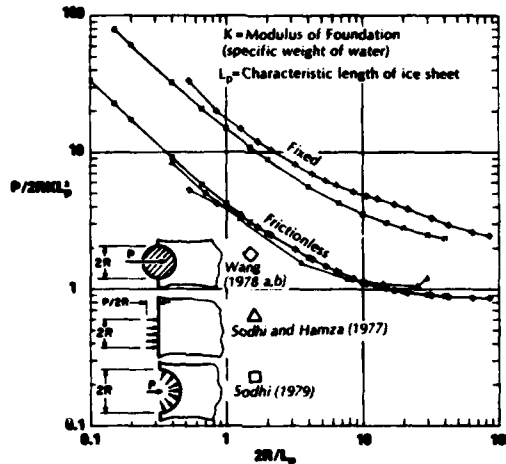

Figure 9.   Plots of nondimensional buckling pressure $P/(2RKL_p^2)$ with respect to $2R/L_p$ for semi-infinite ice sheets.

The results of the third study on the buckling of wedges (Sodhi 1979) are presented in Figure 10 in the form of plots of nondimensional buckling pressure $P/(BKL_p^2)$ with respect to R/L_p for different values of wedge angle α and different boundary conditions (see Fig. 8 for explanation of various parameters). Figure 11 shows the plots of buckling load $P/(KL_p^3)$ with respect to wedge angle α when P acts on a very small area (i.e. P is a concentrated force).
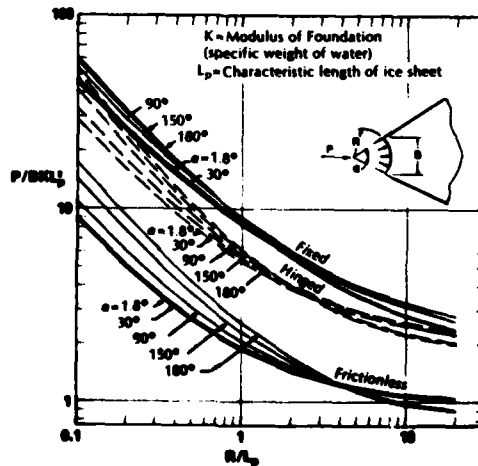

Figure 10.   Plots of nondimensional buckling pressure $P/(BKL_p^2)$ with respect to R/L_p for semi-infinite wedge-shaped ice sheets.
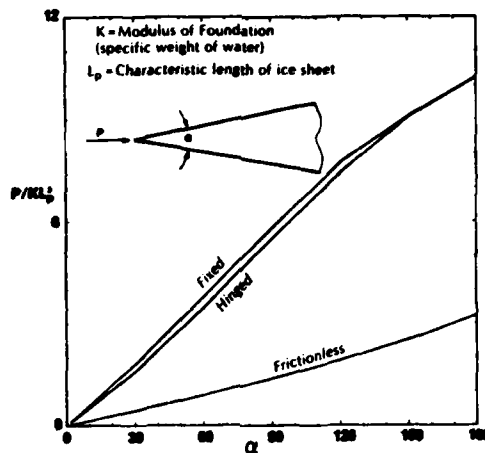
Figure 11.   Plots of concentrated buckling force $P/(KL_p^3)$ with respect to the taper angle α of semi-infinite wedge-shaped ice sheets.

In the study by Sodhi (1979), the buckling analysis is extended to wedges having wedge angles greater than 180°. The results for these cases are shown in Figures 12 and 13 in the form of plots of $P/(2RKL_p^2)$ with respect to $2R/L_p$. The cases considered in Figures 12 and 13 differ in the way the total P is distributed in the ice sheets; in Figure 12 the buckling load P creates a compressive as well as tensile stress field, whereas in Figure 13 the buckling load creates a totally compressive stress field. The buckling pressure for the second case is lower than that in the first case.
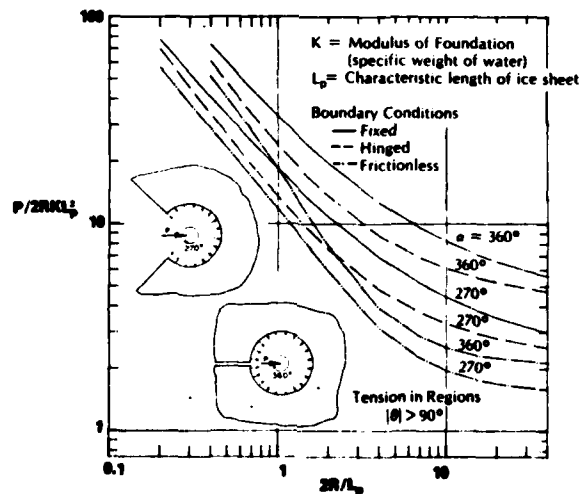

Figure 12.   Plots of buckling pressure $P/(2RKL_p^2)$ with respect to $2R/L_p$ when wedge-angle α is greater than π and when P creates a compressive as well as tensile stress field.
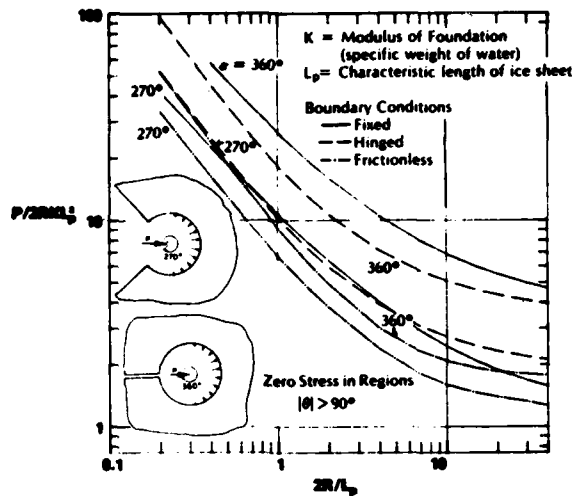
Figure 13.   Plots of buckling pressure $P/(2RKL_p^2)$ with respect to $2R/L_p$ when wedge-angle α is greater than π and when P creates only a tensile stress field.

POST-BUCKLING ANALYSIS OF FLOATING ICE SHEET

An analysis of the post-buckling behavior of floating ice sheets may be conducted to investigate the behavior of the critical load in the neighborhood of the buckling load obtained from the linear analysis already discussed. Kerr (1979) conducted a post-buckling analysis of a semi-infinite floating ice sheet that is loaded by a uniformly distributed in-plane load along the

edge of an ice sheet. Using the perturbation method, he established that the in-plane load required to maintain equilibrium in the post-buckling state would be less than that obtained from the linear analysis. The evaluation of this lower load requires a solution of the non-linear differential equation. This solution has not been obtained as yet.

CONCLUSION

This is a review only of theoretical analyses of the buckling of floating ice sheets in the form of beams and plates resting on elastic foundations. The buckling analysis of uniform cross section and tapered beams on elastic foundations is presented; the results are presented in graphical form. The buckling analysis of plates on elastic foundations is mainly restricted to semi-infinite ice sheets and wedge-shaped ice sheets; the results of these analyses are also presented in graphical form.

The buckling pressure of wedge-shaped ice sheets is very high when the aspect ratio (structure width to the characteristic length of the ice

sheet) is low, and hence the ice sheet fails in the crushing mode. For high aspect ratios, the buckling pressure is low, approaching the values of buckling pressure associated with infinite beams having the same boundary conditions as wedge-shaped ice sheets. The buckling pressure is strongly dependent upon the charactistic length of the ice, which in turn depends upon the modulus of elasticity of ice.

There have not been systematic experiments conducted to verify these theoretical results. The experiments in which the ice sheet failed in the buckling mode were really conducted to *fail the ice sheet in the crushing* mode, and the modulus of elasticity of the ice sheet was not determined. Using an estimated value of the modulus of elasticity, the theoretical values of buckling pressure are generally higher than the experimental values. This may be attributed to the material non-uniformity and material imperfections caused by cracking in the ice sheet prior to failure.

Although the results of various studies cited in this review agree with each other, experimental verification of these results is very desirable.

REFERENCES

Afanas'ev, V.P., Y. V. Dolgopolov and Z.J. Shreishtein (1972) Ice
    pressure on isolated structures in the sea. Trudy Leningrad, Arkt. i
    Antarkt. Inst., vol. 300, p. 61-80. U.S. Army Cold Regions Research
    and Engineering Laboratory, Draft Translation 346.

Hetenyi, M. (1946) Beams on elastic foundations. The University of Michigan
    Press, Chapter VII.

Hirayama, K., J. Schwarz and H. Wu (1973) Model technique for the investigation
    of ice force on structures. In Proceedings of the Second International
    Conference on Port and Ocean Engineering under Arctic Conditions,
    University of Iceland.

Kerr, A.D. (1978) On the determination of horizontal forces a floating ice
    plate exerts on a structure. Journal of Glaciology, vol. 20, no. 82,
    p. 123-134.

Kerr, A.D. (1979) On the buckling force of floating ice plates. IUTAM
    Symposium on the Physics and Mechanics of Ice, Technical University of
    Denmark, Copenhagen, 6-10 August, 1979.

Nevel, D.E. (1979) Bending and buckling of a wedge on an elastic foundation.
    IUTAM Symposium on the Physics and Mechanics of Ice, Technical University
    of Denmark, Copenhagen, 6-10 August, 1979.

Nevel, D.E., R.E. Perham and G.B. Hogue (1977) Ice forces on vertical
    piles. CRREL Report 77-10.

Perham, R. (1977) Personal communication.

Sodhi, D.S. (1979) Buckling analysis of wedge-shaped floating ice sheets.
    5th International Conference on Port and Ocean Engineering under
    Arctic Conditions (POAC 79), NTH, Trondheim, 13-17 August, 1979.

Sodhi, D.S. and H.E. Hamza (1977) Buckling analysis of a semi-infinite ice
    sheet. In Proceedings, 4th International Conference on Port and Ocean
    Engineering under Arctic Conditions (POAC 77), Memorial University of
    Newfoundland, St. John's, Newfoundland, 26-30 Sept., 1977.

Takagi, S. (1978) The buckling pressure of an elastic plate floating on
    water and stressed uniformly along the periphery of an internal hole.
    CRREL Report 78-14.

Wang, Y.S. (1978a) Buckling analysis of a semi-infinite ice sheet moving
    against cylindrical structures. In Proceedings, IAHR Symposium on Ice
    Problems, Lulea, Sweden, 7-9 August, 1978.

Wang, Y.S. (1978b) Buckling of a half ice sheet against a cylinder. In Pro-
    ceedings, ASCE Journal of Engineering Mechanics Division, EM5, October
    1978, p. 1131-1145.

Zabilansky, L.J., D.E. Nevel and F.D. Haynes (1975) Ice force on model
    structures. Second Canadian Hydrotechnical Conference, Burlington,
    Ontario, Canada.

APPENDIX

In the following, a procedure is presented for determining the buckling load of a beam on elastic foundations for a given set of boundary conditions.

The general solution of eq 2 may be assumed as $w = Ae^{m\xi}$. After substituting this solution into eq 2, we get

$$m^4 + 2\lambda m^2 + 1 = 0. \tag{A1}$$

The roots of the above equation are

$$\lambda < 1; \quad m_{1,2,3,4} = \pm(\alpha \pm i\beta)$$

$$\lambda = 1; \quad m_{1,2,3,4} = \pm i\beta, \pm i\beta \tag{A2}$$

$$\lambda > 1; \quad m_{1,2,3,4} = \pm i(\alpha \pm \beta)$$

where

$$\alpha = \sqrt{(1-\lambda)/2} \quad \text{for } \lambda < 1$$

$$= \sqrt{(\lambda-1)/2} \quad \text{for } \lambda > 1 \tag{A3}$$

and

$$\beta = \sqrt{(\lambda+1)/2}$$

The solution of eq 2 may be written in the following form:

Case I $(\lambda < 1)$:

$$w = (C_1 \cosh\alpha\xi + C_2 \sinh\alpha\xi) \cos\beta\xi + (C_3\cosh\alpha\xi + C_4 \sinh\alpha\xi) \sin\beta\xi \tag{A4}$$

Case II $(\lambda = 1)$:

$$w = (C_1 + C_2\xi)\cos\beta\xi + (C_3 + C_4\xi)\sin\beta\xi \tag{A5}$$

Case III $(\lambda > 1)$:

$$w = (C_1\cos\alpha\xi + C_2 \sin\alpha\xi)\cos\beta\xi + (C_3\cos\alpha\xi + C_4 \sin\alpha\xi)\sin\beta\xi \tag{A6}$$

The general procedure for the determination of the buckling load of a beam is to seek a nontrivial solution which satisfies a given set of boundary conditions. As an example, the buckling load of a simply-supported beam of length L is derived to illustrate the procedure.

Using eq A6, the boundary conditions at the ends of a simply-supported beam are expressed by the following set of equations:

$$
\begin{bmatrix} w(o) \\ w''(o) \\ w(L/L_b) \\ w''(L/L_b) \end{bmatrix} = \begin{bmatrix} 1 & 0 & 0 & 0 \\ -\lambda & 0 & 0 & \delta \\ C^\alpha C^\beta & S^\alpha C^\beta & C^\alpha S^\beta & S^\alpha S^\beta \\ \begin{pmatrix} -\lambda C^\alpha C^\beta \\ +\delta S^\alpha S^\beta \end{pmatrix} & \begin{pmatrix} -\lambda S^\alpha C^\beta \\ -\delta C^\alpha S^\beta \end{pmatrix} & \begin{pmatrix} -\lambda C^\alpha S^\beta \\ -\delta S^\alpha C^\beta \end{pmatrix} & \begin{pmatrix} -\lambda S^\alpha S^\beta \\ -\delta C^\alpha C^\beta \end{pmatrix} \end{bmatrix} \begin{bmatrix} C_1 \\ C_2 \\ C_3 \\ C_4 \end{bmatrix} = \begin{bmatrix} 0 \\ 0 \\ 0 \\ 0 \end{bmatrix} \qquad (A7)
$$

where a prime refers to differentiation with respect to ξ, $C^\alpha = \cos(\alpha L/L_b)$, $S^\alpha = \sin(\alpha L/L_b)$, $C^\beta = \cos(\beta L/L_b)$, $S^\beta = \sin(\beta L/L_b)$ and $\delta = \lambda^2 - 1$. For the nontrivial solution of eq A7, the determinant of the matrix is equal to zero, yielding the following characteristic equation:

$$
\cos(\alpha L/L_b) = \pm \cos(\beta L/L_b)
$$

or

$$
(\alpha - \beta)L/L_b = n\pi \qquad (A8)
$$

where $n = 1,3,5, \ldots$ for symmetrical modes

and $n = 2,4,6, \ldots$ for antisymmetrical modes.

The nondimensional buckling pressure can be derived from eq A8, and we get

$$
P/(BKL_b^2) = 2\lambda = (n\pi L/L_b)^2 + 1/(n\pi L/L_b^2) \qquad (A9)
$$

In a similar manner, the characteristic equations for different sets of boundary conditions can be derived and these are given below for all possible cases:

(a) hinged-hinged

$$
2\lambda = \left[(n\pi L/L_b)^2 + 1/(n\pi L/L_b)^2 \right] \qquad (A10)
$$

(b) fixed-fixed

$$
\frac{\sin(\alpha L/L_b)}{\alpha} = \pm \frac{\sin(\beta L/L_b)}{\beta} \quad \text{for } (\lambda > 1) \qquad (A11)
$$

(c) hinged-fixed

$$\frac{\sin(2\alpha L/L_b)}{\alpha} = \pm \frac{\sin(2\beta L/L_b)}{\beta} \quad \text{for } (\lambda > 1) \quad (A12)$$

(d) frictionless-frictionless (i.e. free-free)

$$\frac{\sin(\beta L/L_b)}{\sinh(\alpha L/L_b)} = \pm \frac{\beta}{\alpha} \frac{1-2\lambda}{1+2\lambda} \quad , \quad (\text{for } \lambda < 1) \quad (A13)$$

(e) hinged-frictionless

$$\frac{\sin(2\beta L/L_b)}{\sinh(2\alpha L/L_b)} = \pm \frac{\beta}{\alpha} \frac{1-2\lambda}{1+2\lambda} \quad , \quad (\text{for } \lambda < 1) \quad (A14)$$

(f) fixed-frictionless

$$\frac{2\lambda+1}{2\lambda+2} \sin^2(\beta L/L_b) + \frac{2\lambda-1}{2\lambda-2} \sin^2(\alpha L/L_b) = 1 \quad (\text{for } \lambda > 1)$$

$$(A15)$$

$$\frac{2\lambda+1}{2\lambda+2} \sin^2(\beta L/L_b) - \frac{2\lambda-1}{2\lambda-2} \sinh^2(\alpha L/L_b) = 1 \quad (\text{for } \lambda < 1)$$

For a particular value of L/L_b, the above equations can be solved by trial and error to obtain values of λ. As we are interested in the lowest buckling load for a given set of boundary conditions, the lower envelope plots of $2\lambda = (P/BKL_b^2)$ with respect to L/L_b given in Figure 2 were arrived at by solving eq A12-A15.